GEOPHYSICAL MONOGRAPH SERIES
David V. Fitterman, Series Editor
Michael W. Asten, Volume Editor

NUMBER 12

THE MICROTREMOR SURVEY METHOD

By Hiroshi Okada
Translated by Koya Suto

Published by
SOCIETY OF EXPLORATION GEOPHYSICISTS
with the cooperation of
SOCIETY OF EXPLORATION GEOPHYSICISTS OF JAPAN
AUSTRALIAN SOCIETY OF EXPLORATION GEOPHYSICISTS

Library of Congress Cataloging-in-Publication Data

Okada, Hiroshi, 1934-
The microtremor survey method / by Hiroshi Okada ; translated by Koya Suto.
p. cm. -- (Geophysical monograph series ; no. 12)
Includes bibliographical references and index.
ISBN 1-56080-120-4
1. Microseisms. I. Title. II. Series.
QE539.2.M5 O43 2003
622'.1592--dc22

2003050505

ISBN 0-931830-56-7 (Series)
ISBN 1-56080-120-4 (Volume)

Society of Exploration Geophysicists
P.O. Box 702740
Tulsa, OK 74170-2740

Published 2003
Printed in the United States of America

Contents

Historical note and foreword to the SEG translation

The microtremor survey method (MSM) relies on two paradigms foreign to the practice of conventional seismic exploration. These are (a) the property of seismic surface waves that their penetration into the earth is frequency dependent, hence the dispersion curve (phase velocity versus frequency) for observed data can be inverted to yield a layered-earth model of the subsurface, and (b) the variation of phase velocity with frequency can be measured using array-processing methods.

The MSM applied to the study of near-surface geology has had a fascinating history over the last 50 years, and it is fitting that SEG should publish a Japanese text as a benchmark. For it was a (then) young Japanese seismologist, Keiiti Aki, (1957, 1965) who laid the foundation for the Spatial Autocorrelation (SPAC) method which has become the key to successful extraction of phase-velocity information from surface-wave microtremors. This particular contribution from Aki appears to have been largely ignored in Western literature on the study of microtremors; the great strides in seismic array data processing of the 1960s and 1970s were spurred by the need to locate *direction* to seismic sources, and, hence, beam-forming (or *f-k*) methods (e.g., Capon, 1969) received the greatest emphasis.

Indeed, the very nature of high-frequency microtremors has been a source of significant debate; some authors in past decades attributed them to P-wave energy, and marketed the use of engineering-seismic studies based on comparing spectral peaks of microtremors with P-wave resonances, while others attributed the same energy, and the same spectra, to Rayleigh-wave propagation. See the exchanges by Asten (1979) and Katz (1979) following Asten (1978b) for examples where the debate generated heat as well as light (with somewhat more vigorous debate occurring in unpublished notes sent to the Editor of the day!). More recently, literature originating in the Western Hemisphere has debated whether microtremors are dominated by S-wave resonances or by Rayleigh-wave propagation (e.g., Ibs-von Seht and Wohlenburg, 1999 and references therein; Liu et al., 2000).

The study and use of the spectra of microtremors for engineering-scale studies has developed into a separate and mature science, largely due to the efforts of Japanese seismologists over the last 20 years (Nakamura, 1989; Konno and Ohmachi, 1998). The study and use of phase-velocity dispersion curves of microtremors has developed separately, also in Japan, largely

as a result of the diligence of Prof. Okada and his students, and was cons erably assisted by use of the SPAC technique pioneered by Prof. Aki 45 ye ago.

The SPAC technique is worthy of an additional observation. Array bea forming delivers estimates of wave velocity and direction, and is subject bias in velocity estimates when waves from multiple directions are inco pletely resolved. However, the SPAC technique has the delightful prope that, since the wave *direction* is not sought, estimates of wave *scalar veloc* are unaffected by the superposition of waves from multiple directions. Tl property was described by Aki (1965), a principle subsequently overlook in some literature, e.g., Douze and Laster (1979), but was then reiterated Asten (1983).

In fact, the more omnidirectional the wave energy (assuming single-mo propagation), the better the estimate of scalar velocity. The SPAC techniq thus has the serendipitous property of giving its best results when seisn sources are many. This is why the technique has enormous potential in bui up areas, where microtremor noise militates against the use of convention seismic methods, but that same ubiquitous noise generated by urban acti ity produces an omnidirectional wavefield of high-frequency microtremo ideally suited to the SPAC technique.

I welcome Prof. Okada's learned contribution to the theory, methodolo and case histories for the use of high-frequency microtremors in engineeri geophysics. I warmly endorse his desire to see the method develop into commercially viable survey tool.

I see scope for several further developments not covered in this boc Firstly, the integrated study of both spectral shapes and phase velocities likely to provide more information than either discipline alone. Secondly, t extension of the SPAC technique to detect multimode Rayleigh-wave prop gation (e.g., Asten, 1978a; Henstridge, 1979) should extend the utility of t method developed in this book. Thirdly, the routine use of three-compone seismometers should allow simultaneous detection and use of Love-wave n crotremor energy, using theory by Prof. Okada, which is presented in Engli for the first time in this book, but not yet implemented on published exa ples of field data. Modern data acquisition hardware and portable computi power make the logistics of recording and processing the extra data trivi compared with the size of the task if using the technology of one or tv decades ago. Prof. Okada has positioned us for an immense step forward

the use of seismic methods for engineering and environmental applications in built-up areas.

Michael W. Asten
July, 2001
Department of Earth Sciences
P.O. Box 28E
Monash University
Melbourne, Vic. 3800, Australia.
Email: masten@mail.earth.monash.edu.au

References

Aki, K., 1957, Space and time spectra of stationary stochastic waves, with special reference to microtremors: Bull., Earthq. Res. Inst., **35**, 415–456.

———1965, A note on the use of microseisms in determining the shallow structures of the Earth's crust: Geophysics, **30**, 665–666.

Asten, M. W., 1978a, Phase velocities of mixed-mode high-frequency microseisms (Abstract): EOS, **59**, 1141.

———1978b, Geological control on the three-component spectra of Rayleigh-wave microseisms: Bull., Seism. Soc. Am., **68**, 1623–1636.

———1979, Comments on "Microtremor site analysis study at Beatty, Nevada" by L. J. Katz and R. J. Bellon: Bull., Seism. Soc. Am., **69**, 1623–1636.

———1983, Discussion on "Seismic array noise studies at Roosevelt Hot Springs, Utah Geothermal Area": Geophysics, **48**, 1560–1561.

Capon, J., 1969: High-resolution frequency-wavenumber spectrum analysis: Proc. IEEE, **57**, 1408–1418.

Douze, E. J., and Laster, S. J., 1979, Seismic array noise studies at Roosevelt Hot Springs, Utah Geothermal Area: Geophysics, **44**, 1570–1583.

Henstridge, J. D., 1979, A signal processing method for circular arrays: Geophysics, **44**, 179–184.

Ibs-von Seht, M. and Wohlenburg, J., 1999, Microtremor measurements u to map thickness of soft sediments: Bull., Seis. Soc. Am., **89**, 250–25

Katz, L., 1979, A reply: Bull., Seis. Soc. Am., **69**, 1637–1639.

Konno, K., and Ohmachi, T., 1998, Ground-motion characteristics estim from spectral ratio between horizontal and vertical components of crotremor: Bull., Seis. Soc. Am., **88**, 228–241.

Liu, H. et al., 2000, Comparison of phase velocities from array measurem of Rayleigh waves associated with microtremor and results calculated f borehole shear-wave velocity profiles: Bull., Seis. Soc. Am., **90**, 666–(

Nakamura, Y., 1989, A method for dynamic characteristics estimatio subsurface using microtremors on the ground surface: Quarterly report the Railway Technical Research Institute, Tokyo, **30**, 25–33.

Translator's foreword

The phenomenon of microtremors has long been known to mankind, but it is only quite recently that the microtremor survey method has established itself. It is basically a passive seismic method, whereby "listening" to nature's "voice" gives information enabling us to estimate the subsurface structure under an array of geophones.

Because it is a passive method, the data collection system of the microtremor method is relatively simple, and it can be carried out in areas where access by a conventional seismic crew is prohibitively difficult.

As urban development progresses, the increased level of cultural noise often precludes the use of many of the conventional geophysical survey methods normally used for detecting subsurface structures. The microtremor method provides a viable alternative.

This textbook by Professor Okada is believed to be the first comprehensive textbook in this field. Professor Okada and his team at Hokkaido University have been investigating and developing the method since the early 1980s, and this textbook is a ripe fruit of their collaboration. This textbook was first prepared in 1997 for a seminar of the Japanese SEG, and it has undergone several revisions in the last five years.

The first three chapters of the book are mainly concerned with the nature of microtremors and principles of their detection. Chapter 4 outlines the procedures for data analysis, followed by a chapter on data acquisition and analysis (Chapter 5) and a few case histories in Chapter 6.

The style of the original text reflects the careful and diligent nature of Professor Okada: each building block is carefully explained, laid, and consolidated before the next layer is introduced. Readers may wish to skip details in places, particularly where conceptual discussions take place. However, readers will soon realize that these foundations are necessary steps to understanding the validity of subsequent developments such as practical data collection systems and case histories of their application.

I am a petroleum exploration geophysicist who has been interested in the microtremor survey method for several years, but I am not a native speaker of English. With the help of fellow geophysicists in the Oil Company of Australia Ltd (a subsidiary of Origin Energy Ltd), the English text was carefully refined and made as natural as possible. Acknowledgement for this work is given to Messrs. Justyn Hedges (now with Hardman Resources Ltd) and Damian Kelly (now with Cairn Energy PLC). A special thanks is due to the SEG Volume

Editor, Dr. Michael Asten, who carefully reviewed the technical conten the text and further refined my English.

Koya Suto
Brisbane, 2

Preface

One of the recent innovations in geophysical survey techniques is the application of the microtremor method to the fields of construction and structural engineering. Its main purpose is to estimate the subsurface structure that provides a fundamental basis for analysis of the response of the ground to earthquake movement, particularly in densely populated areas where there is a growing difficulty in utilizing conventional seismic techniques. Therefore development of the "microtremor survey method" (MSM) is eagerly awaited by those concerned with urban engineering.

The history of the microtremor survey method is short, and we can only draw from limited experience and a few case histories. In particular, its application to resource exploration has scarcely been documented. However, application of the microtremor method is gaining popularity in the construction and structural engineering in the area of prevention of potential disaster by earthquakes. This method is well adapted to such an application.

The applicability of the microtremor survey method is, at least theoretically, not limited to any field. It is a basic survey method for delineating subsurface structure, not only for urban applications, but also for exploration of oil, gas, and other resources. In this sense, it is no different from the conventional seismic method.

The microtremor survey method has not been developed as an application or extension of the conventional seismic method, but it is a totally new method based on a totally new idea. Firstly, the wave concerned is different. Consequently, the resultant image of the subsurface structure is, naturally, different from the conventional imaging. As this humble textbook describes, the microtremor method is derived from several assumptions and conditions in its basic theory and development that impose a limitation in applicability. For this reason, the microtremor method is, at present, regarded as unsuitable for detailed surveying.

I present an overview of the practicality and broad applicability of the microtremor method. The charm of this method is its differences from the conventional geophysical methods, in ideas and means. These differences, in turn, may make it difficult for it to be widely accepted as a new geophysical technique. It may still take some time before it becomes a commercially viable survey method. Yet, it is clear the MSM has already reached, to a degree, the realm of practical application, and it is also clear that the

demand for an extended applicability of this method is mounting. We lieve that now is the time to extend the frontiers of the microtremor sur method.

Prof. Hiroshi Okada
Dept of Earth and Planetary Scier
Hokkaido University, Japan

Acknowledgments

A part of this work was supported by the scientific Research Fund from the Ministry of Education of Japan.

On the subject presented in this textbook, the author had many valuable discussions with Dr. Y. Moriya, Dr. T. Sasatani of Hokkaido University, and Mr. O. Nakano of Dia Consultants. For their important contributions to parts of this textbook, the author has pleasure in acknowledging them.

The author is also deeply indebted to Dr. S. Ling for his great assistance in preparing this textbook.

Chapter 1

Introduction

Among geophysical methods, there are many techniques which use the "n ral field," "natural signal," or "natural phenomena." For example, they incl the gravity survey method, the magnetic survey method, the spontaneous tential (SP) measurement in electrical methods, the magnetotelluric met in the electromagnetic methods, and radiometric measurements (Dobrin Savit, 1988; SEGJ, 1989). These are known as "natural field methods." Tl survey methods have been initiated, researched, and developed as mean understanding geological structure by measurement of the respective phys property. They are presently used in their own right or to augment other vey methods, but typically they are utilized as a reconnaissance method p to committing to a detailed survey such as reflection or refraction seis surveys.

The ubiquitous, weak, low amplitude vibrations which may be recor on the surface of the Earth are commonly called microtremors. These f one category of the "natural signals" or "natural phenomena." Until recer there has not been an established method to positively harness this nat phenomenon for estimation of subsurface structure.

Several research projects during the mid-twentieth century documer the kinds of waves that constitute microtremors and the relationship betw microtremors and subsurface structure. Among them Aki (1957) and Tok (1964) suggested a potential application of microtremors to the estimatio subsurface structure.

Research progressed through the 1970s concentrating on the detectio earthquake waves in records contaminated by noise, such as microtrem and pulsation (e.g., Capon, 1969). The success of research was facilitated

the concurrent development of digital recording systems that enabled the recording of earthquake data by multiple array observation networks and the processing and analysing of such data. The results of this research were applied to the detection of traveling waves among other kinds of vibration. In fact, such techniques were used to estimate subsurface structure (e.g., Lacoss et al., 1969; Liaw and McEvilly, 1979; Asten and Henstridge, 1984; Horike, 1985; and Matsushima and Okada, 1990a).

The development of a new exploration method, designated the "microtremor survey method" (MSM) by Okada et al. (1990), for imaging subsurface structure, using natural microtremors has advanced over the last ten years. This survey method, if used effectively, can furnish a preliminary appraisal before a detailed survey for geological structure. Alternatively, this can be a means of extending scarce detailed data from "point data" to "profile data," or "profile data" to "plane data."

As the MSM utilizes the signal found in abundance anywhere on the surface of the Earth, the survey is simple and the operation does not require intensive environmental and safety precautions. In particular, there is no alternative to the microtremor method in areas where conventional seismic methods are difficult or impossible to implement, such as urban or environmentally sensitive areas.

At present, the method of delineating subsurface structure by studying microtremors is poised to progress from the research and development stage to commercial viability. The following chapters expand upon what property of microtremors can be used and how the method can be utilized for delineation of subsurface structure.

Chapter 2

Fundamental properties of microtremors

2.1 What are microtremors?

The surface of the Earth is always in motion at seismic frequencies, even v
out earthquakes. These constant vibrations of the Earth's surface are ca
microseisms or microtremors. The term *microtremor(s)* is more comm
used in the field of earthquake engineering.

The amplitude of these microtremors is, with some extreme excepti
generally very small. Displacements are in the order of 10^{-4} to 10^{-2} mm
below human sensing. Although they are very weak, they represent a sourc
noise to researchers of earthquake seismology; if amplifier gain is increase
record earthquake signals from a distant source, the amplitude of microtrer
proportionally increases, and the desired earthquake signal is buried in
"noise" of microtremors. Elimination of this background noise is technic
extremely difficult or impossible to achieve. Therefore earthquake researc
call microtremors "seismic noise" or, simply, "noise."

It was not until the late nineteenth century, that seismologists could
ploy seismometers to observe the movement of the Earth's surface. Since t
microtremors have been a focus of their strong interest, as is evidence
the large number of research papers published on the subject. Much of
research concerns the source of the vibration and variation of the chara
of the vibration depending on time and location. From this research, we
know that the microtremors are caused by daily human activities such as m
ment of machinery in factories, motor cars, and people walking; and nat

phenomena such as the flow of water in rivers, rain, wind, variation of atmospheric pressure, and ocean waves. Thus microtremors are not a natural phenomenon in *senso stricto*, as human activities constitute some of their sources. However, microtremors are now not regarded as nuisance noise, but rather a useful "signal." In this sense, they are sometimes referred to as "uncontrolled signal."

Both human activity and natural phenomena (such as climate and oceanic conditions) vary with time. Accordingly, microtremor activity varies over time. This variation is very complex and irregular, and not repeatable.

When microtremors are observed simultaneously at several spatially separated stations, it is noted that these tremors are not completely random and that some coherent waves are contained in the records. In other words, microtremors are an assemblage of waves traveling in various directions. In fact, Toksöz and Lacoss (1968) clearly demonstrated from the data of large-aperture seismic array (LASA) that microtremors are an assemblage of body waves and surface waves.

2.2 Power spectra of microtremors

The microtremors originating from human activities are dominated by the components with periods shorter than one second, or higher than 1 Hz in frequency (Kulhanek, 1990, for example), and have clear diurnal variation in both amplitude and period.

On the other hand, the microtremors due to natural phenomena, such as climatic and oceanic condition, have dominant periods greater than one second (frequency lower than 1 Hz), with associated amplitude and period variations corresponding to the vagaries of the respective natural phenomenon.

A detailed analysis reveals that microtremors vary depending upon location. The microtremor survey method has been devised to focus on *this* variation.

A power spectrum of a typical microtremor record observed at a site on the west coast of America is shown in Figure 2.1 (Haubrich, 1967). In the 1960s, it was believed that spectra of microtremors are largely similar worldwide. Figure 2.3 graphically demonstrates the similarity (Peterson, 1993).

In the 1960s, explanations of power spectra were proposed to the effect that the high-power level of the low-frequency components (below 1.0 Hz) and the two characteristic spectral peaks originated from the ocean, while the higher frequency components (above 1.0 Hz) were attributed to human activity

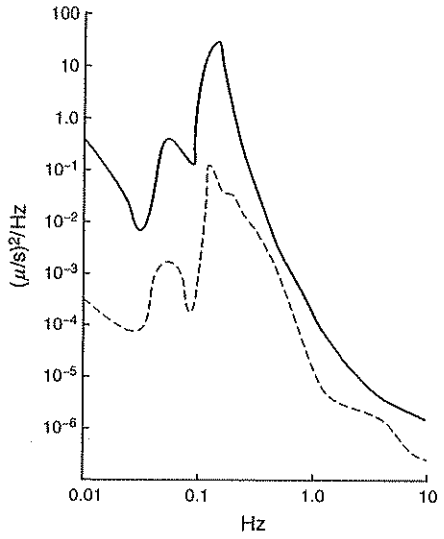

Figure 2.1. Power spectra of microtremors with the frequency between 0.01 and 1(observed on the West Coast of America. Two examples show times of high and power levels.

and climatic conditions. It was believed that the spectral characteristics sl significant variation both locally and temporally.

We have mentioned one of the origins of microtremors as being n ral phenomena such as climatic and marine conditions. Can microtremor observed in the middle of a continent? This is a natural question when considers the limits to application of the microtremor method.

The answer is given in Figure 2.3 (from Peterson, 1993). The dataset collected at 75 permanent seismic stations all over the world (see Figure 2.2 a time of no seismic event due to earthquake or nuclear explosion. These po spectra are calculated for the vertical component of background vibratio the earth including microtremors, wave motions, and even earth tides. T may contain power components whose source is not known to us, hence not investigated, perhaps including some originating in the interior of the Ea Regardless of their sources, these spectra show that the energy of the Ear background seismic vibration exists in abundance at all locations on the Ear surface, and that with an appropriate observation instrument one can rec the microtremor signals. This figure also shows that the microtremors h largely similar spectral structure, as noted in Figure 2.1.

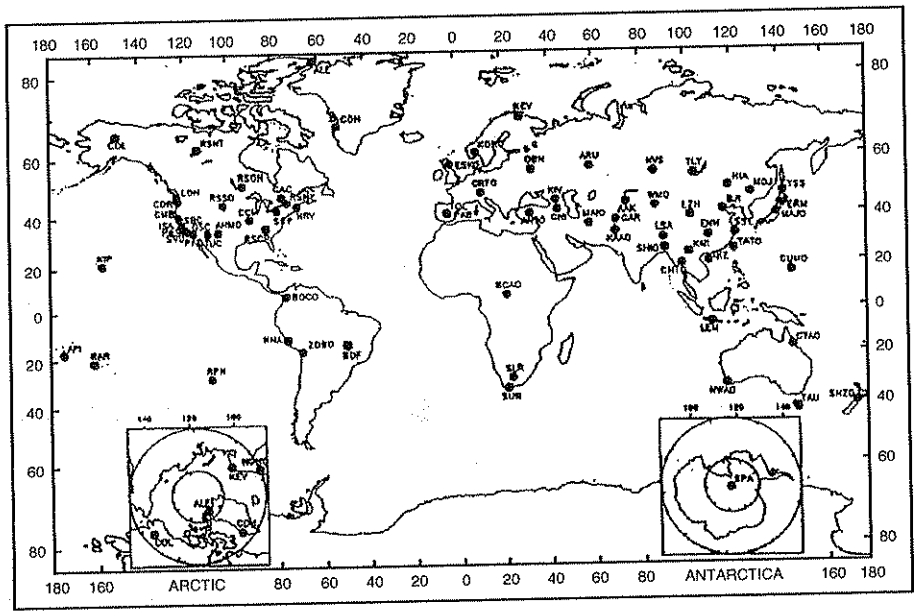

Figure 2.2. Seventy-five permanent seismic observatories in the world, which record common vibration of the earth including microtremors (Peterson, 1993).

The microtremor survey method utilizes signals with periods shorter than several seconds. As seen in Figure 2.3, the signal within this band always exists in seismic records, thereby demonstrating the ubiquitous applicability of the method.

2.3 Temporal and spatial variation of microtremors

Microtremors are a phenomenon that varies both spatially and temporally. As the microtremor survey method assumes both spatial and temporal stationarity of microtremors, it is necessary to investigate this characteristic. Let's look at actual records from observations in Sapporo, Japan.

The data shown in Sections 2.3.1 and 2.3.2 are collected at three stations around Sapporo, the capital city of Hokkaido, at different times:

1. Oyafuru Station (OYF), where thick Ishikari Basin sediments are dominant; during the twelve-day period of 7–19 August 1984 sampling was

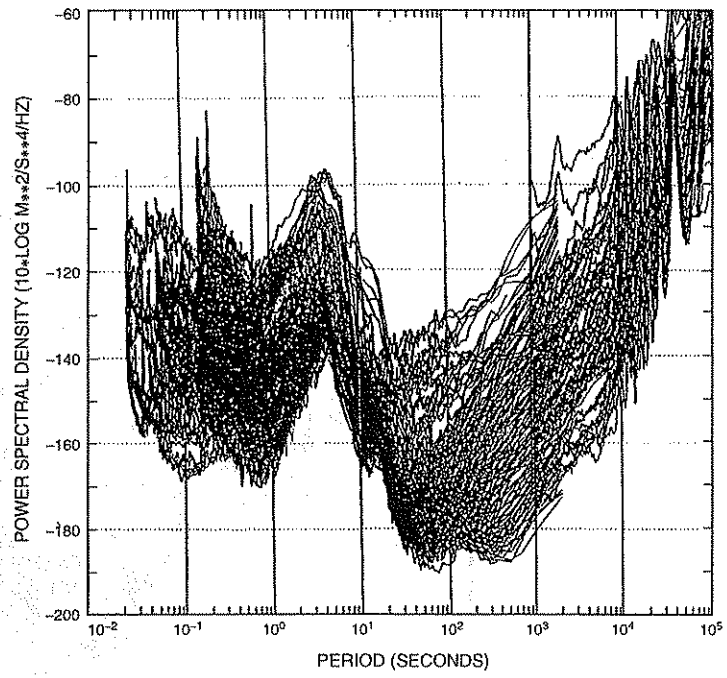

Figure 2.3. The acceleration power spectra of common vibration of the Earth inc ing microtremors recorded at the 75 permanent seismic observatories in the w (Peterson, 1993).

for ten minutes every three hours using a seismometer placed on concrete floor in a garage.

2. A station situated on the campus of Hokkaido University (HKD), am the metropolitan area of Sapporo, still on a sedimentary basin; collec during the one-month period from 4 November to 4 December 19 similarly sampled, the seismometer was set on a concrete block i prefabricated storage building.

3. A station set up in Toyama, nicknamed Misumai (MIS), in a sub of Sapporo during the same period as HKD, directly on the basem rock, similarly sampled, the seismometer placed on a concrete floor reinforced-concrete building.

The type of seismometer used was a compact, long-period, PELS Mode with a natural period of 8 s (Project Team for the Development of

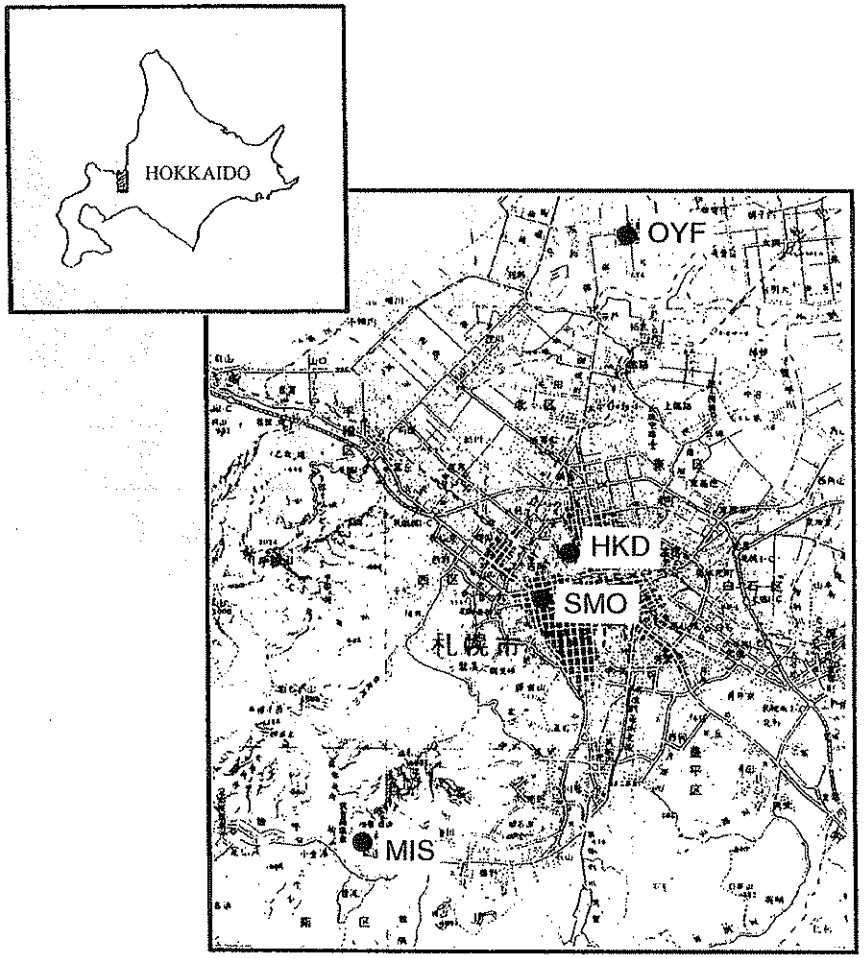

Figure 2.4. Location of Sapporo Meteorological Observatory (SMO) where reference weather data was recorded.

Small-Size Long-Period Seismometer, 1974; Matsumoto and Takahashi, 1977). The recorders used at HKD and MIS were of type Datamark LS-8000SH by Hakusan Industries, and one long-duration recorder designed by the research team of Hokkaido University.

Figure 2.4 shows the location of these three stations. The distance between HKD and MIS is about 14.8 km, and HKD to OYF is about 13.5 km.

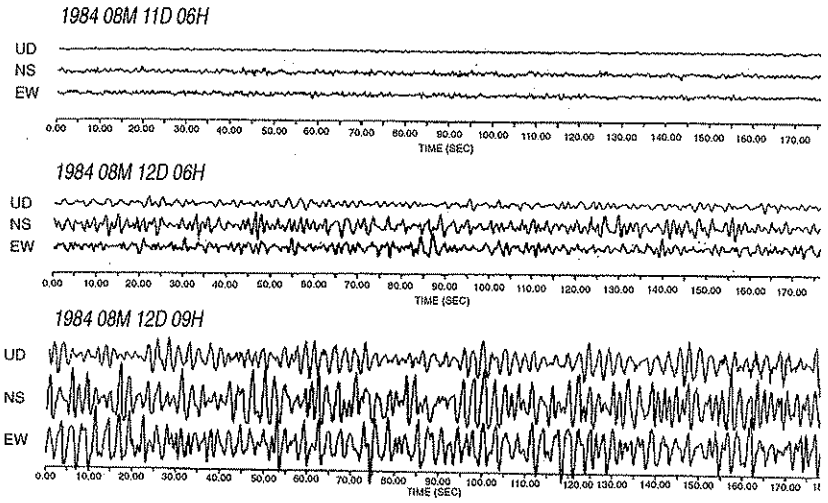

Figure 2.5. An example of three-component microtremor records from Oyafuru : tion (OYF) in suburban Sapporo. The complex waveform continues constantly three minutes, but the amplitude varies in time over three hours and over one day

SMO in Figure 2.4 indicates the location of the Sapporo Meteorological (servatory, where the weather data referred to were recorded.

During the period of observation, it was very quiet at OYF, with little traf At HKD, the level of vibration was considerable, and heavy construction r chines were in operation during weekdays. MIS is located in a naturally qu location. However, tunnel drilling was going on about 500 meters from station, and noise, perhaps due to the drilling, was sometimes observed on record.

For convenience of explanation, a record sample of ten minutes durat is called a "block" in the following sections.

2.3.1 Temporal variation of microtremors

The first example illustrates temporal variation of micrometers within a (Figure 2.5 demonstrates three-component microtremor records and compa microtremors at three different times over two consecutive days: 6 am 11 August, and at 6 am and 9 am on 12 August 1984. The recor

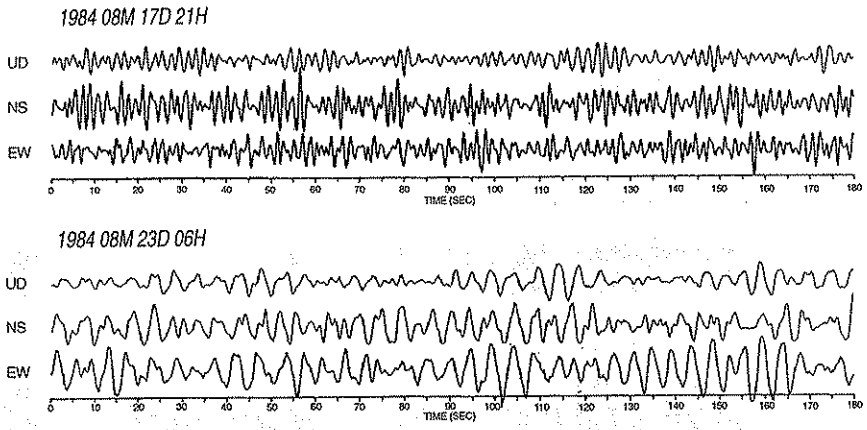

Figure 2.6. An example of a three-component microtremor record from the Oyafuru Station (OYF) at 21 hrs, 17 August 1984 (top) and 06 hrs, 23 August (bottom). Note that the periods are different while the amplitudes are similar over the interval of one week.

microtremors show complex variations, but the degree of complexity does not vary during the recording period of three minutes. However, the amplitude envelope varies vastly between the microtremors recorded one day, or even as little as three hours, apart.

Figure 2.6 shows microtremors recorded at the same location (OYF) about one week apart. They do not differ in amplitude, but their dominant periods (or frequencies) are different.

This variation is integral to the MSM, since the spectrum of the signal determines the lower limit of the depth that can be explored by MSM. When information on deeper structure is desired, data should be acquired at a time when the lower frequency component is dominant.

A sample of 120 blocks (20 hours) of vertical and east-west components of microtremor data were taken from the record collected at HKD and MIS in the fifteen-day period from 19 November to 3 December 1997. Power spectra were calculated for each ten-minute block. Figure 2.7 shows the power spectra of the microtremor records for each time block over-plotted on one axis (Sakaji, 1998). In this explanation, "daytime" refers to 9, 12, 15, and 18 hrs, while "night" refers to 21, 0, 3, and 6 hrs. Figure 2.8 compares the average spectra of day and night. (In both Figures 2.7 and 2.8, the real spectra are not recorded below 0.1 Hz due to the properties of the seismometer.)

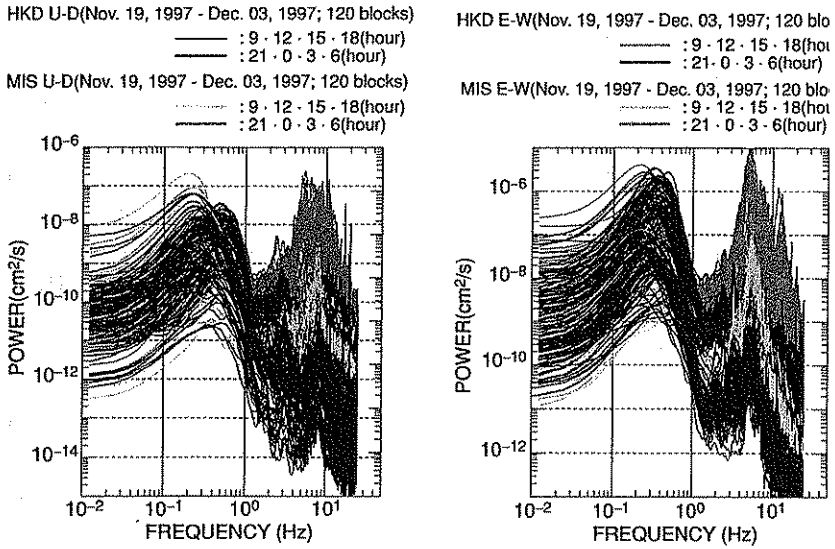

Figure 2.7. Power spectra of the vertical (U-D) and east-west (E-W) components microtremors at HKD and MIS observed in the 15-day period between 19 Novem and 3 December, 1997. The spectra are calculated and overplotted for 120 10-n blocks.

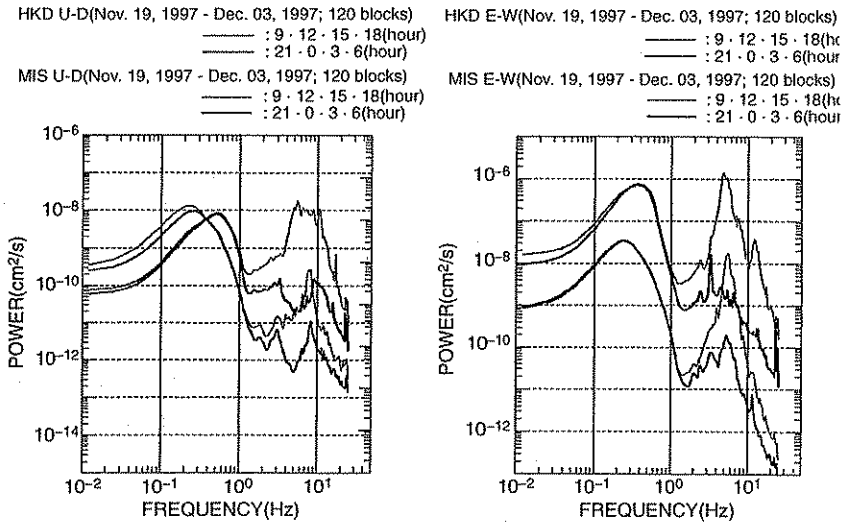

Figure 2.8. Daytime and nighttime averages of power spectra of the vertical (U-I and east-west (E-W) components of microtremors at HKD and MIS, observed in t 15-day period between 19 November and 03 December, 1997.

From Figures 2.7 and 2.8, it is clear that the overall shape of the spectra does not vary in the fifteen-day period, although the power level of the record at the urban HKD station is generally higher than that of suburban MIS. Closer observation reveals temporal variation differences of the power spectra, between these frequencies lower than 1 Hz and those frequencies higher than 1 Hz. For the frequencies under 1 Hz (or periods longer than 1 s), the difference in power between daytime and night is minimal. On the other hand, that difference is significant above 1 Hz (period shorter than 1 s) by one to three orders of magnitude. It is more apparent in the urban HKD station. The conclusion is that the frequency components under 1 Hz are little affected by human activities, while frequency components over 1 Hz are significantly affected. This phenomenon is shown even more clearly in Figure 2.9.

Figure 2.9 is the running power spectra of the east-west component of microtremors obtained from the observations at HKD and MIS. These data were simultaneously sampled for 10 minutes, every three hours beginning at midnight. The data at HKD are from the 29-day period between 5 November and 3 December 1997, and those of MIS are from the 15-day period from 19 November to 3 December 1997. The curve at the top of Figure 2.9 is the atmospheric pressure data at SMO for the corresponding period. It shows a variation from 980 to 1040 hPa. As seen in the graph, the character of spectra of microtremors differs between the ranges higher and lower than 1 Hz.

2.3.1.1 Band under 1 Hz (period longer than 1 s)

The temporal variation of microtremors has a good inverse relationship with the variation of atmospheric pressure: The power of microtremors increases with lower atmospheric pressure, reaching a maximum soon after the minimum in atmospheric pressure. On the other hand, the power decreases when atmospheric pressure increases. This correlation was observed, almost without exception, for the two stations 14.8 km apart for the duration of the recordings. In quantitative comparison of the three-component data of HKD and MIS with atmospheric pressure, Sakaji (1998) calculated cross-correlation coefficients, and found the power maxima of the low-frequency (long period) component of microtremors to lag the minima of atmospheric pressure by from 3 to 15 hours.

Phenomena such as the strong correlation between microtremors and atmospheric pressure, and its lag of 3 to 15 hours, present an interesting area for research. Santo (1960, 1963) may be referred to for additional information;

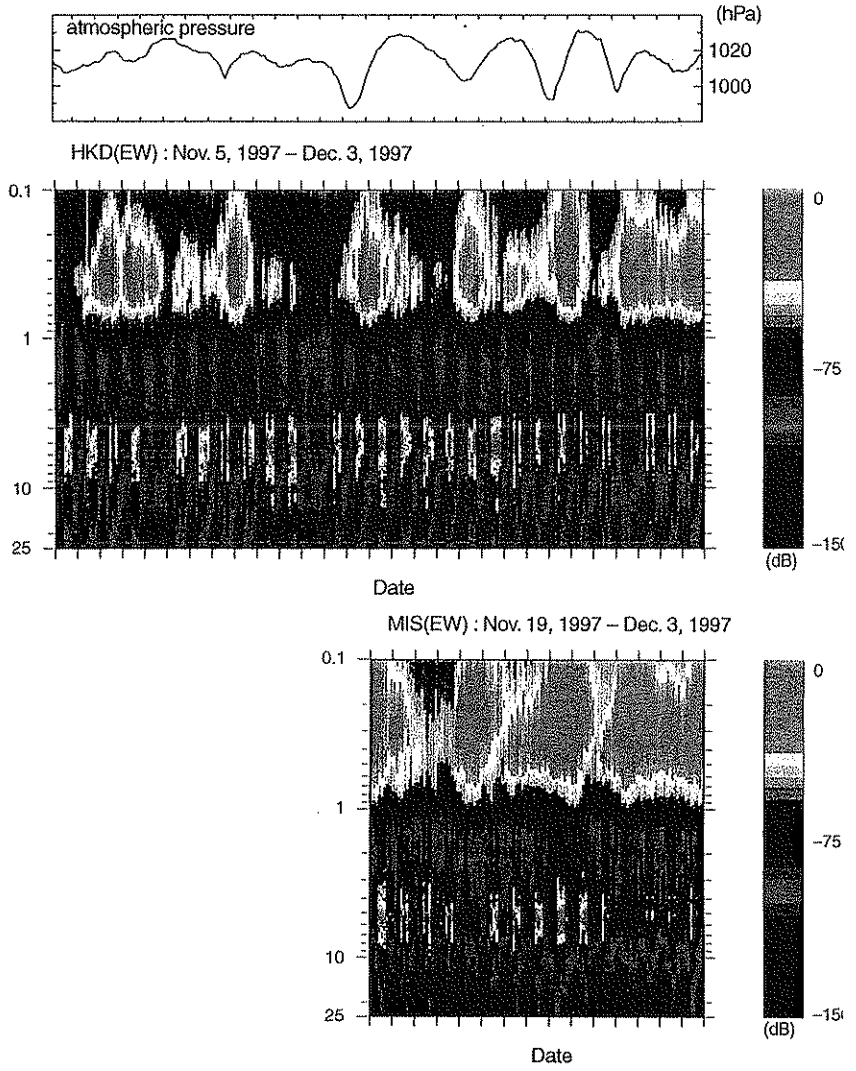

Figure 2.9. Running power spectra of the east-west component of microtremors ol served over the 29-day period between 5 November and 3 December (HKD) an the 15-day period between 19 November and 3 December (MIS) 1997. Atmospher pressure at SMO for this period is shown on the top.

however, these subjects seem to have little to do with the microtremor survey method, and will not be pursued further in this book.

2.3.1.2 Band over 1 Hz (period shorter than 1 s)

As mentioned, the power spectra of higher-frequency microtremors are affected by human activity. This is clear in Figure 2.9. The power spectra of the frequencies between 4 and 7 Hz clearly exhibit diurnal variation. More precise observation may reveal that the relative power of microtremors diminishes relatively around lunchtime and also on Sundays and public holidays. (November 23rd was a public holiday.)

2.3.2 Spatial variation of microtremors

2.3.2.1 Band under 1 Hz (period longer than 1 s)

By examining the power spectra in Figure 2.7, one can observe that the power spectra of both HKD and MIS are affected by atmospheric pressure. However the peak level and its frequency differs between the stations. It varies by time, and the pattern is not consistent. This is seen in the average of the daytime and nighttime power spectra of the shown in Figure 2.8.

The peak frequencies of HKD are about 0.5 Hz for the vertical component and 0.35 Hz for east-west component, while MIS has a peak at approximately the same frequency of 0.25 Hz for both the vertical and east-west components. The peak level of the vertical component is similar between stations, but the peak level of the east-west component at HKD is about 30 times higher than at MIS. In other words, the low-frequency (long-period) east-west component was more easily induced at HKD than MIS.

This demonstrates that, while the variation of atmospheric pressure is considered to be a common phenomenon over a large area, including HKD and MIS and over a relatively long time, it causes different microtremor spectrum structures at different places; that is, output responses to the same input differ with location.

2.3.2.2 Band over 1 Hz (period shorter than 1 s)

The diurnal variation in the peak frequency of the spectrum both at HKD and MIS is large, reflecting the spectral characteristics of the source of the vibration near the stations. While there are differences both in input and output due to amplification characteristics at the site, the diurnal differences in the records are considered to be due mainly to the input.

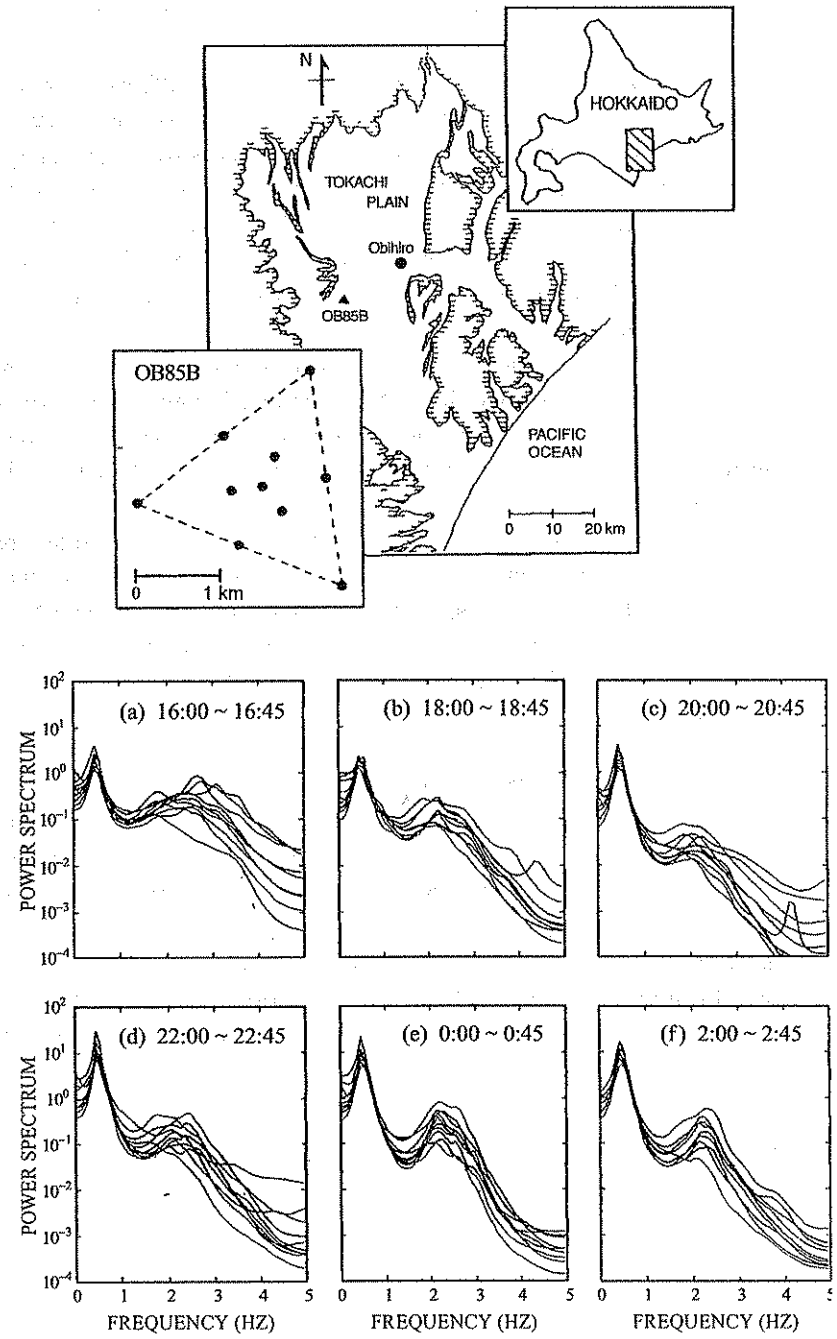

Figure 2.10. Power spectra of ten stations within close proximity for 45-min recor at six different times. The inset OB85B shows the geometry of the 10-station arr used.

The variation of atmospheric pressure is known to affect the low-frequency (long period) component of microtremors over a relatively large area and long time. However, for these high-frequency (short period) components, it is not clear in the power spectra of Figure 2.7 whether the same input causes a different response depending on the location. The extent of "spatial stationarity," which is important for the microtremor survey method, is not obvious. Let us focus our attention on this point and discuss the manner of variation in microtremors in a finer time span.

The spectra in Figure 2.10 are of microtremors simultaneously recorded at ten stations scattered within a 1.5 km radius of suburban Obihiro (see map in Figure 2.10). At each station, six discrete forty-five minute recordings were made, two hours apart, from 16 00 hr on 21 July 1985 to 02 00 hr on the following day.

The overall shape of the spectral structure for the recordings resemble each other, but differences in the frequency component higher than 1.5 Hz for different times and places are noted. The temporal variation in the records is considered to be influenced by the temporal variation of the source of microtremors. On the other hand, the cause of the characteristic spatial differences observed between the numerous locations is attributed to the fact that the microtremors are not satisfying spatial stationarity at these points. However, very little difference is observed in the longer-period spectral components (under 1 Hz) at all of the locations. This leads to the belief that spatial stationarity of the microtremor energy is satisfied within this frequency band.

This example shows that the spectral structure of microtremors with periods less than 1 s is largely stationary over the spatial extent of 1.5 km and a temporal extent of 45 minutes. To discuss the extent of "spatial stationarity" for frequencies greater than 1 Hz (or period shorter than 1 second), it is necessary to analyze the data with an array smaller than one used here.

Chapter 3

Principle of the microtremor survey method

3.1 The microtremor survey method (MSM)

3.1.1 Wave type used in microtremor surveys

Records of microtremors clearly show that microtremors are highly variabl irregular, vibratory phenomena, both temporally and spatially. However, i elasticity theory, microtremors are assemblages of body waves and surfac waves (Toksöz and Lacoss, 1968). As seen before, this vibratory phenomeno comprises a set of stationary and stable spectra with very little variation, withi the temporal and spatial extent of one hour and 1-2 km radius, respectively.

With appropriate instruments, microtremors are observed to be ubiquitou The observed vibrations, in the form of a combination of body and surfac waves, contain, in general,

1) information on complex sources,

2) information on the transmission path, and

3) information on the subsurface structure at the observation station.

MSM is concerned with such elastic waves contained in microtremor Therefore MSM is a kind of elastic-wave survey method in a broad sense, i.e MSM is a seismic survey method.

However, unlike conventional reflection and refraction seismic method which use artificial sources and treat waves as controlled in the phase domai

MSM utilizes uncontrolled natural phenomenon as the source, and treats the various aspects of microtremor spectra (temporal and spatial properties) according to the theory of a stochastic process.

Many of the sources of microtremors can be identified as acting on the Earth's surface or the sea floor. Therefore surface waves are naturally considered to be the dominant component of the microtremors, over body waves. MSM utilizes this dominant surface-wave mode of propagation.

3.1.2 From dispersion of surface waves to subsurface structure

As is well known with dispersion, the velocity of surface waves varies depending on the frequency (or period). Since dispersion is a function of subsurface structure, subsurface structure can, in theory, be estimated from the dispersion. MSM is basically a method to estimate this dispersion of surface waves contained within microtremors.

At present, our level of theoretical knowledge can only solve the characteristics of dispersion of surface waves for parallel, isotropic, and homogeneous layers. Therefore the subsurface structures estimated by MSM are approximated by parallel, isotropic, and homogeneous layers. Consequently, precision of the estimated structure obtained from MSM is lower than that from conventional seismic methods. This is the reason MSM is regarded as a reconnaissance method. However, MSM yields the physical properties of the subsurface structure by exploiting S-wave velocity, which is difficult to measure with conventional engineering-scale seismic surveys. Analysis of the response to earthquake movements identifies S-wave velocity as more important than P-wave velocity in determining subsurface structure. In this regard, the MSM is suitable for the estimation of subsurface structure, such as required by the field of earthquake engineering.

MSM deals with surface waves and it applies surface-wave theory, to be described in the following sections, to detect usable signals.

There are some problems remaining to be solved in MSM, for example:

1) Standardizing the observation system including field procedure and instrumentation

2) The inversion problem; from phase velocity dispersion curves, to velocity structure

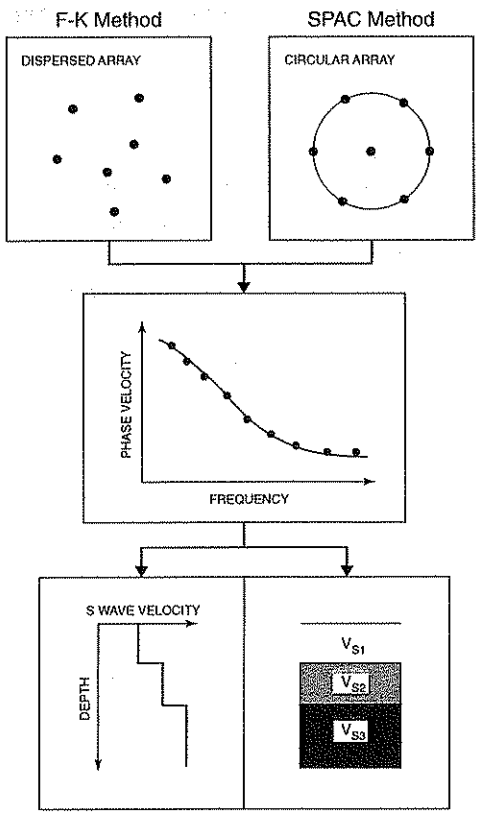

Figure 3.1. Basic procedure of the microtremor survey method.

However the basic scheme of MSM for estimating subsurface structure has been more or less completed. This basic scheme and its procedure are shown in Figure 3.1. It consists of three steps:

1) Observation by the seismometer network (array) arranged on the ground surface

2) Estimation of the dispersion of the surface wave as a response to the subsurface structure directly below the array

3) Estimation of the subsurface structure causing the dispersion by means of inversion

3.2 Spectral representation of microtremors

The body and surface waves contained in the microtremors originate in both temporally and spatially random sources by a range of mechanisms, and travel through a variety of geological conditions. Consequently, records of microtremors have a very complex waveform, and no simple mathematical equation describes it. Therefore, the amplitude of microtremors at a particular time and location cannot be predicted. It is, indeed, a stochastic phenomenon. In other words, the amplitude of microtremors is indeterminate and unrepeatable.

By regarding the amplitude of microtremors as a stochastic variable, a probability can be defined. By this probability, the probability distribution or probability density function of the amplitude of microtremors can also be defined.

Nogoshi and Igarashi (1970) stated that the frequency distribution of the amplitude of microtremors approaches a normal distribution as the number of samples increases. Using the large amount of data collected at HKD and MIS as mentioned before, Sakaji (1998) re-examined this under various conditions. The following examples are from his contribution to examining the temporal stability of microtremors by estimating frequency distribution of microtremors as a stochastic variable and its autocorrelation function.

Figure 3.2 shows estimates of frequency distribution (i.e., probability density function) from the vertical component of microtremors, estimated by progressively widening the sampling windows from two minutes to ten minutes. The data are taken from one 10-min block from 29 November 1997 at MIS and HKD.

The amplitude is normalized by the maxima within the sampling interval to facilitate visual comparison. The numbers in the upper right corner of each histogram are the average a and the standard deviation s of amplitude. The average a is expressed by the deviation from the average of amplitude in the whole 10-min interval. The values of a and s show very little variation. The curves superimposed in the histograms represent the probability density function of the normal distribution with the average and standard deviation posted in each column. Although some disturbance is observed in the data of the first 2 min at MIS, both MIS and HKD records show that the distribution becomes smooth as the sampling interval is increased; and that the distribution is well approximated by the normal distribution when data length exceeds 4 min.

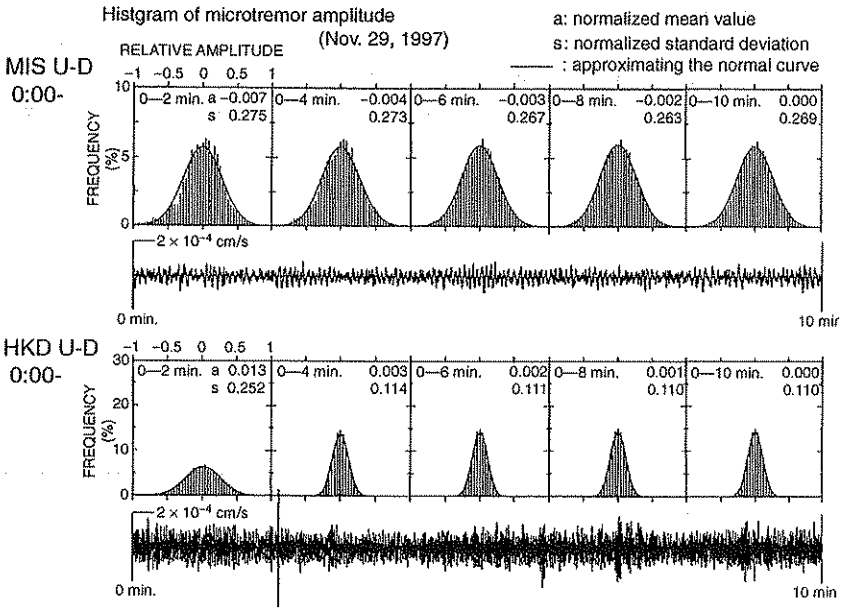

Figure 3.2. A record of microtremors for 10 min and the histogram of its amplitude The curve is the probability density function determined by assuming the histogram follows normal distribution.

Figure 3.3 shows the first 10 s of the autocorrelation function of the five 2-min segments of the 10-min data at HKD used in Figure 3.2. The average a and variance s^2 of the amplitude are posted in each figure, in which the average is expressed as a deviation from the average of the entire 10-min data set. The variation of both average and variance do not vary widely; they are almost constant.

For the data length of 10 min studied, Figures 3.2 and 3.3 demonstrate that the average, variance, and autocorrelation function of amplitude of microtremors are constant regardless of the time of sampling, and, therefore microtremors satisfy the properties of a stationary stochastic process.

Such a stochastic nature of microtremors is repeatable for data at different times. However, this is not always true with data samples that are more than 3 hr apart. This suggests that the stationarity of microtremors does not last more than 3 hr.

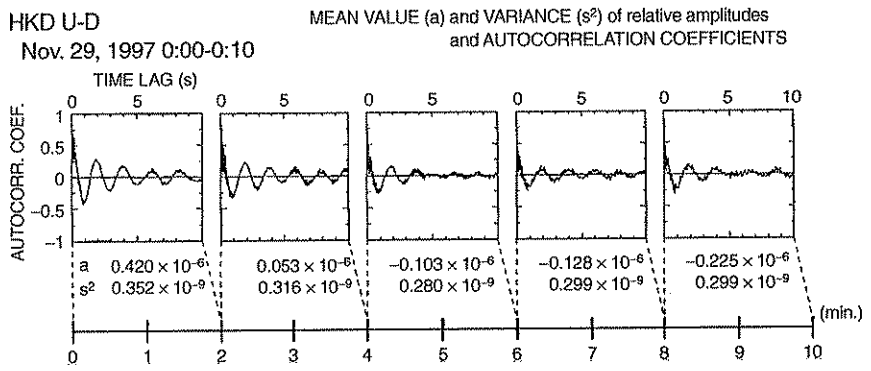

Figure 3.3. Autocorrelation coefficient of the microtremor records for the first 10 s of log: A 10-min record was blocked into five 2-min segments and the autocorrelation was calculated for each of the segments.

The frequency distribution of the amplitude of microtremors may deviate considerably from the normal distribution, when a transient impulse noise such as footsteps and a passing car interferes with the data during acquisition. Even in the absence of such extreme cases, the observed frequency distribution of amplitude may at times deviate from a normal distribution. The data from urban station HKD contain such periods. MSM uses a method of analysis based on the normal process, i.e., the *f-k* method (refer to Figure 3.1). It is not appropriate to apply this method to data sets whose amplitudes deviate from a normal distribution.

Now, we consider microtremors in terms of the theory of a stochastic process[1]. This foundation will assist in understanding the subsequent discussion. Two assumptions are made here regarding microtremors whose amplitude is indeterminate:

1) Within a certain extent of space, microtremors are a stochastic process both temporally and spatially[2];

2) A microtremor record at a certain point over a limited period of time within the same domain can be regarded as a sample record (or sample function) of the stochastic process[3].

[1]For fundamental issues of the theory of stochastic process, the author referred to Yaglom (1962), Priestley (1981), and Sunahara (1981).

[2]More strictly, stationary ergodic process.

[3]Sometimes referred to as "sample process."

The first assumption means that the probability density function (or probability distribution) is not dependent on either space or time. In other words if a probability density function of amplitude of microtremor is determined once for a point of time, then the form of the function does not vary over much larger periods of time.

3.2.1 Spectral representation of a stochastic process

This section explains, in general terms, the spectral description of a stochastic process. This is to provide a foundation before considering the application to microtremors.

Let $\{X(t): -\infty < t < \infty\}$ be a zero-mean stochastically continuous stationary process. Then there exists an orthogonal stochastic process $\{Z(\omega)\}$ such that for all t, $X(t)$ may be expressed as:

$$X(t) = \int_{-\infty}^{\infty} \exp(i\omega t) dZ(\omega), \tag{3.1}$$

where ω is angular frequency[4] (Yaglom, 1962; Priestly, 1981). This integral is defined in the "mean square sense."[5] The $\{Z(\omega)\}$ in equation (3.1) is a complex-valued stochastic process satisfying the following conditions on its expectation values:

i) $\mathrm{E}[dZ(\omega)] = 0$ (for all ω); (3.2)

ii) $\mathrm{E}\left[|dZ(\omega)|^2\right] = dH(\omega)$ (for all ω), (3.3)

where $H(\omega)$ is the integrated spectrum of $X(t)$;

iii) for different ω and ω' ($\omega \neq \omega'$);

$$\mathrm{E}[dZ^*(\omega) \cdot dZ(\omega')] = 0, \tag{3.4}$$

where $dZ(\omega) = \{Z(\omega + d\omega) - Z(\omega)\}$ and

$dZ(\omega') = \{Z(\omega' + d\omega') - Z(\omega')\}$;

[4]The stochastic process $\{X(t)\}$ cannot be expressed by a Fourier series or Fourier integral. Therefore, the total energy or total power cannot be considered by separating into its frequency components. This spectral representation resembles, in form, the Fourier-Stieltjes integral, but the $Z(\omega)$ here can contain undifferentiable functions. If $Z(\omega)$ is differentiable, the equation (3.1) is identical to the common Fourier integral.

[5]$X(t)$ does not have a practical sense unless one considers a quantity of the order of $X^2(t)$ such as variance and covariance.

and condition (iii) means that $dZ(\omega)$ and $dZ(\omega')$ are independent of each other. Such a stochastic process is called an orthogonal process. Here * denotes the complex conjugate.

The above property of the stationary stochastic process $\{X(t)\}$ and its spectral representation are assumed to be a fundamental nature of microtremors. These properties play the most important role in the subsequent data analysis of microtremors.

3.2.2 Spectral representation of microtremors

Microtremors as a stationary stochastic process are a phenomenon which is a function of time, t, and position vector $\xi(x, y)$. A record of microtremors over a certain finite time span can be regarded as a sample function of a stationary stochastic process. It can also be described as a spectral representation such as equation (3.1), except that this requires three parameters for X.

Suppose a recorded sample function of microtremors

$$X(x, \xi)(-\infty < t < \infty, -\infty < x < \infty, -\infty < y < \infty)$$

is a stationary stochastic process with average 0 and is continuous with respect to t and ξ. A doubly orthogonal process $Z'(\omega, \mathbf{k})$ exists and $X(t, \xi)$ is expressed in a spectral representation as

$$X(t, \xi) = \iiint_{-\infty}^{\infty} \exp(i\omega t + i\mathbf{k}\xi) dZ'(\omega, \mathbf{k}), \tag{3.5}$$

where $\omega = 2\pi f$ and $\mathbf{k} = (k_x, k_y)$. In these expressions, ω is the angular frequency, $\mathbf{k}$ is the wavenumber vector, and k_x and k_y are its x and y components, respectively. Then $Z'(\omega, \mathbf{k})$ satisfies the following relationships:

i) $\mathrm{E}[|dZ'(\omega, \mathbf{k})|] = 0$ (for all ω and $\mathbf{k}$); (3.6)

ii) $\mathrm{E}\left[|dZ'(\omega, \mathbf{k})|^2\right] = dH'(\omega, \mathbf{k})$ (for all ω and $\mathbf{k}$); (3.7)

iii) for any two distinct angular frequencies ω and $\omega'(\omega \neq \omega')$ and two distinct wavenumber vectors $\mathbf{k}$ and $\mathbf{k}'$ $(\mathbf{k} \neq \mathbf{k}')$,

$$\mathrm{E}[dZ'^{*}(\omega, \mathbf{k}) dZ'(\omega', \mathbf{k}')] = 0, \tag{3.8}$$

where * denotes the complex conjugate.

The relationship (iii) above means that the stochastic process $Z'(\omega, \mathbf{k}$ has a special property that its increments at different values of ω and $\mathbf{k}$ ar uncorrelated, i.e.,

$$dZ'(\omega, \mathbf{k}) = \{Z'(\omega + d\omega, \mathbf{k} + d\mathbf{k}) - Z'(\omega, \mathbf{k})\} \text{ and}$$
$$dZ'(\omega', \mathbf{k}) = \{Z'(\omega' + d\omega', \mathbf{k}' + d\mathbf{k}') - Z'(\omega', \mathbf{k}')\}$$

are uncorrelated for two distinct angular frequencies and two distinct wav number vectors.

If the spectrum of microtremors $X(t, \xi)$ is continuous and differentiab with respect to frequency and wavenumber, the right-hand side of equ tion (3.7) becomes $dH'(\omega, \mathbf{k}) = h'(\omega, \mathbf{k})\, d\omega\, d\mathbf{k}$, where $h'(\omega, \mathbf{k})$ is the spectr density function of $X(t, \xi)$. Then equation (3.7) can be rewritten as:

$$E\left[|dZ'(\omega, \mathbf{k})|^2\right] = h'(\omega, \mathbf{k}) d\omega\, d\mathbf{k}. \tag{3.}$$

3.3 Detection of surface waves

Microtremors contain surface waves in abundance. As stated, these surfac waves are generated randomly, both in a temporal and spatial sense, by a variet of mechanisms, and travel through a wide range of geological condition Naturally, microtremors become a very complex assemblage of elastic wav containing not only body waves and surface waves, but also scattered an diffracted waves. To separate surface waves from this assemblage, researche have tried various methods. For example, when microtremors were recorde by analog instruments, here is the procedure used:

- Microtremors were recorded at three points forming a tripartite array, an wavelets resembling each other were identified. By reading the wavelet it was possible to derive apparent periods and velocities (Ikegami, 1964
- More quantitatively, a band-pass filter was applied to microtremo recorded by a tripartite array, to derive the phase velocity versus fr quency (Kudo et al., 1976);
- By digital processing, the autocorrelation of similar wavelets in tripartit array records were used to derive periods and phase velocities quantita tively.

Since the development of digital recording of microtremors, the analysis method has advanced to understanding microtremors as a type of stochastic process. At present, the methods used to detect surface waves are known as (Okada et al., 1990)

- Frequency-wavenumber spectral method (*f-k* method) and
- Spatial autocorrelation method (SPAC method).

The *f-k* method is an application of the technique developed in the United States in the late 1960s to detect nuclear explosions using a seismic network with a diameter as large as 200 km. The statistical parameter, called the *f-k* spectrum, played a central role in the detection of nuclear explosions (Capon, 1969; Capon et al., 1967; Lacoss et al., 1969). The *f-k* method uses this *f-k* spectrum. Its principle is "to detect a relatively strong wave from within the complex assemblage of microtremors."

This method does not question the nature of the wave, i.e., whether it is dispersive or not. If a higher-mode surface wave is dominant, such a higher-mode wave is detected, and if a body wave is dominant, the body wave is detected. Also, there is no logic in the fundamental theory of *f-k* spectral analysis to identify surface waves or to judge the dispersion of the surface waves. In this sense, the *f-k* method is not a way to detect surface waves alone. Yet, if the *f-k* method is used in analysis for the microtremor survey method, it is assumed that surface waves are relatively dominant over other kinds of waves mixed into the microtremor assemblage.

The SPAC method is an application of observation with a circular array combined with a data analysis method used for understanding the transmission properties of a variety of waves generated by earthquake movement. It is based on the (then) newly developed the theory of a stochastic process by Aki (1957) who attempted to estimate the subsurface structure from microtremor records by assuming the microtremors are isotropic waves coming from all directions.

The basic principles of the SPAC method are

1) Assume the complex wave motion of microtremors to be a stochastic process in time and space;
2) A spatial autocorrelation coefficient for microtremor data, as observed with a circular array, can be defined when the waves composing the microtremors are dispersive like surface waves; and, hence,

3) The spatial autocorrelation coefficient is a function of phase velo and frequency.

This method clearly states its basic theory, and it is regarded as an excel method to separate surface waves from microtremors. This research, at time of its presentaion, was to suggest a new frontier of geophysical sur methods. However, its actual application had to wait for more than twe years. Some of its few applications include Okada and Sakajiri (1983), Hid (1985), and Matsuoka et al. (1996).

In a simple expression, these two methods are based on theories to de signals from noise. The detection theories owe their foundation to the the of a stochastic process for complexly varying phenomenon. In this sense, estimation of subsurface structure by microtremors is also an applicatio the theory of the stochastic process.

The next section deals with the detection of surface waves by these methods.

3.4 Detection of Rayleigh waves from the vertical component of microtremors (frequency-wavenumber method)

As stated previously, the method of detection of surface waves is criti to the microtremor survey method. To date, two methods have been veloped: the frequency-wavenumber method and the spatial autocorrelat method. The properties common to both methods are, the microtremors regarded as a stochastic process, and their spectra form the basis of analy Both methods observe the vertical component of microtremors in orde extract the Rayleigh wave, a type of surface wave.

Of the methods fundamentally based on these common grounds, th seem to be more case histories reported using the frequency-wavenum method, including Asten and Henstridge (1984), Horike (1985), Matsushi and Ohshima (1989), Matsushima and Okada (1990a), Tokimatsu et al. (19 etc. The frequency-wavenumber method will be explained in this section.

The frequency-wavenumber method acquires microtremor data us an array whose size is appropriate to the target depth, then calculates frequency-wavenumber power spectral density function (*f-k* spectra). T

surface wave contained in the microtremors is detected as a function of phase velocity and frequency (or period). The method of detecting surface waves by the parameter of the *f-k* spectra is, hereafter, simply called the *f-k* method. The *f-k* method owes its origin to the research for LASA by Lacoss et al. (1969) and Capon (1969). The method was comprehensively described in the textbook by Aki and Richards (1980), and some appropriate parts of that textbook are quoted in the following sections[6].

3.4.1 Frequency-wavenumber power spectral density function

In general, a phenomenon which can be regarded as a temporally stochastic process can be characterized by its power spectral density function (or simply power spectra). This function defines the frequency composition of the power of the phenomenon. Similarly, a phenomenon which can be regarded as a stochastic process, both temporally and spatially, can be characterized by a frequency-wavenumber power spectral density function. With this function, the frequency composition and the propagation velocity vector of phenomena can be described.

Microtremors can be considered as a stochastic process, both temporally and spatially, that contains propagating waves. The *f-k* spectra of microtremors can be estimated from either of the following two methods:

1) Estimate the autocorrelation function of the microtremors and perform a Fourier transform on it
2) Perform the Fourier transform directly on the microtremor record and average the square of its absolute values

The first method is the very definition of a power spectrum density function. It corresponds to the well-known "Wiener-Khinchine theorem" for the single variable case. Expressed mathematically, let $R(\xi, \eta, \tau)$ be the autocorrelation function[7] of microtremors $X(x, y, t)$:

$$R(\xi, \eta, \tau) = \mathrm{E}[X(x, y, t) \cdot X(x + \xi, y + \eta, t + \tau)]; \qquad (3.10)$$

[6]This textbook is not suitable for practical data processing nor a guide to programming such software. For practical application, see Capon (1969).

[7]It may be more correct to call this the "time-space autocorrelation function," as opposed to the one-dimensional case.

then estimating its *f-k* power spectral density function $P(k_x, k_y, \omega)$:

$$P(k_x, k_y, \omega) = \iiint_{-\infty}^{\infty} R(\xi, \eta, \tau) \exp\{i(\omega\tau - k_x\xi - k_y\eta)\} d\tau d\xi d\eta. \qquad (3$$

The second method is an estimation of the power spectral density func by the finite Fourier transform. The more practical method uses the FFT. following explanation involves use of the discrete power spectrum. A p of equality of the two methods is beyond the scope of this textbook, interested readers are referred to Bendat and Piersol (1986) for a proof in single variable case. Their proof implicitly suggests the validity of the pract method frequently used in the Microtremor Survey Method, i.e., estima the power spectrum density function of a set of observation data over a fi time by subdividing the data into several temporal blocks.

Suppose P_{lmk} is a power spectral density function:

$$P_{lmk} = \lim_{L,M,K\to\infty} \frac{\mathrm{E}\left[|F_{lmk}|^2\right]}{L\Delta x \cdot M\Delta y \cdot K\Delta t}, \qquad (3$$

where F_{lmk} is the finite Fourier transform of microtremor record $X(l\Delta x, m$ $k\Delta t)$, which is digitized in the three-dimensional space of distances Δx Δy and time Δt:

$$F_{lmk} = \sum_{l'=0}^{L-1} \sum_{m'=0}^{M-1} \sum_{k'=0}^{K-1} X(l'\Delta x, m'\Delta y, k'\Delta t) \times \exp\{-2\pi i(ll'/L + mm'/M - kk'/K)\}\Delta x\Delta y\Delta t. \qquad (3.$$

Strictly speaking, microtremors are not always a perfectly stationary p cess in the time-space domain. They depend on atmospheric pressure ocean wave motion, which are subject to transitional variation, and in sp the subsurface structure is inhomogeneous. Therefore the above principle c not be applied universally to actual data. However, the microtremor data estimation of geological structure are collected over a finite extent of time space, and the data are required to be "stationary"[8] within that extent. S eral *f-k* spectrum methods have been developed for the above principle: "beam-forming method" and the "maximum likelihood method" for exam

[8]To examine whether it is stationary or not, one can compare power spectra at stations.

3.4.2 Beam-forming method

The beam-forming method (BFM) is the simplest of the methods for estimating the f-k spectrum. This is also called the conventional method. This method treats the microtremor data collected with an array of multiple observation stations as a record from a single seismograph. It assembles the data and estimates the velocity and direction of the wave with the highest power.

For the purpose of beam-forming, consider the time shift of the wave with wavenumber k_x and k_y and frequency ω observed at a station (x_i, y_i) by t with respect of the base station (x_0, y_0):

$$t = t_0 + k_x(x_i - x_0)/\omega + k_y(y_i - y_0)/\omega + \tau_i, \tag{3.14}$$

where t_0 is the arrival time of the wave at the base station (x_0, y_0) and τ_i designates the characteristic delay at the observation station (x_i, y_i), sometimes called the "station residual."

If the microtremor record at the station i is $X_i(t)$, the output of the beam is written as

$$b(k_x/\omega, k_y/\omega, t) = \frac{1}{N}\sum_{i=1}^{N} X_i(t + t_i). \tag{3.15}$$

The estimated value of the power spectrum of the time series $b(k_x/\omega, k_y/\omega, t)$ can be obtained as

$$\hat{P}(k_x, k_y, \omega) = \int \exp(i\omega\tau)d\tau \cdot \frac{1}{N^2} E\left[\sum_{i=1}^{N} X_i(t + t_i)\sum_{j=1}^{N} X_j(t + \tau + t_j)\right]. \tag{3.16}$$

This can be rewritten using equation (3.10):

$$\hat{P}(k_x, k_y, \omega) = \int \exp(i\omega\tau)d\tau \cdot \frac{1}{N^2}\sum_{i,j=1}^{N} R(x_j - x_i, y_j - y_i, t_j - t_i + \tau). \tag{3.17}$$

By introducing a weighting function $W(\kappa_x, \kappa_y)$ of the form

$$W(\kappa_x, \kappa_y) = \frac{1}{N^2}\sum_{i,j=1}^{N} \exp[-i\kappa_x(x_i - x_j) - i\kappa_y(y_i - y_j) + i\omega(\tau_i - \tau_j)], \tag{3.18}$$

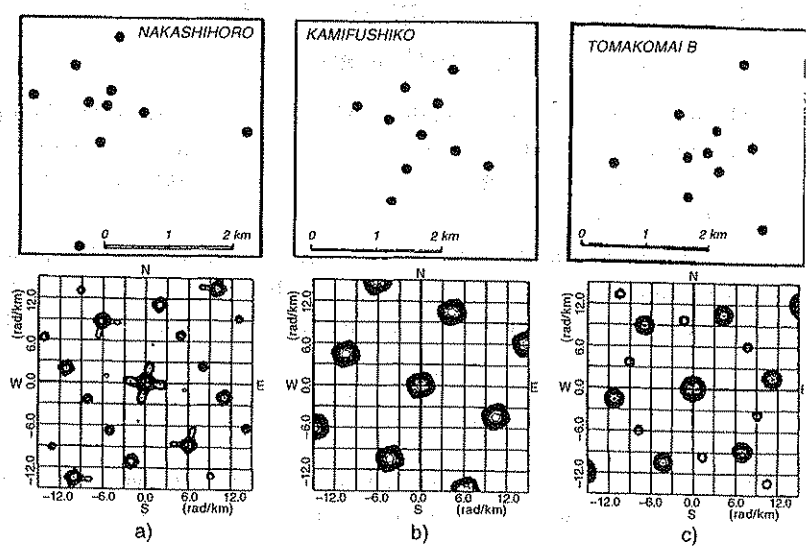

Figure 3.4. Examples of array responses used in microtremor surveys.

the estimated value of the power spectrum can be written as a weighted avera of the true power spectrum:

$$\hat{P}(k_x, k_y, \omega) = \iint_{-\infty}^{\infty} W(\kappa_x - k_x, \kappa_y - k_y)P(k_x, k_y, \omega)d\kappa_x d\kappa_y. \tag{3.}$$

The weighting function $W(\kappa_x, \kappa_y)$ is unique to the distribution of static for observation (x_i, y_i), and is calculated by equation (3.18). This is called "array response."

Figure 3.4 shows three examples of an observation array for microtrem observation, together with the associated array response. Several large s lobes are seen around the major peak at the center. These side lobes rem in the f-k power spectra as apparent peaks. In order to reduce the error estimation, the number of seismometers and their distribution should be su that the array response approaches a two-dimensional δ-function.

If the weighting function is a δ-function with its center at $\kappa_x = \kappa_y = 0$, estimated value of the spectra in the left hand side of equation (3.19) wo perfectly coincide with the true value of the spectra.

3.4.3 Maximum likelihood method or high-resolution method

The maximum likelihood method (MLM) was developed by Capon (1969). This method has better resolution than the BFM, but its mathematical elaboration is a little more difficult. Aki and Richards (1980) concisely explain the method as follows.

Suppose a dataset $d_{t,i}$ with a finite length N has a normal distribution with mean value s_t and covariance matrix ρ.[9] Then, for the number of the stations M, the $d_{t,i}$ has $M \times N$ values, and its probability density function is:

$$f = \frac{|\Phi|^{1/2}}{(2\pi)^{MN/2}} \exp\left\{-\frac{1}{2}\sum_{i,j=1}^{M}\sum_{k,l=1}^{N}\Phi_{ij}^{kl}(d_{k,i}-s_k)(d_{l,j}-s_l)\right\}, \tag{3.20}$$

where Φ_{ij}^{kl} is an element of an $MN \times MN$ matrix Φ which is the inverse of the covariance matrix. The element of the covariance matrix is

$$\rho_{ij}^{kl} = E[(d_{k,i}-s_k)(d_{l,j}-s_l)], \tag{3.21}$$

where the suffixes i and j correspond to station numbers, and k and l correspond to time.

Now, we consider the simplest case of a single observation station, i.e., $M = 1$ in equation (3.20). The probability density function for N variables d_t $(t = 1, 2, \ldots, N)$ can be written as

$$f = \frac{|\Phi|^{1/2}}{(2\pi)^{N/2}} \exp\left\{-\frac{1}{2}\sum_{k,l=1}^{N}\Phi^{kl}(d_k-s_k)(d_l-s_l)\right\}. \tag{3.22}$$

Here Φ^{kl} is an element of the $M \times N$ matrix Φ which is the inverse matrix of the covariance matrix ρ^{kl}. An element of the covariance matrix ρ^{kl} is

$$\rho^{kl} = E\left[(d_k-s_k)(d_l-s_l)\right]. \tag{3.23}$$

Here we assume that the form of the signal s_k has a known shape as $f_k (k = 1, 2, \ldots, N)$ while its amplitude includes an unknown factor c, that is

$$s_k = cf_k. \tag{3.24}$$

[9] In section 3.2, we discussed that there are cases where the amplitude of microtremor data does not show normal distribution. The following discussion is not applicable for such data.

Now the best estimate of the factor c is what we desire to know. Using a matrix expression, the inside of the exponential term of equation (3.22) is rewritten as:

$$-\frac{1}{2}(\mathbf{d}-c\mathbf{f})^T\,\Phi\,(\mathbf{d}-c\mathbf{f}),$$

where $\mathbf{d}$ and $\mathbf{f}$ are column vectors of d_k and f_k and ^{T} stands for transposition of the vector. Then, differentiating the equation with respect to c,

$$-\frac{1}{2}(\mathbf{d}-c\mathbf{f})^T\,\Phi\,(\mathbf{d}-c\mathbf{f}) = -\frac{1}{2}[\mathbf{d}^T\Phi\mathbf{d} - c\mathbf{d}^T\Phi\mathbf{f} - c\mathbf{f}^T\Phi\mathbf{d} + c^2\mathbf{f}^T\Phi\mathbf{f}]; \tag{3.25}$$

and letting the result 0, the most likely estimate of c is

$$\hat{c} = (\mathbf{d}^T\Phi\mathbf{f})\cdot(\mathbf{f}^T\Phi\mathbf{f})^{-1}. \tag{3.26}$$

In deriving equation (3.26), the symmetrical property of Φ,

$$\mathbf{d}^T\Phi\mathbf{f} = \mathbf{f}^T\Phi\mathbf{d}, \tag{3.27}$$

was used.

From equation (3.27) the maximum likelihood estimate of the signal vector $\mathbf{s}$ is

$$\hat{\mathbf{s}} = \hat{c}\mathbf{f} = (\mathbf{d}^T\Phi\mathbf{f})\cdot(\mathbf{f}^T\Phi\mathbf{f})^{-1}\mathbf{f}, \tag{3.28}$$

and, if $\mathbf{d} = c\mathbf{f}$, then $\mathbf{s} = c\mathbf{f}$, i.e., there is no distortion introduced into the signal, the variance of the estimated value of c can be calculated.

From

$$\hat{c} - c = (\mathbf{d}-c\mathbf{f})^T\Phi\mathbf{f}(\mathbf{f}^T\Phi\mathbf{f})^{-1}, \tag{3.29}$$

and using

$$\mathrm{E}\left[(\mathbf{d}-c\mathbf{f})(\mathbf{d}-c\mathbf{f})^T\right] = \rho,\ \rho = \Phi^{-1}, \tag{3.30}$$

we reach

$$\begin{aligned} E\left[(\hat{c}-c)^2\right] &= E\left[(\hat{c}-c)^T(\hat{c}-c)\right] \\ &= (\mathbf{f}^T\Phi\mathbf{f})^{-1}\mathbf{f}^T\Phi\rho\Phi\mathbf{f}(\mathbf{f}^T\Phi\mathbf{f})^{-1} \\ &= (\mathbf{f}^T\Phi\mathbf{f})^{-1} \\ &= (\mathbf{f}^T\rho^{-1}\mathbf{f})^{-1}. \end{aligned} \tag{3.31}$$

Summarizing the above result, the maximum likelihood estimate of the amplitude of the signal c is given by $(\mathbf{d}^T\ \mathbf{\Phi f})(\mathbf{f}^T\mathbf{\Phi f})^{-1}$ and the variance of its estimate is equal to $(\mathbf{f}^T\rho^{-1}\mathbf{f})^{-1}$, where ρ is the covariance matrix of the noise (or microtremors) and $\mathbf{\Phi} = \rho^{-1}$.

The maximum likelihood estimate of the power spectrum used by Capon (1969) is the variance of the signal estimate of a sine wave signal with amplitude $= 1$: $f_k = \exp\{i\omega(k-1)\Delta t\}$, where ω is the angular frequency at which the power spectrum is to be estimated.

In conclusion, the estimate of the power spectrum becomes

$$(\mathbf{f}^T\mathbf{\Phi f}^*)^{-1} = \left(\sum_{k=1}^{N}\sum_{l=1}^{N}\Phi^{kl}\exp\left[i\omega\,(k-l)\,\Delta t\right]\right)^{-1}, \tag{3.32}$$

where $\mathbf{f}^*$ is the conjugate of the complex number $\mathbf{f}$.

Equation (3.32) is a reasonable estimate of the power spectrum, because this is the variance of the maximum likelihood estimate of sine-type vibration with a certain frequency. The covariance gives a high-resolution estimate of the power spectrum of the noise with nearby frequencies.

By expanding equation (3.32) to the two-dimensional space, the estimate of f-k spectrum by Capon (1969) is

$$P'(k_x, k_y, \omega) = \left\{\sum_{i=1}^{N}\sum_{j=1}^{N}\phi_{ij}(\omega)\exp[ik_x(x_i - x_j) + ik_y(y_i - y_j)]\right\}^{-1}, \tag{3.33}$$

where $\phi_{ij}(\omega)$ is an element of the matrix $\mathbf{\Phi}(\omega)$ and (x_i, y_i) is the position coordinates of the station i. Here $\mathbf{\Phi}(\omega)$ is the inverse matrix of the Fourier transform of the covariance matrix $\rho_{\tau,i,j}$ below:

$$\rho_{\tau,i,j} = \mathrm{E}[X_{t,i}\cdot X_{t+\tau,j}], \tag{3.34}$$

where $X_{t,i}$ stands for noise at station i.

3.4.4 Phase velocity and direction of wave propagation

3.4.4.1 Estimating phase velocity

In the f-k method, the phase velocity of the most dominant wave in the f-k spectrum is sought. From the wavenumber vector $\mathbf{k}_0$, which is drawn at the

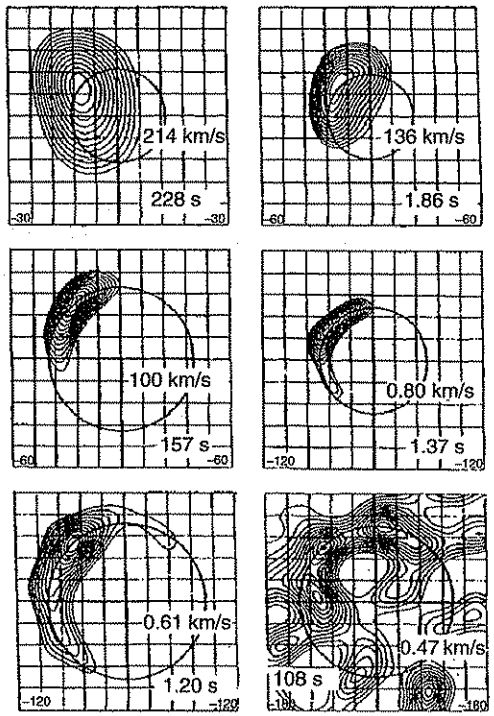

Figure 3.5. The f-k spectra and phase velocity of the wave with the highest power Each plot shows spectral power contoured in two-dimensional wavenumber space, fo a specified frequency. The six plots show six frequencies corresponding to period ranging from 2.28 s to 1.08 s. On each plot, the circle drawn passes through the peal of the contoured spectrum; the radius of this circle is the wavenumber of the dominan wave energy at the specified period.

peak of the f-k spectrum in the wavenumber coordinates (k_{xo}, k_{yo}) of frequency f_0 (period T_0), the phase velocity c_0 can be obtained as

$$c_0 = \frac{2\pi f_0}{|\mathbf{k}_0|} = \frac{2\pi}{T_0\sqrt{k_{xo}^2 + k_{yo}^2}}. \tag{3.35}$$

Figure 3.5 shows the relationship between an f-k power spectrum an phase velocity. The data used in the figure are microtremor data collecte in the campus of Hokkaido University, and the analysis method used is th MLM.

3.4.4.2 Estimating the direction of the wave origin

The microtremor survey method, even if the phase velocity of the wave originated from nonparallel layers, cannot estimate the structure of nonparallel layers. This is because the MSM must use a characteristic equation derived on the assumption of parallel layered subsurface structure in the inversion of observed phase velocity to subsurface structure. In practical applications, this is a limitation of MSM. However, in the case of the *f-k* method, which is commonly used, the direction of propagation of the most dominant wave can be estimated from the *f-k* power spectrum.

Suppose a coordinate system of an observation array with the positive direction of the y-axis to the north and positive direction of the x-axis to the east. Taking the bearing ϕ clockwise from the north, the direction of the origin of the most dominant wave ϕ_0 is calculated from the wavenumber coordinates of the peak of the spectrum (k_{xo}, k_{yo}) as:

$$\phi_0 = \tan^{-1}\left(\frac{k_{x_0}}{k_{y_0}}\right). \tag{3.36}$$

3.4.5 Calculation of cross-spectra by block averaging

We have seen that the variance derived from the *f-k* spectrum is the most important estimate in detecting surface waves from the microtremors. The more accurate the estimation of the *f-k* spectrum, the more accurate the subsequent estimation of the subsurface structure. In estimating the *f-k* spectrum, a calculation of cross-spectrum is necessary[10]. There are several different algorithms in the BFM and MLM methods.

Okada et al. (1990) and Matsushima et al. (1990a), due to the limits of the data processing systems of the time, chose one or more blocks from the records, and estimated the *f-k* spectrum for each block, then averaged them to reach the final phase velocity.

If there is no limit to the data processing system, the cross-spectrum can be calculated by the Capon's (1969) method. Using this method, the *f-k* spectrum is estimated by the block averaging or the direct segment method: A record of long duration is divided into M segments, and the cross-spectra of the segments are averaged. The phase velocity is estimated from this averaged cross-spectrum. The theory of stochastic process guarantees that this method can obtain a more stable estimate.

[10]The following method is applicable to the calculation of cross-spectrum by the SPAC method discussed later.

The following is a description of the cross-spectrum calculation m thod from Capon (1973). It is rather lengthy; however, this is an importa fundamental of the interpretation method, so the explanation is consider necessary.

In the block averaging method, a microtremor record $\{X_{ij}\}$ with its leng L is divided into M segments. The number of data points in each segment set to N, i.e., $L = M \times N$. First, the power spectra and cross spectra of ea segment are calculated for each station and pair of stations, respectively. T *f-k* spectrum of the entire data is then estimated by averaging the spectra the M segments. Phase velocity is estimated from this averaged *f-k* spectru The following explanation shows why the estimate can become stable by usi this algorithm.

Let P_{jn} be the Fourier transform of X_{jn}, the nth segment of a microtrem record at the jth station at the frequency f:

$$P_{jn}(f) = \frac{1}{\sqrt{N}} \sum_{m=1}^{N} X_{j,m+(n-1)N} \exp(imf), \; j = 1, 2, \ldots, K, \quad n = 1, 2, \ldots, M, \tag{3.3}$$

where K is the number of the stations. The estimate of the cross spectrum $\hat{S}$ obtained by averaging the M segments is

$$\hat{S}_{jk}(f) = \frac{1}{M} \sum_{n=1}^{M} P_{jn}(f) \cdot P_{kn}^{*}(f) \quad j, k = 1, 2, \ldots, K, \tag{3.3}$$

where * indicates complex conjugate.

The mean of $\hat{S}_{jk}(f)$ is

$$\begin{aligned}
&\mathrm{E}[\hat{S}_{jk}(f_0)] \\
&= \mathrm{E}\left[\frac{1}{M}\sum_{n=1}^{M} P_{jn}(f_0) \cdot P_{jn}^{*}(f_0)\right] \\
&= \mathrm{E}\left[\frac{1}{MN}\sum_{n=1}^{M}\sum_{m,m'=1}^{N} X_{j,m+(n-1)N} X_{k,m'+(n-1)N} \exp\{i(m-m')f_0\}\right] \\
&= \frac{1}{N}\sum_{m,m'=1}^{N} \rho_{jk}(m-m') \exp\{i(m-m')f_0\} \\
&= \int_{-\pi}^{\pi} S_{jk}(f) |W_N(f - f_0)|^2 \frac{df}{2\pi},
\end{aligned} \tag{3.3}$$

where $\rho_{jk}(m-m')$ is covariance and $|W_N(f)|^2$ is the Bartlett window, which is given by Blackman and Tukey (1958) as

$$|W_N(f)|^2 = \frac{1}{N}\left|\frac{\sin[(N/2)f]}{\sin[(1/2)f]}\right|^2. \tag{3.40}$$

Since

$$\int_{-\pi}^{\pi} |W_N(f)|^2 \frac{df}{2\pi} = 1, \tag{3.41}$$

we reach

$$\mathrm{E}[\hat{S}_{jk}(f_0)] \approx S_{jk}(f_0). \tag{3.42}$$

Therefore, $\hat{S}_{jk}(f_0)$ is the asymptotically unbiased estimate for $S_{jk}(f)$. At the same time, the mean square value of $\hat{S}_{jk}(f_0)$ is

$$\mathrm{E}\left[\{\hat{S}_{jk}(f_0)\}^2\right] = \mathrm{E}\left[\frac{1}{M^2N^2}\sum_{n,n'=1}^{M}\ \sum_{m,m',m'',m'''=1}^{N} X_{j,m+(n-1)N}X_{k,m'+(n-1)N}\right.$$
$$\left.\times X_{j,m''+(n'-1)N}X_{k,m'''+(n'-1)N}\exp\{i(m-m')f_0\}\exp\{i(m''-m''')f_0\}\right]. \tag{3.43}$$

Assuming the microtremors are a multidimensional normal process, the following equation is satisfied:

$$\begin{aligned}&\mathrm{E}\left[X_{j,m+(n-1)N}X_{k,m'+(n-1)N}X_{j,m''+(n'-1)N}X_{k,m'''+(n'-1)N}\right]\\ &\quad=\rho_{jk}(m-m')\rho_{jk}(m''-m''')\\ &\qquad+\rho_{jj}\{m-m''+(n-n')N\}\rho_{kk}\{m'-m'''+(n-n')N\}\\ &\qquad+\rho_{jk}\{m-m'''+(n-n')N\}\rho_{kj}\{m'-m''+(n-n')N\}.\end{aligned} \tag{3.44}$$

The variance of the expected values can be obtained by substituting equation (3.44) for equation (3.43) and using equation (3.39), as

$$\begin{aligned}&\mathrm{Var}\{\hat{S}_{jk}(f_0)\}\\ &=\int_{-\pi}^{\pi}\int_{-\pi}^{\pi}\left[\frac{1}{M}+\frac{2}{M}\sum_{n=1}^{M-1}\left(\frac{M-n}{M}\right)\exp\{inN(f-f')\}\right]\\ &\quad\times\left[S_{jj}(f)S_{kk}(f')|W_N(f-f_0)W_N(f'-f_0)|^2+S_{jk}(f)S_{jk}(f')\right.\\ &\quad\left.\times W_N(f-f_0)W_N^*(f+f_0)W_N(f'+f_0)W_N^*(f-f_0)\right]\frac{df}{2\pi}\frac{df'}{2\pi},\end{aligned} \tag{3.45}$$

where * designates the complex conjugate. If $S_{jk}(f)$ is a constant in th vicinity of the frequency f_0, equation (3.45) can be approximated as

$$\begin{aligned}\mathrm{Var}\{\hat{S}_{jk}(f_0)\} &\approx \frac{1}{M}S_{jj}(f_0)S_{kk}(f_0) \quad f_0 \neq 0, \pi\\ &\approx \frac{1}{M}\left[S_{jj}(f_0)S_{kk}(f_0)+S_{jk}^2(f_0)\right] \quad f_0 = 0, \pi.\end{aligned} \tag{3.46}$$

As $\mathrm{Var}\{\hat{S}_{jk}(f_0)\} \to 0$ when $M \to \infty$, it becomes apparent that $\hat{S}_{jk}(f)$ is convergent on the value of $S_{jk}(f)$.

In the BFM for example, the mean and variance of the estimate of the f-spectra by this algorithm, $\hat{P}(f_0, \mathbf{k}_0)$, are

$$\mathrm{E}[\hat{P}(f_0,\mathbf{k}_0)] = \int_{-\pi}^{\pi}\int_{-\infty}^{\infty}\int_{-\infty}^{\infty} P(f,\mathbf{k})|W_N(f-f_0)B(\mathbf{k}-\mathbf{k}_0)|^2\frac{df}{2\pi}dk_x dk \tag{3.47}$$

and

$$\begin{aligned}\mathrm{Var}\{\hat{P}(f_0,\mathbf{k}_0)\} &= \frac{1}{M}[\mathrm{E}\{\hat{P}(f_0,\mathbf{k}_0)\}]^2 \quad f_0 \neq 0, \pi\\ &= \frac{2}{M}[\mathrm{E}\{\hat{P}(f_0,\mathbf{k}_0)\}]^2 \quad f_0 = 0, \pi,\end{aligned} \tag{3.48}$$

where $|B(\mathbf{k})|^2$ is the beam-forming array pattern which is defined by

$$B(\mathbf{k}) = \frac{1}{K}\sum_{j=1}^{K}\exp(i\mathbf{k}\cdot\mathbf{r}_j), \tag{3.49}$$

where $\mathbf{r}_j$ is the position vector of the observation station j.

In MLM, on the other hand, the mean and variance of $P'(f_0, \mathbf{k}_0)$, are

$$\begin{aligned}\mathrm{E}[P'(f_0,\mathbf{k}_0)] &= \left(\frac{M-K+1}{M}\right)\int_{-\pi}^{\pi}\int_{-\infty}^{\infty}\int_{-\infty}^{\infty} P(f,\mathbf{k})\\ &\quad\times|W_N(f-f_0)B'(f_0,\mathbf{k},\mathbf{k}_0)|^2\frac{df}{2\pi}dk_x dk_y\end{aligned} \tag{3.50}$$

and

$$\begin{aligned}\mathrm{Var}\{P'(f_0,\mathbf{k}_0)\} &= \frac{1}{M-K+1}[\mathrm{E}\{P'(f_0,\mathbf{k}_0)\}]^2 \quad f_0 \neq 0, \pi\\ &= \frac{2}{M-K+1}[\mathrm{E}\{P'(f_0,\mathbf{k}_0)\}]^2 \quad f_0 = 0, \pi,\end{aligned} \tag{3.51}$$

where B' is:

$$B'(f, \mathbf{k}, \mathbf{k}_0) = \sum_{j=1}^{K} A_j(f, \mathbf{k}_0) \exp\{i(\mathbf{k} - \mathbf{k}_0) \cdot \mathbf{r}_j\}. \qquad (3.52)$$

As seen clearly in equations (3.47), (3.48), (3.50), and (3.51), the variance in the BFM depends on the number of segments M, but not the number of the stations K. On the other hand, in the MLM, it is a function of both M and K. In short, in the BFM, increasing the number of stations does not result in a decrease of variance.

3.5 Detection of Rayleigh waves from the vertical component of microtremors (spatial autocorrelation method)

The spatial autocorrelation method (SPAC) is based on the theory developed by Aki (1957) to determine the relationship between the temporal and spatial spectra of seismic waves, when the distribution of wavenumber vectors is too complicated for phase analysis.

The significance of the Aki's theory is its treatment of the complex wave phenomenon as a stochastic process in temporal and spatial dimensions. Of course this complex wave phenomenon includes the microtremors. The idea forms an important foundation when considering a method of extracting necessary information from the complex "noise."

Aki (1957), as an example of the application of his theory, tried to estimate the subsurface structure from a record of short period (<1 s) microtremors. In his time, the digital data recording system was not available and the result of his experiment cannot be regarded as "excellent." However, the idea of understanding the natural noise as a signal and suggesting a new direction in geophysical prospecting for meaningful subsurface structure, using that signal, is highly respected.

Later applications of the microtremor method are published by Okada and Sakajiri (1983), Hidaka (1985), Okada et al. (1990), Ferrazzini et al. (1991), Hough et al. (1992), Malagnini et al. (1993), Ling (1994), and Matsuoka et al. (1996)[11].

[11] According to the Aki's (1957) theory, the observation system seems to require many stations on a circular array. This was a severe restriction in applying this theory. However, Okada and Sakajiri (1983) and Hidaka (1985) demonstrated an equilateral triangle is sufficient to form a circular array. This eliminated a difficulty in spreadi the array and was a leap towards a practical application of the method. The meth that deploys this simple array is, hence, called "spatial autocorrelation method."

There are not many reports on the application of the spatial aut correlation method (SAM). However, it has two advantages over t frequency-wavenumber method:

1) It requires fewer stations and a smaller array than the frequenc wavenumber method to achieve a similar result. The size of the array the microtremor observation is very important, because
   - a large array increases the field effort and decreases field efficiency
   - a large array may affect the assumption of the microtremor meth that the layers are subparallel under the array.
2) By recording the vertical and both horizontal components of the m crotremor signal, not only the Rayleigh-wave, but also the Love-wa can be detected (Okada and Matsushima, 1989). Its theoretical bas is an extension of the Rayleigh wave detection and is easy to unde stand.

Aki's papers (1957, 1965) have a limitation in that they do not detect Lov wave energy, and using his method will not separate Love waves from Rayleig waves. Ferrazzini et al. (1991) observed three-component microtremors volcanic origin near the Pu'u O'o volcano in Hawaii, and he estimated tl subsurface structure from the phase velocities of the Rayleigh wave and tl Love wave. Their method included the "limitation" mentioned above. Oka and Matsushima (1989) improved the method and developed a new algorith (see Section 3.6). Matsushima and Okada (1990b) and more recently Y mamoto (2000) applied the new algorithm to microtremor data, and separat out the Love-wave energy. Their result demonstrated that the S-wave veloci structure estimated from propagating Love waves strongly agreed with th estimated from Rayleigh waves.

The microtremor survey method seeks ultimately to estimate the sul surface S-wave velocity structure. Therefore, as the Love wave consists sole of S-wave energy, the potential of the SPAC method, which can separate o the Love-wave, is considered to be immense. To date, only a few applicatio have been published, and they are limited to prospecting using the Rayleig wave from observations of the vertical component of microtremors. Howeve

the method has the possibility of wider application, and the data collection, processing, and analysis are much simpler. Therefore the SPAC method is clearly superior to the frequency-wavenumber method.

Theoretically, the SPAC method requires a peculiar array with multiple seismometers arranged in a circular pattern. By defining the spatial autocorrelation coefficient for dispersing waves in microtremor data observed by a circular array, the theory demonstrates that the spatial autocorrelation coefficient is a function of the frequency and phase velocity based on the radius of the array. The following sections describe the theoretical basis of the spatial autocorrelation method.

3.5.1 Spectral representation of microtremors in a polar coordinate system

In analyzing microtremor data by the SPAC method, it is convenient to use a polar coordinate system for microtremor spectra. By using polar coordinate relations,

$$\boldsymbol{\xi} = r\,(\cos\theta, \sin\theta) \quad \text{and} \quad \mathbf{k} = k\,(\cos\phi, \sin\phi)\,, \tag{3.53}$$

equation (3.5) is rewritten as

$$X(t, r, \theta) = \int_{-\infty}^{\infty}\int_{0}^{\infty}\int_{0}^{2\pi} \exp\{i\omega t + irk\cos(\theta - \phi)\} d\varsigma\,(\omega, k, \phi)\,, \tag{3.54}$$

where

$$\begin{aligned} d\zeta\,(\omega, \mathbf{k}, \phi) &= k d\zeta'\,(\omega, k, \phi) \\ &= dZ'\,(\omega, \mathbf{k}) \quad \text{in (3.5).} \end{aligned} \tag{3.55}$$

From equation (3.54) the microtremors as a stationary stochastic process can be expressed as a continuous sum of the waves of various angular frequency ω and wavenumber k independently (i.e., without correlation) arriving from various directions ϕ.

The $\zeta(\omega, k, \phi)$ of equation (3.54) satisfies the following relationships:

$$\text{i) } \mathrm{E}\,[d\zeta\,(\omega, k, \phi)] = 0 \qquad \text{(for all } \omega, k, \phi\text{)}, \tag{3.56}$$

$$\text{ii) } \mathrm{E}\left[|\, d\zeta\,(\omega, k, \phi)\,|^2\right] = dH\,(\omega, k, \phi) \quad \text{(for all } \omega, k, \phi\text{)}, \tag{3.57}$$

iii) for any two distinct ω, and ω' (where $\omega \neq \omega'$), and two distinct se (k, ϕ) and (k', ϕ') (where $k \neq k'$ and $\phi \neq \phi'$),

$$\mathrm{E}[d\zeta^*(\omega, k, \phi) d\zeta(\omega', k', \phi')] = 0, \tag{3.5}$$

where * denotes the complex conjugate.

Now we make two assumptions:

Assumption 1: The microtremors consist mainly of surface waves, and o of their modes (often the fundamental mode) is dominant.

Assumption 2: Hence, ω and k are related as a function of each other, and or ζ, namely the microtremors expressed as a stochastic process, ha significance only on a curve $[\omega, k(\omega)]$.

When we discuss the vertical component of the microtremors, the surfa wave referred to is the Rayleigh wave. In this case, the spectral representatic of equation (3.54) becomes

$$X(t, r, \theta) = \int_{-\infty}^{\infty}\int_{0}^{2\pi} \exp\{i\omega t + irk(\omega)\cos(\theta - \phi)\} d\varsigma\,(\omega, \phi)\,. \tag{3.5}$$

In general, as the spectra of the microtremors are considered to be conti uous and differentiable with respect to frequency and direction, the stochast process $\zeta(\omega, \phi)$ satisfies the following relationship:

$$\begin{aligned} \mathrm{E}\left[|d\zeta\,(\omega, \phi)|^2\right] &= dH\,(\omega, \phi) \\ &= h\,(\omega, \phi)\, d\omega\, d\phi, \end{aligned} \tag{3.6}$$

where $h(\omega, \phi)$ may be called "frequency-direction spectral density," an $h(\omega, \phi)\, d\omega\, d\phi$ represents the average contribution to the total power from th components of the waves coming from the directions between ϕ and $\phi + d$ with angular frequencies between ω and $\omega + d\omega$.

When this average contribution is summed up (i.e., integrated), with re spect to all directions, the power spectral density function (or simply "powe spectrum") of microtremors at one station $h_0(\omega)$is obtained as

$$h_0(\omega) = \int_{0}^{2\pi} h\,(\omega, \phi) d\phi. \tag{3.61}$$

3.5.2 The spatial autocorrelation function and the spatial covariance function

For the sake of simplicity of expression, hereafter the coordinates on the Earth's surface (x, y) are expressed as (r, θ) in polar coordinate space.

Now, suppose there are two microtremor observation stations A and B, the distance between which is r. Let A be the origin of the coordinate system (0, 0), then the coordinates of station B are (r, θ).

From equation (3.59), the microtremor record at station A can be represented as

$$X(t, 0, 0) = \int_{-\infty}^{\infty} \int_{0}^{2\pi} \exp(i\omega t) d\varsigma(\omega, \phi), \tag{3.62}$$

and the record at B as

$$X(t, r, \theta) = \int_{-\infty}^{\infty} \int_{0}^{2\pi} \exp\{i\omega t + irk\cos(\theta - \phi)\} d\varsigma(\omega, \phi). \tag{3.63}$$

The spatial autocorrelation function between A and B is

$$\begin{aligned} S(r, \theta) &= \mathrm{E}\left[X^*(t, 0, 0) X(t, r, \theta)\right] \\ &= \lim_{T\to\infty} \frac{1}{2T} \int_{-T}^{T} X^*(t, 0, 0) X(t, r, \theta)\, dt \\ &= \int_{-\infty}^{\infty} \int_{0}^{2\pi} \int_{-\infty}^{\infty} \int_{0}^{2\pi} \exp\{i(\omega' - \omega)t + irk'\cos(\theta - \phi')\} \\ &\quad \times \mathrm{E}[d\zeta^*(\omega, \phi)\, d\zeta(\omega', \phi')]. \end{aligned} \tag{3.64}$$

This equation is reduced by equations (3.57), (3.58), (3.59), and (3.60) to

$$S(r, \theta) = \int_{-\infty}^{\infty} \left[\int_{0}^{2\pi} \exp\{irk\cos(\theta - \phi)\} h(\omega, \phi)\, d\phi\right] d\omega \tag{3.65}$$

$$= \int_{-\infty}^{\infty} g(\omega, r, \theta)\, d\omega, \tag{3.66}$$

where

$$g(\omega, r, \theta) = \int_{0}^{2\pi} \exp\{irk\cos(\theta - \phi)\} h(\omega, \phi)\, d\phi \tag{3.67}$$

is called the spatial covariance function of the microtremors at the angular frequency ω (Henstridge, 1979).

This equation at the origin (0, 0) is evaluated as

$$\begin{aligned} g(\omega, 0, 0) &= \int_{0}^{2\pi} h(\omega, \phi)\, d\phi \\ &= h_0(\omega), \end{aligned} \tag{3}$$

and gives the power spectrum of equation (3.61). In the same way, the sp autocorrelation function at the origin is

$$\begin{aligned} S_0 \equiv S(0, 0) &= \mathrm{E}\left[|X(t, 0, 0)|^2\right] \\ &= \int_{-\infty}^{\infty} h_0(\omega)\, d\omega. \end{aligned} \tag{3}$$

Here, $h_0(\omega)\, d\omega$ is the average contribution to the total power from the cor nents of microtremors $X(t, r, \theta)$ with angular frequency between ω and $d\omega$ observed at one station (A or B) within the space where the array is spr Therefore S_0 in the left-hand side of equation (3.69) gives the total powe the stochastic process (i.e., microtremor record) at one station within the a space.

3.5.3 The spatial autocorrelation coefficient of a circular array and its relation to phase velocit

Suppose we lay an array consisting of several stations on a circle with a radi around the origin A. We define the averaged spatial autocorrelation funct and spatial autocorrelation coefficient for the microtremors observed by circular array. For simplicity, consideration is given to one component wi particular frequency ω.

Now, let $g(\omega, r, \theta)$ be the spatial covariance function between the ce and one point on the circumference of the circular array at the frequency We can then define the *directional average* of the spatial covariance funct by averaging $g(\omega, r, \theta)$ over all the directions:

$$\overline{g}(\omega, r) = \frac{1}{2\pi} \int_{0}^{2\pi} g(\omega, r, \theta) d\theta. \tag{3.}$$

By substituting the integrand with equation (3.67), we obtain

$$\overline{g}(\omega, r) = \frac{1}{2\pi} \int_{0}^{2\pi} \int_{0}^{2\pi} \exp\{irk\cos(\theta - \phi)\} h(\omega, \phi) d\phi\, d\theta. \tag{3.}$$

In equation (3.71), the integral along θ is

$$\frac{1}{2\pi}\int_0^{2\pi} \exp\{irk\cos(\theta-\phi)\}d\theta = J_0(rk), \tag{3.72}$$

which is the Bessel function of the first kind of zero order with the variable rk. Therefore equation (3.71) is simply

$$\begin{aligned}\overline{g}(\omega, r) &= \int_0^{2\pi} J_0(rk)\, h(\omega, \phi)d\phi \\ &= J_0(rk)\int_0^{2\pi} h(\omega, \phi)d\phi. \end{aligned}\tag{3.73}$$

Using equations (3.61) or (3.68), equation (3.73) is further simplified to

$$\overline{g}(\omega, r) = h_0(\omega)\, J_0(rk) \tag{3.74}$$

or

$$\overline{g}(\omega, r) = g(\omega, 0, 0)\, J_0(rk). \tag{3.75}$$

Similarly, the directional average of the spatial autocorrelation function defined by equation (3.64) is reduced to

$$\overline{S}(r) = \int_{-\infty}^{\infty} h_0(\omega)\, J_0(rk)\, d\omega. \tag{3.76}$$

The terms to be integrated in equation (3.74) or (3.76) mean that, for the total power of the microtremors within the array space, the average contribution of the components of the waves between ω and $\omega + d\omega$ is always weighted by the coefficient $J_0(rk)$, which is related to the subsurface structure. Therefore $\overline{S}(r)$, the left-hand side of (3.76), gives the total power of all the microtremors propagating under the influence of the subsurface structure directly beneath the circular array of radius r.

Now we define the "spatial autocorrelation coefficient at the angular frequency ω," $\rho(\omega, r)$, or simply "spatial autocorrelation coefficient," $\rho(f, r)$, as the power spectra of microtremors at one station within the array space (the center of the circle, i.e., origin, for instance) normalized to $h_0(\omega)$:

$$\rho(\omega, r) \equiv \overline{g}(\omega, r)\,/\,h_0(\omega). \tag{3.77}$$

$$\rho(f, r) = J_0(2\pi fr/c(f))$$

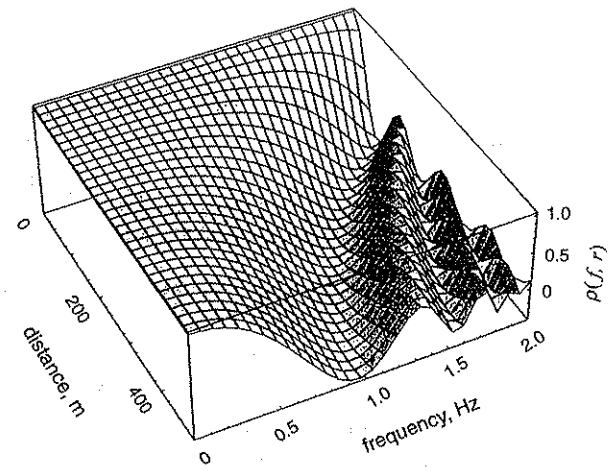

Figure 3.6. A schematic graph of the spatial autocorrelation coefficient.

Using equation (3.74),

$$\rho(\omega, r) = J_0(rk), \tag{3.7}$$

or from $k = \omega/c(\omega)$ (where $c(\omega)$ is the phase velocity),

$$\rho(\omega, r) = J_0(r\omega/c(\omega)), \tag{3.7}$$

and from $\omega = 2\pi f$,

$$\rho(f, r) = J_0(2\pi fr/c(f)). \tag{3.8}$$

Therefore the spatial autocorrelation coefficient at the frequency f is related the phase velocity $c(f)$ via the Bessel function of the first kind of zero orde Figure 3.6 is a schematic diagram of the spatial autocorrelation coefficie controlled by the two variables f and r.

As is clear in the above theoretical derivation, the phase velocity of certain frequency can be calculated by the spatial autocorrelation coefficie

of the component of the wave whose frequency is ω, from the microtremors recorded with a circular array of radius r[12].

The spatial autocorrelation coefficient defined above is a quantity unique to the location of the array, and it reflects the subsurface structure directly below the array.

3.6 Detection of Love waves from microtremors (spatial autocorrelation method)

So far we have considered the vertical component of waves in microtremors; the polarization of waves propagating over a horizontal plane has not been considered. For the horizontal component of the waves in microtremors, two types of polarization should be considered: waves with vibration parallel and perpendicular to the direction of propagation. We again assume these polarized waves to be a stationary stochastic process.

To discuss these polarized waves, we consider the components of the waves parallel and perpendicular to the direction of the line through two observation stations. They are, hereafter, called "radial" and "tangential" components of waves, respectively.

3.6.1 The spectral representation of horizontally polarized waves in microtremors

We again consider a circular array which, however, consists of three-component seismometers equally spaced on a circle with radius r and a three-component seismometer at the center.

Let radial and tangential components of the waves in microtremors observed at a station (r, θ) on the array be a stationary random process $\mathbf{X}_r(t, r, \theta)$ and $\mathbf{X}_\theta(t, r, \theta)$, which inevitably includes surface waves, that is, both Rayleigh and Love waves.

Assuming that $\mathbf{X}^R(t, r, \theta)$ and $\mathbf{X}^L(t, r, \theta)$ are a complex assemblage of horizontal components of Rayleigh waves and that of Love waves, respectively, and are also regarded as stationary stochastic processes, the radial and tangential components of the waves consisting of these processes propagated

[12]In practical data processing, this is performed by dividing the observed data into as many segments as possible, and calculating finite Fourier transform and block averaging for each segment.

through the array with direction ϕ may be written as

$$\mathbf{X}_r(t, r, \theta) = \mathbf{X}_r^R(t, r, \theta) + \mathbf{X}_r^L(t, r, \theta),$$
$$\mathbf{X}_\theta(t, r, \theta) = \mathbf{X}_\theta^R(t, r, \theta) + \mathbf{X}_\theta^L(t, r, \theta), \quad (3$$

where

$$X_r^R = X^R \cos(\theta - \phi) \quad X_\theta^R = -X^R \sin(\theta - \phi),$$
$$X_r^L = X^L \sin(\theta - \phi) \quad X_\theta^L = X^L \cos(\theta - \phi), \quad (3$$

and subscripts r and θ refer to the radial and tangential components of wa

Following the representation in the preceding sections, these proce may also be written in the polar coordinate system as

$$\mathbf{X}_{r,\theta}^R(t, r, \theta) = \int_{-\infty}^{\infty}\int_0^{\infty}\int_0^{2\pi} \exp\{i\omega t + irk^R \cos(\theta - \phi)\} dZ^R(\omega, k^R, \cdot$$

$$\mathbf{X}_{r,\theta}^L(t, r, \theta) = \int_{-\infty}^{\infty}\int_0^{\infty}\int_0^{2\pi} \exp\{i\omega t + irk^L \cos(\theta - \phi)\} dZ^L(\omega, k^L, \cdot$$

(3

where $k^{R(L)}(=\omega/c^{R(L)})$ is the wavenumber for the Rayleigh (Love) w with phase velocity $c^{R(L)}$ and $Z^{R(L)}$, the doubly orthogonal process for crotremors including the Rayleigh (Love) wave, ω is the angular freque and ϕ, the direction of waves propagating through the array.

3.6.2 The spatial autocorrelation function for horizontally polarized waves

For these processes, we assume again that the stochastic process Z^R and Z concentrated on curves $[\omega, k^R(\omega)]$ and $[\omega, k^L(\omega)]$, respectively. This assu tion provides that the increments of the processes dZ^R and dZ^L in equa (3.83) are

$$dZ^R(\omega, k^R, \phi) = dZ^R(\omega, \phi), \text{ and } dZ^L(\omega, k^L, \phi) = dZ^L(\omega, \phi). \quad (3$$

In this case, the spectral representation of equation (3.83) may be writte

$$\mathbf{X}_{r,\theta}^R(t, r, \theta) = \int_{-\infty}^{\infty}\int_0^{2\pi} \exp\{i\omega t + irk^R \cos(\theta - \phi)\} dZ^R(\omega, \phi);$$

$$\mathbf{X}_{r,\theta}^L(t, r, \theta) = \int_{-\infty}^{\infty}\int_0^{2\pi} \exp\{i\omega t + irk^L \cos(\theta - \phi)\} dZ^L(\omega, \phi). \quad (3$$

For the processes at the center of a circular array and a point on a circle with radius r, the spatial autocorrelation functions for radial and tangential components are defined as

$$S_r(r,\theta) = \mathrm{E}[X_r^*(t,0,\theta)\cdot X_r(t,r,\theta)];$$
$$S_\theta(r,\theta) = \mathrm{E}[X_\theta^*(t,0,\theta)\cdot X_\theta(t,r,\theta)]. \tag{3.86}$$

Assuming that no coupling takes place between the Rayleigh and Love waves in the processes in other words, dZ^{R*} and dZ^L or dZ^R and dZ^{L*} are uncorrelated,

$$\mathrm{E}[dZ^{R*}(\omega,\phi)\cdot dZ^L(\omega,\phi)] = 0, \text{ or } \mathrm{E}[dZ^R(\omega,\phi)\cdot dZ^{L*}(\omega,\phi)] = 0 \tag{3.87}$$

The properties (i), (ii), and (iii) discussed in Section 3.2.2 for the process Z' for the vertical component of microtremors are also applicable to these processes. Then using equation (3.81), equations (3.86) reduce to

$$S_r(r,\theta) = \mathrm{E}\left[X_r^{R*}(t,0,\theta)\cdot X_r^R(t,r,\theta) + X_r^{L*}(t,0,\theta)\cdot X_r^L(t,r,\theta)\right];$$
$$S_\theta(r,\theta) = \mathrm{E}\left[X_\theta^{R*}(t,0,\theta)\cdot X_\theta^R(t,r,\theta) + X_\theta^{L*}(t,0,\theta)\cdot X_\theta^{L*}(t,r,\theta)\right]. \tag{3.88}$$

Following Section 3.5.1, a frequency-direction spectral density function of the horizontally polarized waves in microtremors $h^{R(L)}(\omega,\phi)$ is defined by

$$\mathrm{E}\left[|dZ^{R(L)}(\omega,\phi)|^2\right] = dH^{R(L)}(\omega,\phi),$$
$$= h^{R(L)}(\omega,\phi)\,d\phi\,d\omega, \tag{3.89}$$

which gives the average contribution to the total power from components in $X^{R(L)}$ coming from the directions between ϕ and $\phi + d\phi$ with angular frequencies between ω and $\omega + d\omega$, where $H^{R(L)}$ is the integrated spectrum of $X^{R(L)}$. When the average contribution to the total power from components in $X^{R(L)}$ is integrated with respect to all the directions, the power spectral density function of components in $X^{R(L)}$ at one station $h_0^{R(L)}(\omega)$ is obtained as

$$h_0^{R(L)}(\omega) = \int_0^{2\pi} h^{R(L)}(\omega,\phi)\,d\phi. \tag{3.90}$$

The spatial autocorrelation function for radial and tangential componen of the waves in microtremors at angular frequency ω may be written fro equations (3.85), (3.88), and (3.89) as

$$S_r(\omega,r,\theta) = \int_0^{2\pi} \cos^2(\theta-\phi)\exp\{irk^R\cos(\theta-\phi)\}h^R(\omega,\phi)\,d\phi + \int_0^{2\pi} \sin^2(\theta-\phi)\exp\{irk^L\cos(\theta-\phi)\}h^L(\omega,\phi)\,d\phi; \tag{3.9}$$

$$S_\theta(\omega,r,\theta) = \int_0^{2\pi} \sin^2(\theta-\phi)\exp\{irk^R\cos(\theta-\phi)\}h^R(\omega,\phi)\,d\phi + \int_0^{2\pi} \cos^2(\theta-\phi)\exp\{irk^L\cos(\theta-\phi)\}h^L(\omega,\phi)\,d\phi. \tag{3.9}$$

If the average over azimuth θ is taken for the respective functions, the ave aged spatial autocorrelation function for radial and tangential components obtained as

$$\overline{S}_r(\omega,r) \equiv \frac{1}{2\pi}\int_0^{2\pi} S_r(\omega,r,\theta)\,d\theta = \frac{1}{2}\left[\{J_0(p) - J_2(p)\}h_0^R(\omega) + \{J_0(q) + J_2(q)\}h_0^L(\omega)\right] \tag{3.9}$$

and

$$\overline{S}_\theta(\omega,r) \equiv \frac{1}{2\pi}\int_0^{2\pi} S_\theta(\omega,r,\theta)\,d\theta = \frac{1}{2}\left[\{J_0(p) + J_2(p)\}h_0^R(\omega) + \{J_0(q) - J_2(q)\}h_0^L(\omega)\right], \tag{3.9}$$

where J_0 and J_2 are the Bessel function of the first kind of zero order an of second order, respectively; $p = rk^R$ and $q = rk^L$. The averaged spati autocorrelation functions for radial and tangential components at the arra center are, by inserting $r = 0$ into equations (3.93) and (3.94),

$$\overline{S}_r(\omega,0) = \overline{S}_\theta(\omega,0) = \frac{1}{2}\left\{h_0^R(\omega) + h_0^L(\omega)\right\} \equiv \frac{1}{2}H_0(\omega). \tag{3.9}$$

3.6.3 The spatial autocorrelation coefficient for horizontally polarized waves and wavenumber equation of Love waves

We define the spatial autocorrelation coefficient at frequency ω for radial and tangential components, $\rho_r(\omega, r)$ and $\rho_\theta(\omega, r)$ as

$$\rho_r(\omega, r) = \overline{S}_r(\omega, r)/\overline{S}_r(\omega, 0);$$
$$\rho_\theta(\omega, r) = \overline{S}_\theta(\omega, r)/\overline{S}_\theta(\omega, 0). \tag{3.96}$$

The coefficients thus defined, however, help only to understand the calculation of the process, and are not necessarily required for discrimination between the Rayleigh and Love waves from microtremors.

Using equations (3.93), (3.94), and (3.95), equation (3.96) can be rewritten as

$$\rho_r(\omega, r) = \left[\{J_0(p) - J_2(p)\} h_0^R(\omega) + \{J_0(q) + J_2(q)\} h_0^L(\omega)\right]/H_0(\omega);$$
$$\rho_\theta(\omega, r) = \left[\{J_0(p) + J_2(p)\} h_0^R(\omega) + \{J_0(q) - J_2(q)\} h_0^L(\omega)\right]/H_0(\omega). \tag{3.97}$$

The presence of variables p and q in these equations states that the spatial autocorrelation coefficients for radial and tangential components are related to a subsurface structure beneath the array, (i.e., the wavenumbers k^R and k^L are a function of frequency ω as causing Rayleigh- and Love-wave dispersion). In addition, these equations show that the autocorrelation coefficients also depend on the power of microtremors, or more precisely, the power ratio of Rayleigh or Love waves in microtremors observed at the array. Therefore the spatial autocorrelation coefficients thus defined cannot be regarded as a unique parameter to characterize an underground structure.

Depending on the stationary condition for microtremors observed, the coefficients may vary even in the same array.

This is different from the spatial autocorrelation coefficient for vertical component of the waves defined by equation (3.77) or (3.78) in Section 3.5.3.

Rearranging equations (3.93), (3.94), and (3.95), an equation for the wavenumber of the Love waves, k^L can be obtained:

$$\lambda J_0(q) - J_2(q) = \lambda J_0(p) + J_2(p) \tag{3.98}$$

or

$$\lambda = \frac{J_2(p) + J_2(q)}{-J_0(p) + J_0(q)}, \tag{3.99}$$

where $J_0(p)$and $J_2(p)$ are determined by the spatial autocorrelation coefficient for the vertical component of microtremors, assuming that the Rayleigh waves have the same wavenumbers for the vertical and horizontal components. The quantity λ is a function of the frequency ω and the radius of the circular array r, and is given by the observed quantities as

$$\lambda(\omega, r) = \frac{\Sigma^- + J_2(p) H_0(\omega)}{\Sigma^+ - J_0(p) H_0(\omega)}, \tag{3.100}$$

where

$$\Sigma^+ = \overline{S}_r(\omega, r) + \overline{S}_\theta(\theta, r),$$

and

$$\Sigma^- = \overline{S}_r(\omega, r) - \overline{S}_\theta(\theta, r).$$

The terms are derived from equation (3.88), the first equations of (3.93) and (3.94), and $H_0(\omega)$ is determined by equation (3.95). Then, we can solve equation (3.98) or (3.99) for $q(= rk^L)$ which gives the phase velocity of Love waves c^L at frequency ω.

The power spectral density functions of the Rayleigh waves and the Love waves can be obtained for the same frequency by substituting the variables in equations (3.93) and (3.94) with $J_0(q)$ and $J_2(q)$ thus obtained, and $J_0(p)$ and $J_2(p)$ determined for the vertical component.

As is evident from equation (3.99), the quantity λ is independent of the power of microtremors, but is a function of only the radius of the array r and variables p and q, directly related to the wavenumbers k^R and k^L. In other words, the quantity λ can be regarded as a parameter to relate dispersions of both Rayleigh and Love waves under the array of a given radius. Therefore, in the SPAC method using the three-component observation, Rayleigh waves and Love waves complement each other in determining subsurface S-wave velocity structure.

Chapter 4

Estimating phase velocity and subsurface structure

4.1 Estimating phase velocity

The basic principle of the microtremor survey method, as previously stated, is described as "detecting the form of dispersion of the surface wave contained in the microtremors, i.e., determining the relationship between phase velocity and frequency (or period)." Here, the band of frequencies relates to the range of the depth of investigation. The longer the period used, the deeper the depth of investigation becomes. However, the relationship between them is not known before a survey.

The basic variables used to determine the nature of the structure, phase velocity c and frequency f, are implicitly related in the characteristic equation:

$$F\left(c, f; v_{p1}, v_{s1}, \rho_1, h_1; v_{p2}, v_{s2}, \rho_2, h_2; \ldots; v_{pN}, v_{sN}, \rho_N\right) = 0, \quad (4.1)$$

where v_{pj}, v_{sj}, ρ_j and h_j are parameters for the jth layer of the structure consisting of N layers, i.e., P-wave velocity, S-wave velocity, density, and thickness, respectively. This equation cannot be explicitly solved for c as a function of the independent variable f. However, as a formality, by supposing this equation has a solution, it can be written as

$$c = c\left(f; v_{p1}, v_{s1}, \rho_1, h_1; v_{p2}, v_{s2}, \rho_2, h_2; \ldots; v_{pN}, v_{sN}, \rho_N\right). \quad (4.2)$$

Hereafter, the layer parameters are omitted for simplicity, and equation (4.2) is rewritten as

$$c = c(f). \quad (4.3)$$

The surface wave consists of a multitude of wave modes, and the phase velocity resolved by equation (4.1) is not unique when the frequency is higher than a certain value. Moreover, the number of the solutions increases with frequency. However, in most surface waves, the fundamental mode is dominant. The exception is when the Poisson's ratio of the subsurface structure is great, i.e., the ratio of S-wave velocity to P-wave velocity (v_s/v_p) is very small. Therefore, in practice, the higher-mode components greater than the second order are regarded as negligible, and a unique phase velocity is obtained for each frequency component of the surface wave. Hence, equation (4.3) represents the relationship between the fundamental-mode phase velocity and frequency, and the velocity c can be regarded as a single-valued function of frequency f.

In summary, the procedure for detecting surface waves from microtremors is to find the relationship of equation (4.3) from observation, and to estimate the layer parameters of equation (4.1) or (4.2).

As stated in the previous chapter, there are two methods for detecting the surface waves, i.e., finding the relationship (4.3): the *frequency-wavenumber* (*f-k*) *method* and the *spatial autocorrelation (SPAC) method.*

Recent case histories of the estimating subsurface structure by microtremors are dominated by the *f-k* method. But this method has two main shortcomings: the first is that it uses a relatively narrow frequency range for the size of array required, and the second is the difficulty in accurately estimating the phase velocity due to the degeneration phenomenon of *f-k* spectra (Okada et al., 1995). To avoid degeneration, this method requires a large array and a large number of observation stations. However, a large array size adversely affects the lateral resolution. With these defects of the *f-k* method in mind, this chapter is a discussion of data acquisition and processing using the SPAC method, which is free from these defects.

4.1.1 Spatial autocorrelation (SPAC) method

Observations of the vertical component of microtremors show that the phase velocity c in equation (3.80) corresponds to the phase velocity of the fundamental mode Rayleigh wave. As stated, this is because the fundamental mode is dominant in the surface wave.

Consider the case of estimating the phase velocity of the Rayleigh wave in microtremors observed by a circular array of radius r. Assuming $r = r_0$,

i.e., $A = 2\pi r_0 (= \text{const.})$, equation (3.80) is written as

$$\rho_{r_0}(f) = J_0(Af/c) = J_0(x), \tag{4.4}$$

where $x = Af/c$ and c is a function of f. Since it is clear that there may be more than one value of x that satisfies equation (4.4) for a given frequency, the phase velocity c to satisfy equation (4.4) is not always unique.

The simplicity of equation (4.4) appears to suggest a possibility of easily finding the optimum Bessel function $J_0(x)$ from a range of observed values of f and $\rho_{r_0}(f)$ by, say, the least-squares fitting method. However, the relationship between frequency f and x in the right-hand side of equation (4.4) is not linear. Therefore, no matter how densely the values of $\rho_{r_0}(f)$ are sampled for a wide range of f, it is impossible to obtain the unique Bessel function to satisfy equation (4.4) by the least-squares fitting method. This is because the solution to the equation (4.4) is theoretically not unique.

In practice, the estimation of the phase velocity c from a dataset collected by an array of a certain size is carried out for each frequency f by

$$c(f) = Af/x.$$

This generates a solution for the variable x of the Bessel function $J_0(x)$ which is equal to the known autocorrelation coefficient.

The phase velocity is, in fact, obtained by this method. A problem with this method is the frequently encountered difficulty of finding a unique phase velocity c near the minima and maxima of $\rho_{r_0}(f)$ (see Figure 4.1). This is a serious difficulty in finding the phase velocity from an array of a single size.

This problem can be avoided by (1) repeating observation at the same station with arrays of different sizes, or, if provided with sufficient equipment, (2) using a combination of arrays of different radii. The latter is called a *multiple circular array* or a *complex array.*

Analysis of such data employs the *extended spatial autocorrelation method* by Ling and Okada (1993), an extension of the SPAC method.

4.1.2 Extended spatial autocorrelation (ESPAC) method

The SPAC method requires a circular array for data collection, and it seems practically difficult to locate a multitude of stations on a circle in a given

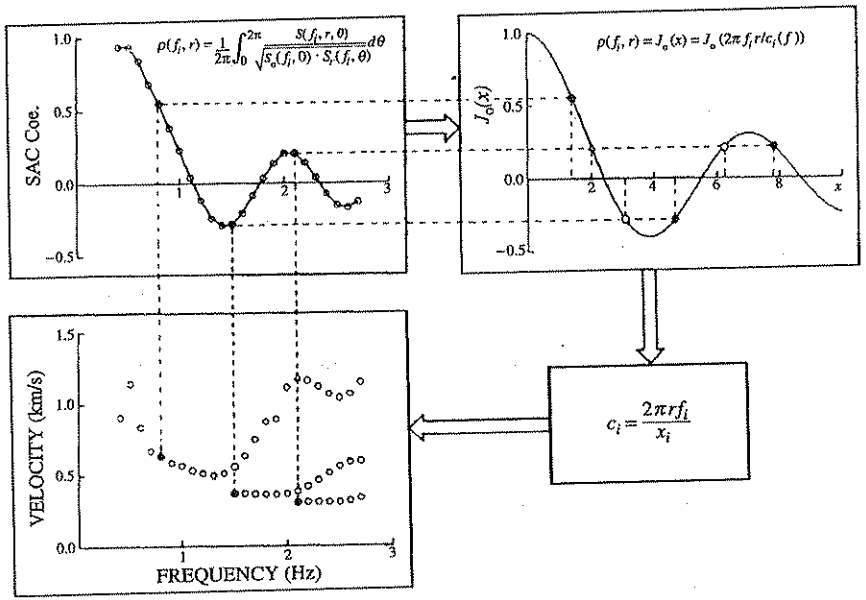

Figure 4.1. Flowchart to estimate phase velocity by the SPAC method.

geographical setting. However, reducing the number of stations on the circle can ease this difficulty.

For example, an array of only four stations arranged at the corners and center of an equilateral triangle should not be too difficult to configure. In fact, an equilateral triangle array with such a small number of stations can achieve a spatial autocorrelation coefficient with considerable precision. Then, by using an equilateral triangle as a unit and varying its size, several datasets can be collected with a multitude of different arrays. An apparent problem with this manner of data collection is the different times of observation for data from different arrays. However, the data collected in different time can be jointly processed; there is no need to treat them separately.

This joint processing method is called the extended spatial autocorrelation (ESPAC) method (Ling and Okada, 1993), as distinct from the spatial autocorrelation method, which deploys a single circular array. The ESPAC method can also be applied to data simultaneously collected with multiple circular arrays. Incidentally, such a dataset may be analyzed using the *f-k* method as well.

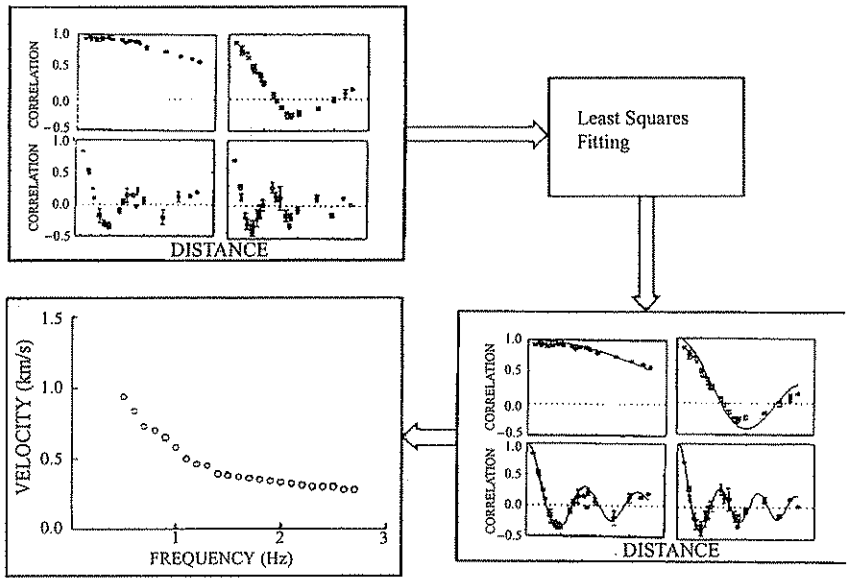

Figure 4.2. Flowchart to estimate phase velocity by the ESPAC method.

The word "extended," is used, as a matter of convenience, to indicate ar extended array size according to the time of observation. It is not intended tc mean a development or extension of the autocorrelation principle.

The theory of the ESPAC method is clear from the definition of the spatia autocorrelation coefficient from equation (3.78) or (3.80). A more precisc account is given in the following section.

Now, let's think of the equation (3.80) with a constant f. By substituting $f = f_0$, $c_0 = c(f_0)$, and $B = 2\pi f_0/c_0 (= const.)$, this becomes

$$\rho_{f_0}(r) = J_0(Br). \tag{4.5}$$

The left-hand side of this equation is a single value function of the vari able r. Provided with the values of $\rho_{f_0}(r)$ for various values of r, the optimun Bessel function J_0 can be found by the least-squares method (see Figure 4.2) The ESPAC method is based on this principle. To improve the precision o the solution, a large number of $[r, \rho_{f_0}(r)]$ pairs from a large area without any particular bias towards location is sought.

There are two ways to achieve this:

1) Repeat observations while varying the size of the array; and
2) Use a concentric circle array or composite array, whereby various circular arrays can be extracted from one simultaneous observation.

Option 1 requires fewer stations but the observation takes longer, while option 2 takes less time but requires more recording equipment. In either the case, the scale of data acquisition becomes relatively large. However this method has merits:

1) Data from different observations can be jointly processed
2) The array does not strictly have to be circular, if the space is reasonably isotropic

4.2 Estimating subsurface structure from phase velocity

4.2.1 Procedure for estimating subsurface structure

Rayleigh wave microtremors are generally dominated by the fundamental mode, and higher mode components are rarely dominant. In theory, the dispersion property of Rayleigh waves can be solved only for parallel layers. Considering these restrictions, the following assumptions are made for estimating subsurface structure of a layered earth:

Assumption 1. The phase velocity obtained from observation of microtremors is that of the fundamental mode of Rayleigh waves.

Assumption 2. The structure under the array of observation is parallel.

At present (1999), a general method for directly obtaining the P- or S-wave velocity structure for a given phase velocity of Rayleigh waves is yet to be developed. Therefore, to estimate subsurface structure from a given phase velocity, we must rely on past experience, at least in the earlier stage of interpretation. The procedure is, roughly,

1) Calculate the phase velocity for an assumed S-wave velocity structur of several layers with reference to available data
2) Refine the model parameters to match the phase velocity calculated fron observation

The initial assumption and subsequent refinement of the model have to b performed manually.

When the manual iteration of procedures (1) and (2) reaches maximun improvement of the model, the following inversion algorithm can be used fo further refinement. The inversion process uses the final manual model as th initial input and refines it in a layer-by-layer manner. The refinement algorithn is, in principle, no different from the manual iteration:

1) Find the difference between the calculated and observed values of phas velocity for a variety of frequencies and subsurface structures
2) Estimate the modified parameters required to refine the subsurfac layered-earth model
3) The modified parameters are used for the next iteration

Processes (1) to (3) are repeated until the difference between the calculatec and observed values of phase velocity becomes smaller than a certain value.

4.2.2 Inversion

There are many methods for calculating the phase velocity of Rayleigh wave from a layered-earth model. Here a method by Schwab and Knopoff (1972) is introduced. The parameters required for calculation of phase velocity are number of layers (N), P-wave velocity (v_p), S-wave velocity (v_s), density (ρ) and thickness (h) of each layer. The phase velocity c is expressed as a functior of the subsurface parameters as shown in equation (4.2), shown again below:

$$c = c\left(f; v_{p1}, v_{s1}, \rho_1, h_1; v_{p2}, v_{s2}, \rho_2, h_2; \ldots v_{pN}, v_{sN}, \rho_N\right). \qquad (4.2)$$

By applying Taylor's expansion to equation (4.2) and removing terms of second order and higher, the difference between the observed phase velocity and that calculated for a model can be approximated by a first order partial differential equation. Consider c_i^{obs} and c_i^{cal} to be observed and calculated phase

velocity for ith frequency on an N layer model, respectively:

$$\begin{aligned}\Delta c_i &= c_i^{obs} - c_i^{cal} \\ &= \sum_{j=1}^{N}\left(\frac{\partial c_i}{\partial v_{pj}}\Delta v_{pj} + \frac{\partial c_i}{\partial v_{sj}}\Delta v_{sj} + \frac{\partial c_i}{\partial \rho_j}\Delta \rho_j\right) + \sum_{j=1}^{N-1}\frac{\partial c_i}{\partial h_j}\Delta h_j \\ & \qquad i = 1, 2, \ldots, M, \end{aligned} \tag{4.6}$$

where the partial derivatives such as $\partial c_i/\partial v_{pj}$ are calculated for the model. When phase velocities are obtained for M frequencies, M simultaneous equations of equations (4.6) are solved for $4N-1$ variables by the method of least squares. The model is refined by using this solution as the next input. Therefore, it is required that the number of the known phase velocities M has to be greater than the number of variables $4N-1$, i.e., $M > 4N-1$. However, simply having the number of variables satisfying this condition is not enough; the range of frequencies for which the phase velocities are known must be influenced by the structure down to the Nth layer. For these restrictions, a reduction of the number of parameters is desired prior to the inversion. In practice, two constraints are added to the model:

Condition 1: thickness of the layer h is fixed prior to inversion.

Condition 2: v_p and ρ are assumed to be functions of v_s which is generally known.

For condition 2, for example, results shown in Figure 2 and Figure 6 (pages 212 and 214, respectively) in *Geophysical Exploration—A Pictorial* (SEGJ, 1989) can be used. Equation (4.6) is simplified as

$$\begin{aligned}\Delta c_i &= \sum_{j=1}^{N}\left[\left(\frac{\partial c_i}{\partial v_{pj}}\right)\frac{dv_{pj}}{dv_{sj}} + \left(\frac{\partial c_i}{\partial v_{sj}}\right) + \left(\frac{\partial c_i}{\partial \rho_j}\right)\frac{d\rho_j}{dv_{sj}}\right]\Delta v_{sj} \\ & \qquad i = 1, 2, \ldots, M, \end{aligned} \tag{4.7}$$

and $\Delta v_{sj} (j = 1, 2, \ldots, N)$ are the only unknown independent variables. In short, only the S-wave velocity structure is the variable directly estimated from the phase velocity of the observed Rayleigh wave.

The damped least-squares method (Marquardt, 1963) is available to solve equation (4.7). It is explained in the following section.

4.2.3 Estimating adjustment parameters

To calculate the adjustment parameters for a subsurface structure, first, equation (4.7) is rewritten in matrix form:

$$\mathbf{P} = \mathbf{GV_S}, \tag{4.8}$$

where $\mathbf{P}$ is a column vector consisting of M residuals of phase velocities in equation (4.7), $\mathbf{G}$ is a coefficient matrix of $M \times N$ for the model, and $\mathbf{V}$ is a column vector of N unknown parameters. The least squares solution of equation (4.8) $\hat{\mathbf{V}}_\mathbf{S}$ is given as

$$\hat{\mathbf{V}}_\mathbf{S} = \left(\mathbf{G}^\mathrm{T}\mathbf{G}\right)^{-1}\mathbf{G}^\mathrm{T}\mathbf{P}, \tag{4.9}$$

where $\mathbf{T}$ denotes the transposed matrix. The least-squares solution $\hat{\mathbf{V}}_\mathbf{S}$ is obtained to minimize the square sum of the residual:

$$|\mathbf{e}|^2 = (\mathbf{P} - \mathbf{GV_S})^\mathrm{T}(\mathbf{P} - \mathbf{GV_S}). \tag{4.10}$$

In equation (4.9), the normalized equation matrix $\mathbf{G}^\mathrm{T}\mathbf{G}$ often become singular or close to it, which makes the solution of equation (4.9) unstable. In such a case, a stable solution is obtained using the damped least-square method developed by Marquardt (1963). This method tries to minimize the following value in place of equation (4.10):

$$(\mathbf{P} - \mathbf{GV_S})^\mathrm{T}(\mathbf{P} - \mathbf{GV_S}) + \mathbf{V_S^T}\Theta\mathbf{V_S},$$

where

$$\Theta = \begin{bmatrix} \sigma^2/\sigma_1^2 & 0 & \cdots & 0 \\ 0 & \sigma^2/\sigma_2^2 & \cdots & 0 \\ \vdots & \vdots & \ddots & \vdots \\ 0 & 0 & \cdots & \sigma^2/\sigma_N^2 \end{bmatrix}, \tag{4.11}$$

which is a weighting matrix. The σ^2 is the variance of the residuals defined by the square sum of residuals divided by the degree of freedom, i.e.,

$$\sigma^2 = (\mathbf{P} - \mathbf{GV_S})^\mathrm{T}(\mathbf{P} - \mathbf{GV_S})(M-N)^{-1}. \tag{4.12}$$

The σ_j^2 is the variance of the jth component of the solution. Here σ/σ_j is called the damping factor.

The solution by this method is given as the following equation in place of equation (4.9):

$$\hat{\mathbf{V}}_\mathbf{S} = \left(\mathbf{G}^\mathrm{T}\mathbf{G} + \Theta\right)^{-1}\mathbf{G}^\mathrm{T}\mathbf{P}. \tag{4.13}$$

The relationship between $\hat{\mathbf{V}}_\mathbf{S}$, the solution by equation (4.13), and $\mathbf{V}_\mathbf{S}$, the true solution, is given as

$$\hat{\mathbf{V}}_\mathbf{S} = \mathbf{R}\mathbf{V}_\mathbf{S}, \tag{4.14}$$

where $\mathbf{R}$ is called resolution matrix and it is obtained from equations (4.8) and (4.13):

$$\mathbf{R} = \left(\mathbf{G}^\mathrm{T}\mathbf{G} + \Theta\right)^{-1}\mathbf{G}^\mathrm{T}\mathbf{G}. \tag{4.15}$$

When $\mathbf{R}$ is identical to unit matrix $\mathbf{I}$, the solution is unique and the components of $\hat{\mathbf{V}}_\mathbf{S}$ and $\mathbf{V}_\mathbf{S}$ have one to one correspondence. However, when $\mathbf{R}$ is far from $\mathbf{I}$, the solution $\hat{\mathbf{V}}_\mathbf{S}$ is no longer unique. Accordingly, R_{ii}, the ith diagonal element of $\mathbf{R}$, is called the resolution, which is an indicator of the reliability of the ith solution.

When the data are independent of each other and their variance is σ^2, the covariance matrix $\mathbf{C}$ can be written as

$$\mathbf{C} = \sigma^2\mathbf{R}\left(\mathbf{G}^T\mathbf{G} + \Theta\right)^{-1}, \tag{4.16}$$

and the ith diagonal element C_{ii} gives the variance σ^2 of the ith element of the solution for equation (4.11).

4.2.4 Calculation procedure

When the adjustment parameters are obtained by the method described in the last section, the layered-earth model is corrected using them. The calculation then is repeated with the corrected model and a new set of adjustment parameters is obtained. In this iteration, when σ, the square root of the variance, becomes smaller than a certain value and the resolution R_{ii} reaches greater than a certain threshold, the iteration is terminated and the solution is regarded as having converged. Note the number and thickness of the layers, N and h_j, are given as predetermined values to reduce the number of parameters, and are not adjusted through the iteration.

In practice, the procedure for the calculation is as follows:

1) Establish the limit of depth estimation as half of the maximum wavelength calculated from the phase velocity of the observed data set.

2) The number and thickness of layers, N and h_j, are set. The maximu value of N should be around half of the number of data points. T thickness h_j may be set as equal divisions of the limit of estimation, o may be chosen with fine intervals near the surface and coarse interv at depth.

3) Assign an S-wave velocity v_s, an unknown parameter, to each layer. Tl initial model is determined by referencing the statistical v_s data for t lithology of the top and bottom layers and roughly interpolating for t layers between.

4) An alternative and quite effective method of creating the initial mod is as follows: Calibrate the known phase velocity as a function of wav length, so that each phase velocity is assigned as an S-wave to t layer at a depth of half the corresponding wavelength. By exami ing this spatial distribution of S-wave velocity, several S-wave velo ity boundaries may be seen as large velocity contrasts. These veloci boundaries can be used as formation boundaries of the initial veloci model, and smoothed v_s values between the boundaries are assigned t the layer.

5) A preliminary inversion is performed on this initial model. If there a adjacent layers with similar velocities, then these layers are combine into one. On the other hand, if there is a layer boundary with poor res lution, then combine the layers above and below to form one layer, eac of one velocity. This should make the number of layers appropriate t the precision of the calculation. This inversion is iterated.

6) When the above convergence conditions are satisfied, the model is r garded as final.

In practice, the resolution of the shallowest layer often does not improv In such a case, the calculation must be performed with a fixed velocity for th first layer.

4.2.5 Effective variables for refining a model

During the inversion, among the unknown parameters of equation (4.($\left(\Delta v_{pj}, \Delta v_{sj}, \Delta\rho_j, \Delta h_j\right)$, only Δv_{sj} is independent due to conditions 1 and 2 Therefore equation (4.7) is used in the inversion. This approximation fc

performing the calculation is not always appropriate; however, in many cases, numerical experiments have confirmed that the variation of phase velocity of a Rayleigh-wave is most sensitive to that of the S-wave velocity. This means that among the quantities known as partial derivatives of phase velocity for the unknown parameters of equation (4.6) $(\partial c_i/\partial v_{pj})$, $(\partial c_i/\partial v_{sj})$, $(\partial c_i/\partial \rho_j)$, the second term is the largest by an order of magnitude in most cases. Therefore the contribution of the first and the third terms are very small, and the S-wave velocity acts as the most important parameter in the inversion. Thus it follows that the most reliable parameters gained from the phase velocity of a Rayleigh wave are the S-wave velocities of the layers.

Chapter 5

Data acquisition and analysis methods

This chapter discusses the methods of acquisition and analysis of microtrer data suitable for the detection of surface waves by the frequency-wavenum (f-k) method and the spatial autocorrelation (SPAC) method.

The f-k method requires a relatively large number of observation static Therefore, its field effort is more intensive than for the SPAC method. At same time, the spatial extent of the array becomes larger than that of SPAC method, resulting in the violation of the assumption of "horizo layers." However, when there are several dominant modes of surface wave the microtremors, or when it contains strong body waves, this method th retically has the potential to separate these waves. Additionally, by this metl the direction of the source of the wave can be estimated, and the phase velo of waves of a wide frequency range can be obtained.

The SPAC method is simpler in field data acquisition and data ana sis than the f-k method. Using an array of three-component seismomet the SPAC method can separate Rayleigh and Love waves. However, wl higher-mode surface waves are mixed in the data, the SPAC method can separate the fundamental-mode surface wave. Such a case is rather rare, where such a condition exists, the f-k method is available.

5.1 Observing microtremors

5.1.1 Observation array

5.1.1.1 For the *f-k* method

More flexibility is allowed in array design for the *f-k* method than for the SPAC method. The ideal array spread should have a large lateral extent with varied distance between seismometers. In general, topography and other constraints on seismometer location dictate the shape and size of the array. By considering the data analysis process, and taking the possibility of later application of the SPAC method into account, a desired array configuration would be a seismometer at the center of a spread with other seismometers arranged to form equilateral triangles of various sizes concentric with the central station.

A larger number of observation stations provides greater precision in the *f-k* spectra. For example, the gigantic LASA in America deploys 525 seismometers in the array with a diameter of about 200 kilometers. However, considering restrictions in station setting and analysis time, around ten seismometers may be a practical number for the purpose of exploring subsurface structure.

5.1.1.2 For the SPAC method

The observation array to collect data for analysis by the SPAC method requires, as seen in Figure 5.1 for example, at least four seismometers, three of them arranged on a circle of radius r and one at the center. It is expected that a larger number of seismometers will give a better result.

If the three stations on the circle form a equilateral triangle, the directional calculation becomes simpler, and the distance r in (3.80) can take two values,

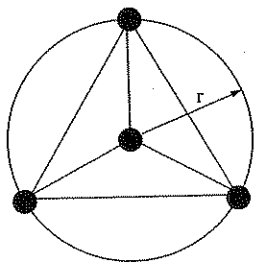

Figure 5.1. A four-point array.

i.e., the radius r and the length of the side of the equilateral triangle $\sqrt{3}r$. two or more arrays with different r are spread at the same location, a wid range of phase velocity can be estimated.

The extended spatial autocorrelation method does not require an equila eral triangle array, and it allows an array similar to the frequency-wavenumb method.

5.1.2 Data acquisition system

There are two types of data acquisition systems: one with all the stations an array connected and recorded with a multichannel recorder, and the oth with each station recorded independently.

The former system has the advantage that no time correction is necessar since all the stations are recorded against the same clock. This system is we suited to a small array, for estimation of shallow structure. However, there a operational disadvantages for large arrays; the difficulty of wiring restric selection of station sites, and the requirement for maintenance of the wi throughout the observation.

The second system requires time calibration among the stations, for e ample, by using a GPS clock installed in each recorder to synchronize t records. However, it imposes little restriction in selection of the station site Considering all the advantages and disadvantages, the independent syste seems more suited to the recording of microtremors.

Finally, it is desirable for the data to be in digital form to facilitate da processing.

5.1.3 Time for data collection

The time of day for data collection, i.e., day or night, does not affect the conte of the data. However, it is best to avoid areas subject to noise, e.g., areas wi heavy traffic which disturbs the stationarity of microtremors required for dat Data for many of the examples in this book were collected at night, the reaso being that there is little unstable cultural noise at night, and the microtremo as a stationary process dominate in the data.

The data length is typically forty-five minutes to one hour for long perio microtremors. However, thirty minutes may be sufficient for microtremo with a period shorter than one second.

Microtremor data recorded at independent stations require some preprocessing. One of the requirements is synchronization of each station.

5.2 Data analysis

5.2.1 Data analysis by frequency-wavenumber method

Figure 5.2 is a data processing flow chart using the frequency-wavenumber method. Since the theory of the data analysis was explained in Chapter 3, only the practical data processing sequence is presented here.

It is believed that the MLM is superior to the BFM in detecting surface waves from microtremor records. Therefore, this chapter follows the data analysis sequence of the MLM.

Equation (3.33) gives $P'(\mathbf{k}, \omega)$, the estimated f-k power spectrum. Following Capon (1969), this may be transformed as

$$P'(\mathbf{k}, \omega) = (\mathbf{a}^T \boldsymbol{\Phi} \mathbf{a}^*)^{-1} \tag{5.1}$$

or

$$P'(\mathbf{k}, \omega) = \left\{ \sum_{i=1}^{N} \sum_{j=1}^{N} \phi_{ij}(\omega) \exp[i\mathbf{k}(\mathbf{r}_i - \mathbf{r}_j)] \right\}^{-1}$$
$$= \sum_{i=1}^{N} \sum_{j=1}^{N} A_i^*(\mathbf{k}, \omega)\ A_j(\mathbf{k}, \omega)\, \hat{S}_{ij}(\omega) \exp[i\mathbf{k}(\mathbf{r}_i - \mathbf{r}_j)], \tag{5.2}$$

where

$$A_i(\mathbf{k}, \omega) = \frac{\sum_{j=1}^{N} q_{ij}(\mathbf{k}, \omega)}{\sum_{i=1}^{N} \sum_{j=1}^{N} q_{ij}(\mathbf{k}, \omega)}, \tag{5.3}$$

and $q_{ij}(\mathbf{k}, \omega)$ is an element of the inverse matrix of matrix

$$\{\hat{S}_{ij}(\omega) \exp[i\mathbf{k}(\mathbf{r}_i - \mathbf{r}_j)]\}.$$

$A_i(\mathbf{k}, \omega)$ is called the optimum weighting function which is a kind of optimization filter. This filter passes the plane waves with a velocity corresponding to the peak of the f-k spectra, and attenuates waves with other velocities.

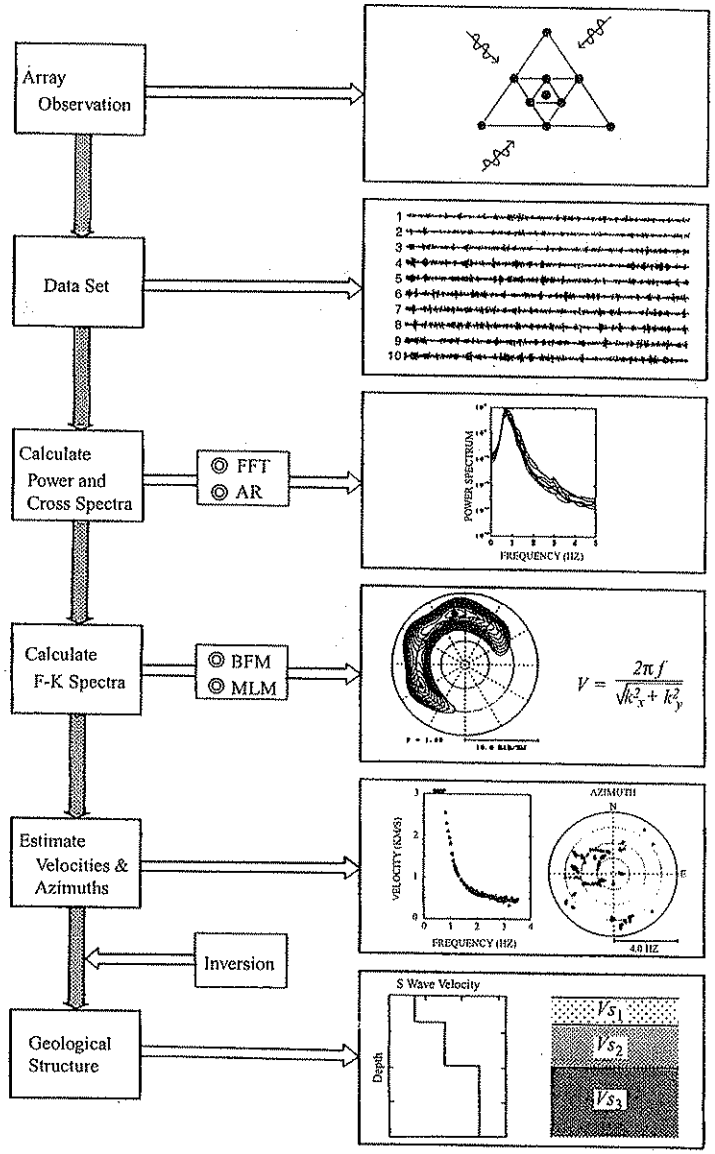

Figure 5.2. Flow of data analysis by the f-k method.

The vector **a** in equation (5.1) is of the form

$$\mathbf{a}^T = \{\exp(i\mathbf{kr}_1), \exp(i\mathbf{kr}_2), \ldots, \exp(i\mathbf{kr}_N)\}, \tag{5.4}$$

and * denotes the complex conjugate. The parameters are:

N: number of stations

$\hat{S}_{ij}(\omega)$: estimated cross-spectrum between the signals at the ith and jth stations for the angular frequency $\omega = 2\pi f$

$\mathbf{r}_i$: The position of the ith station

The calculation of the cross-spectra of equation (5.2), as described in Chapter 3, uses the direct Fourier transform, or the block averaging method. Smoothing of the raw spectra is required for the direct Fourier transform. The Parzen window, shown below, can be used for smoothing:

$$W(f) = \frac{3}{4}u\left(\frac{\sin\frac{\pi uf}{2}}{\frac{\pi uf}{2}}\right)^4, \tag{5.5}$$

where u is a constant in seconds. Figure 5.3 shows the shape of this window. In the figure, b is the resolution bandwidth and is given as:

$$b = \frac{1}{\int_{-\infty}^{\infty} W^2(f)\,df}. \tag{5.6}$$

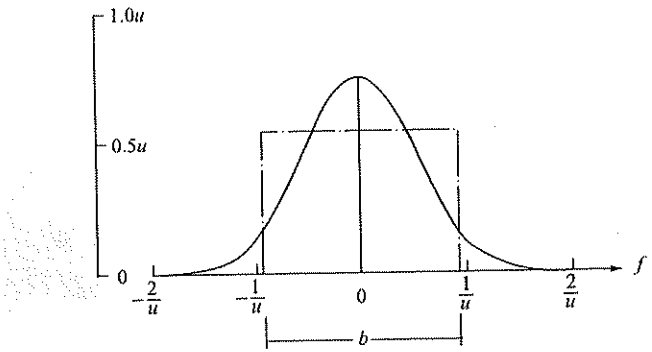

Figure 5.3. Parzen window (from Ohsaki, 1976).

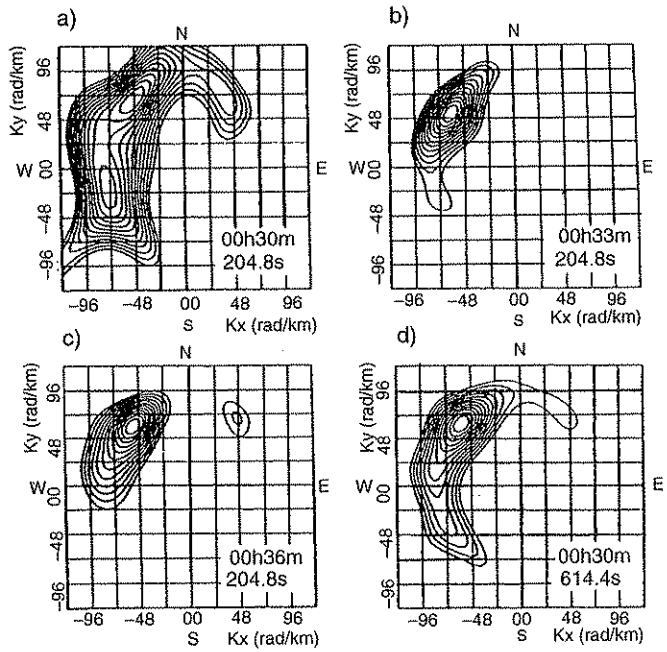

Figure 5.4. The f-k spectra at 0.833 Hz. Data lengths are 204.8 s for (a), (b), and (c); 614.4 s for (d).

Smoothing of the raw spectra $S(f)$ is performed by

$$\hat{S}(f) = \int_{-\infty}^{\infty} S(f)\cdot W(f-g)\,dg. \tag{5.7}$$

Figure 5.4 shows the f-k spectra at 0.833 Hz in frequency (Matsushima and Okada, 1989) of microtremors observed by eight stations that formed an array of 2 km by 1 km on the campus of Hokkaido University. Setting the maximum amplitude to be 0 dB, and contoured to –12 dB with a contour interval 1dB. This figure shows the temporal variation of the spectra by using three data sets, each 204.8 s long, lagged by 3 min (a, b, and c) and the spectra calculated from the longer 614.4-s record. The shorter records show some variation in spectra, but the position of the peak is approximately the same regardless of the time of observation. In this calculation, the resolution band of the Parzen window was set to $20\Delta f$,where Δf is the frequency interval of the cross-spectra.

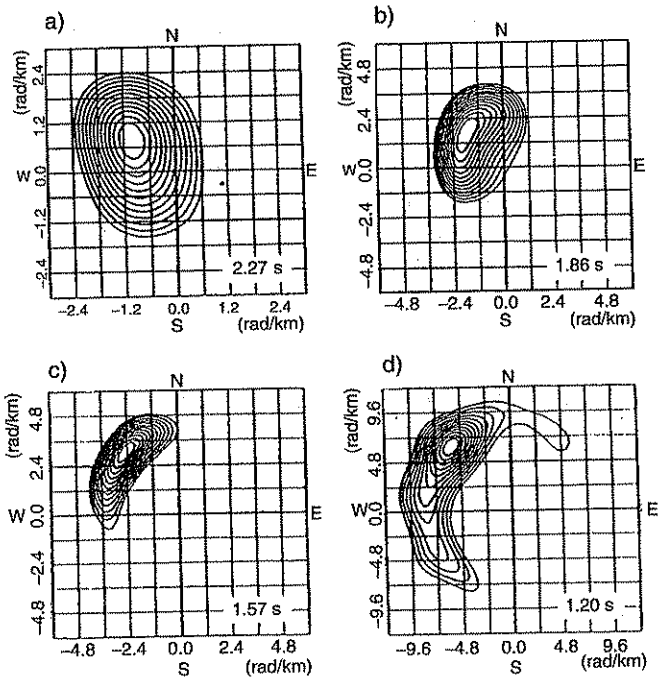

Figure 5.5. The f-k spectra of four different periods: 2.27, 1.86, 1.57, and 1.20 s (corresponding frequency 0.440, 0.538, 0.637, and 0.833 Hz, respectively).

Figure 5.5 shows examples of the f-k spectra for four different periods, 2.27, 1.86, 1.57, and 1.20 s (i.e., 0.440, 0.538, 0.637, and 0.833 Hz in frequency, respectively) calculated from the same data as Figure 5.4. Such f-k spectra can be calculated for a wider range of frequencies at a finer interval. Then the phase velocity of the dominant wave with each frequency component can be obtained by reading the coordinates of the peak spectrum (k_{x_0}, k_{y_0}) of each frequency in each plot. Note the frequency interval cannot be finer than the resolution bandwidth of the smoothing window, $20\Delta f$.

5.2.2 Data analysis by spatial autocorrelation method

The work flow for data analysis by the spatial autocorrelation method is shown in Figure 5.6. The theory of the analysis was explained in Chapter 3, and several problems in practical data analysis are presented in this section.

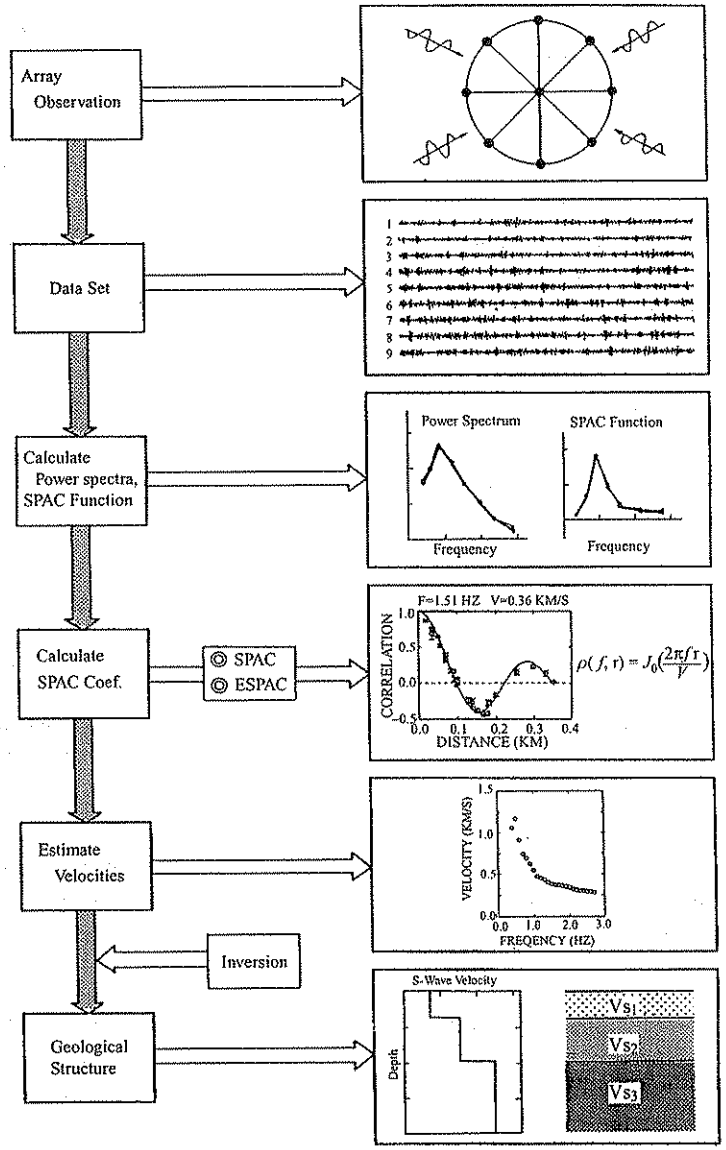

Figure 5.6. Flow of data analysis by the SPAC and ESPAC methods.

5.2.2.1 Standardization of the spatial autocorrelation function

In observing microtremors with a circular array, it is ideal for all the seismometers and recorders to have identical properties, such as frequency response. In addition, it is desirable that the conditions of installation of seismometers, e.g., coupling with the ground, be the same. In practice, it is rare to have such an ideal situation. Usually the frequency characteristics of seismometers and recorders vary, and conditions of installation may be different from place to place. When calculating the spatial autocorrelation function under such circumstances, it is necessary to standardize the spatial autocorrelation function (3.77) by the power spectra density function of each station. In other words, the spatial autocorrelation coefficient should be calculated by

$$\rho(\omega_0, r) = \frac{1}{2\pi}\int_0^{2\pi} \frac{\hat{S}(\omega_0, r, \theta)}{\sqrt{\hat{S}_0(\omega_0)\,\hat{S}_r(\omega_0)}} d\theta, \tag{5.8}$$

where

$$\begin{aligned} \hat{S}(\omega_0, r, \theta) &= \mathrm{E}[\hat{X}(t, \omega_0, 0, 0)\,\hat{X}(t, \omega_0, r, \theta)], \\ \hat{S}_0(\omega_0) &= \mathrm{E}[|\hat{X}(t, \omega_0, 0, 0)|^2], \\ \hat{S}_r(\omega_0) &= \mathrm{E}[|\hat{X}(t, \omega_0, r, \theta)|^2]. \end{aligned} \tag{5.9}$$

In equation (5.9), $\hat{X}(t, \omega_0, 0, 0)$ and $\hat{X}(t, \omega_0, r, \theta)$ are the records of components with the frequency ω_0 at the central station (0,0) and the station (r,θ), respectively. Through the characteristics of the recording system and ground conditions, the original microtremors at the ith station X_i is magnified by a_i times and recorded as $\hat{X}_i$ $(= a_i X_i)$, where a_i is a constant independent of frequency, and the spectral density function is assumed to be constant throughout the array, i.e.,

$$E\left[|X(t, r, \theta)|^2\right] = \text{const.} \tag{5.10}$$

In short, the spatial autocorrelation coefficient of equation (5.8) is a directional (or azimuthal) average of the coherency between the records at the center and at the circumference of the circular array for a certain frequency ω_0.

5.2.2.2 The size of sample N and the analysis interval T_r

There is no standard for the size of sample, i.e., the length of the data segment for analysis. It is chosen based on the required precision for the estimated

value. It may be practical to decide these values by considering parameters such as the highest expected frequency (f_N), standard error of the power spectrum (ε_r), the resolution bandwidth desired in the power spectrum analysis (B_e), etc. However, the size of the sample may be dictated by other factors such as limitation in the length of the record and precision of observations. Exceptional cases aside, the following relationships may be used as rules of thumb in data processing, using the power spectra analysis method (Bendat and Piersol, 1986):

5.2.2.2.a For calculating the estimated value of the power spectra from the estimated autocorrelation function. *Lag in correlation function*: The maximum lag number m is chosen by

$$m = \frac{1}{B_e h} \qquad (h = \Delta t), \tag{5.11}$$

where B_e is the desired resolution bandwidth in the power spectra analysis.

Sample size and time window for analysis: The size of the sample size N is chosen by

$$N = \frac{m}{\varepsilon_r^2}, \tag{5.12}$$

where ε_r is the standard error desired in the calculation. The corresponding minimum window for analysis (i.e., minimum record length) T_r is

$$T_r = Nh = N\Delta t. \tag{5.13}$$

Degree of freedom and standard error: The degree of freedom n is given by

$$n = 2B_e T_r = \frac{2N}{m}, \tag{5.14}$$

and the standard error is

$$\varepsilon_r = \sqrt{\frac{1}{B_e T_r}} = \sqrt{\frac{m}{N}}. \tag{5.15}$$

Therefore, when N is constant, a smaller m gives a smaller ε_r.

5.2.2.2.b For calculating the estimated power spectra by the Fourier transform. Here, the commonly used smoothing in the frequency domain is assumed. When the spectra are white noise within a limited range, the estimated spectra at the frequency interval of $1/T_r$ essentially have no correlation. Therefore, when l frequency components near the estimated values of the raw spectra are averaged, the smoothed estimate value of the spectra $\hat{G}_k$ results in

$$\hat{G}_k = \frac{1}{l}\left[\bar{G}_k + \bar{G}_{k+1} + \cdots + \bar{G}_{k+l-1}\right]. \tag{5.16}$$

This $\hat{G}_k$ is a χ^2 variable with degree of freedom approximately $n = 2l$ by the addition theorem of χ^2 of independent variables. The resultant effective resolution bandwidth is approximately $B'_e = lB_e$, where $B_e = 1/T_r$. Therefore this averaging in the frequency domain gives

$$B'_e = lB_e = l/T_r = l\Delta f; \tag{5.17}$$

$$N = 2B'_eT_r = 2l. \tag{5.18}$$

The standard error is

$$\varepsilon_r = \sqrt{\frac{1}{B'_eT_r}} = \sqrt{\frac{1}{l}}. \tag{5.19}$$

The estimated value $\hat{G}_k$ is considered to represent the midpoint of the frequency range from f_k to f_{k+l-1}. Altogether N/l such estimated values are calculated.

5.2.2.3 Calculation of the phase velocity

When the spatial autocorrelation function method is used, the phase velocity at the array center is obtained by equation (3.80). From $x_0 = 2\pi f_0 r_0/c\,(f_0)$, the phase velocity for the frequency f_0 is

$$c\,(f_0) = \frac{2\pi f_0 r_0}{x_0}, \tag{5.20}$$

where x_0 is the variable of the Bessel function of the first kind of zero order. The value of the spatial autocorrelation coefficient ρ_0 is satisfied by x_0 for a certain frequency obtained from a dataset observed by a circular array of radius r_0.

In this case, there may be a frequency range in which the spatial autocorrelation coefficient does not satisfy the Bessel function due to errors in data

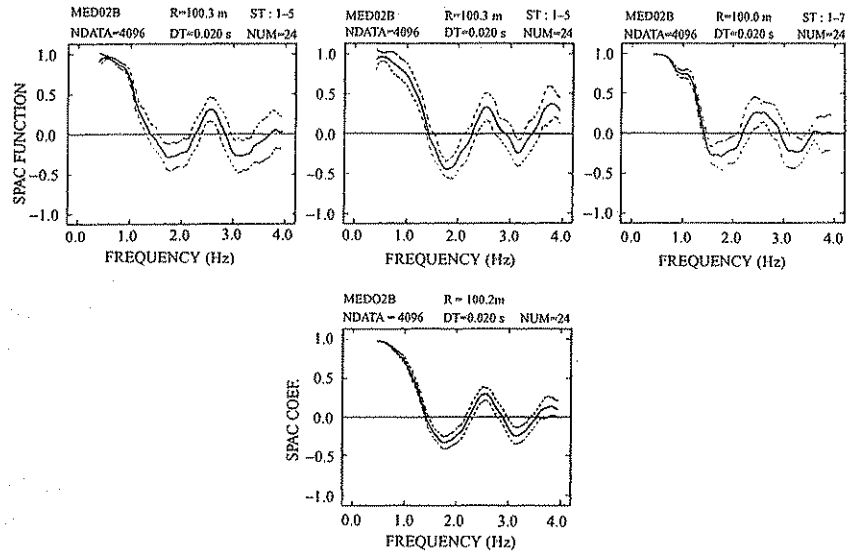

Figure 5.7. Top: the integrand in equation (5.8) (coherency); bottom: the result of the integration (5.8) (spatial autocorrelation coefficient).

acquisition and processing and insufficient power in the microtremors. Estimation is not possible in such cases. To fill the gap in the phase velocity, it may be necessary to reprocess using the data from a different time window or re-acquire data with a different array radius.

5.2.2.4 An example of spatial autocorrelation function

The data in this example were collected by the array shown in Figure 5.1. The example shown in Figure 5.7 is for $r = 100$ m. The three graphs on the top row of the figure show spatial covariance function $g\,(\omega, r, \theta)$ calculated from equation (3.67), each corresponding to the function for different directions from the center station to the three apex stations. These show coherency given by the integrand of equation (5.8). Here, a standardization is applied for plotting.

The spatial autocorrelation coefficient $\rho\,(\omega_0, r)$ is shown in the bottom row. Theoretically this should be the Bessel function of the first kind of zero order. In the high-frequency range, the maxima in the amplitudes of ρ tends to become smaller than the value of the Bessel function. This is because either

the power of the microtremors diminishes in that frequency range, severely reducing correlation, or it is affected by spatial aliasing due to the number of stations on the circumference. To increase precision in this area, it is necessary to employ a smaller array size or to increase the number of stations on the circumference.

5.2.3 Case history of estimating phase velocity

As discussed, during data acquisition for analysis by the spatial autocorrelation (SPAC) method, the arrangement of stations is often restricted, because it requires a special circular array. On the other hand, the extended spatial autocorrelation (ESPAC) method assumes that the spatial covariance function at a given frequency is approximately constant in every direction, eliminating the restrictions in observation and increasing freedom in array design. For example, a dataset collected for the *f-k* method can be analyzed by the ESPAC method. This section shows an example of the application of the ESPAC method to records of the vertical component of microtremors, collected by both a circular array and an arbitrary array. The aim here was to estimate the velocity of the Rayleigh wave with the ESPAC method, then compare the result with the *f-k* method. Also presented is an example of separating the Rayleigh and Love waves from the data acquired by a circular array of three-component seismometers.

5.2.3.1 Analysis of vertical component data from the circular array

Three-component microtremor data were collected in the Tokachi Plain in eastern Hokkaido, using three semicircular arrays of different radii (Figure 5.8, top right). The vertical component is used for the analysis in this example. The duration of observation is 45 min for the large array and 30 min for the medium and small arrays. Each array contains nine seismometers arranged in equal angle spacing of 22.5 degrees. The radii of the array are 180, 90, and 50 m.

In addition, two triangular arrays (array-L and array-S), of ten vertical-component seismometers, were used for data analysis by the *f-k* method. The size of the arrays is about 1100 and 400 m, respectively (Figure 5.8, bottom), and the record length is 45 min.

Figure 5.9a shows a sample of the microtremor data collected by the large semicircular array. Figure 5.9b is a 2500-s running power spectrum at Station 1 of the large array. From the running power spectrum, it is clear that the record of microtremors is very stable for the duration of the 2500-s sample. The

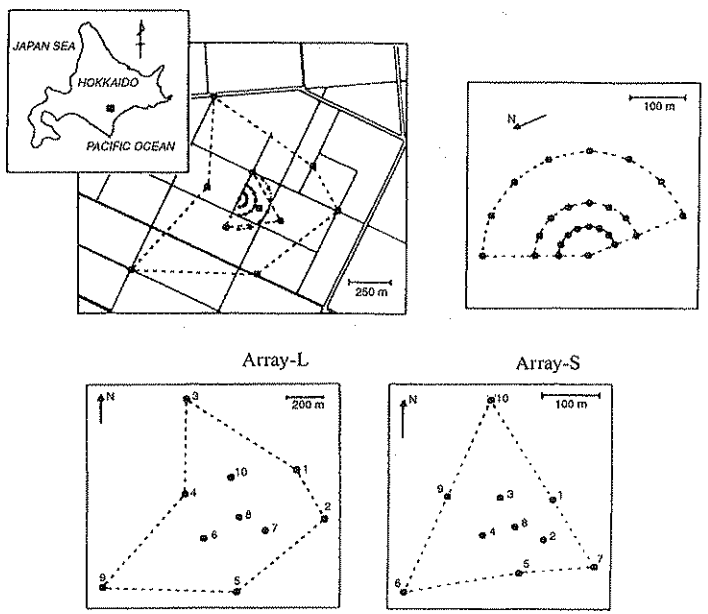

Figure 5.8. Various arrays used in microtremor observation in the Tokachi Plain, Hokkaido.

running power spectra of other stations, whose figures are not presented here, show very similar characteristics.

Three graphs, a, b, and c, in Figure 5.10 are the power spectra of microtremors recorded with the large, medium, and small arrays, respectively. They show that the power is characteristically high at about 0.4 Hz and 2.5 Hz, and low around 1.0 Hz. Two band-pass filters, centered at 1.0 Hz and 2.0 Hz, were separately applied to the records. The results are shown in Figure 5.11. Notice that while (b), with a 2.0-Hz filter, shows waves with good correlation among the stations, (a), with a 1.0-Hz filter, does not show obvious correlation. This suggests difficulty in estimating the phase velocity near 1.0 Hz.

Figure 5.12 shows examples of fitting the Bessel functions of the first kind of zero order to the $r \sim \rho(r)$ curves for $f = 0.5$, 1.5, and 2.5 Hz. In the figure, a, b, and c correspond to small, medium, and large arrays, respectively, while d is the sum of the three. As is well known, the precision of the calculation in fitting a Bessel function to the observed data is improved by increasing the number of stations.

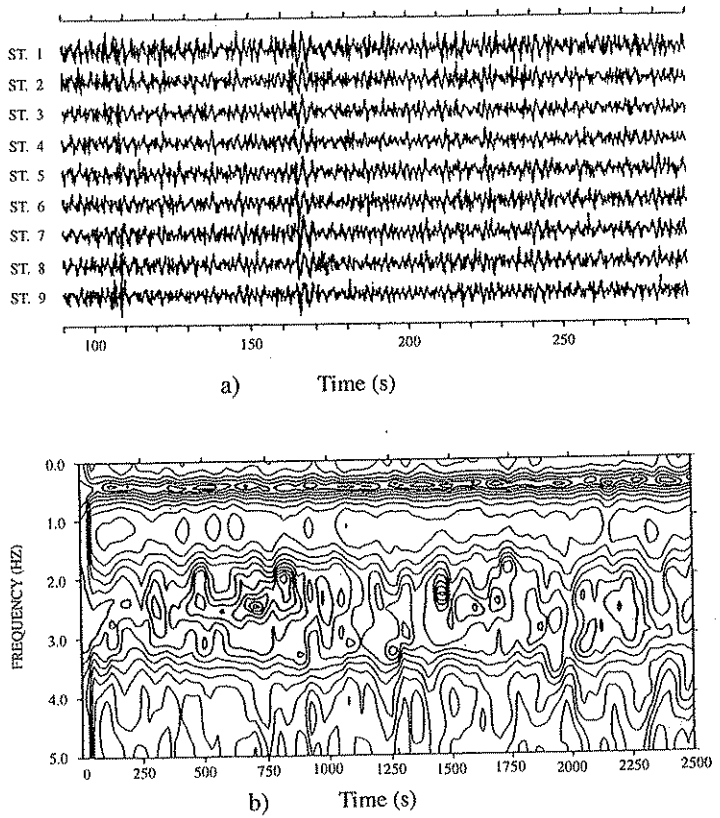

Figure 5.9. (a) A part of the microtremor record for the large semicircular array; (b) running power spectra of the whole record of the large array at station 1.

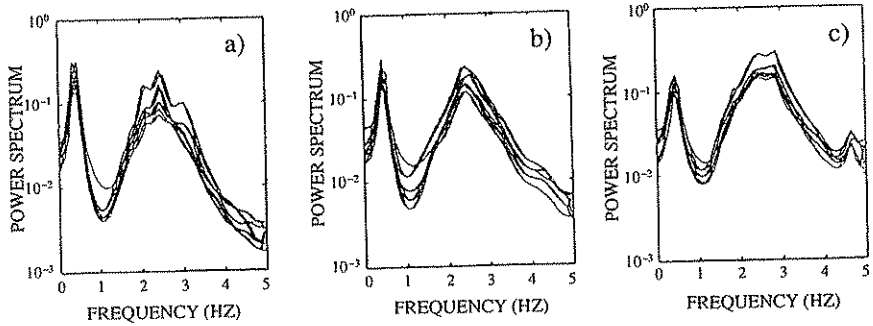

Figure 5.10. Power spectra of the three semicircular arrays.

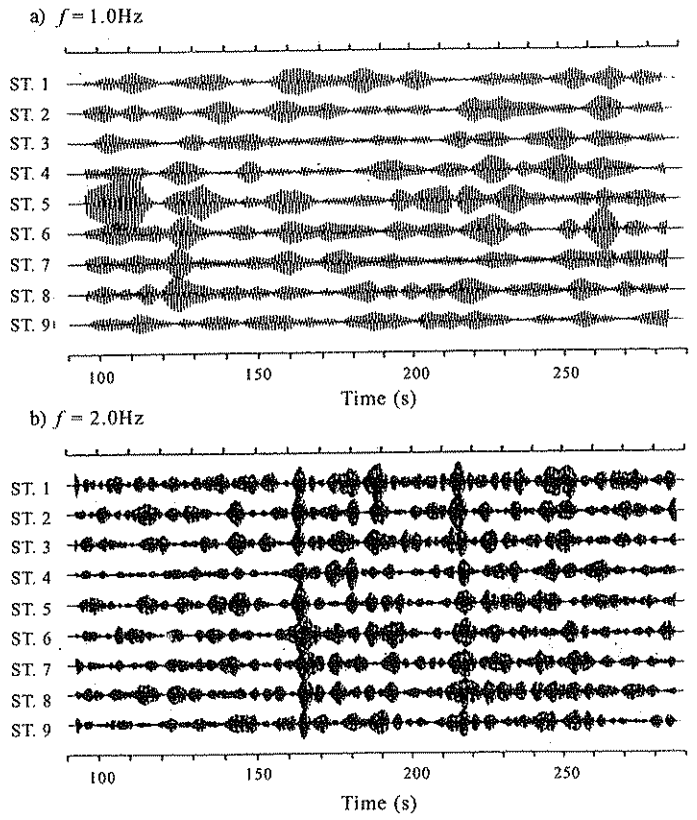

Figure 5.11. A part of the microtremor record collected by the large semicircular array processed through band-pass filters (the central frequencies are: (a) $f = 1.0$ Hz; (b) $f = 2.0$ Hz.

This method can use a combination of data from different arrays or recorded at different times, as long as the station is not moved. An example of combined data analysis using the records from three different arrays is shown in Figure 5.13, together with the Bessel function of best fit to $\rho(r)$. The velocity values shown on the top of the graphs are the estimated optimum phase velocities. As these graphs show, and as expected from the power spectra, the power is weak in the vicinity of 1.0 Hz (e.g., 0.8 ~1.2 Hz). So the result in this range is poor as the correlation is poor. However, one Bessel function fits almost all the other frequency ranges.

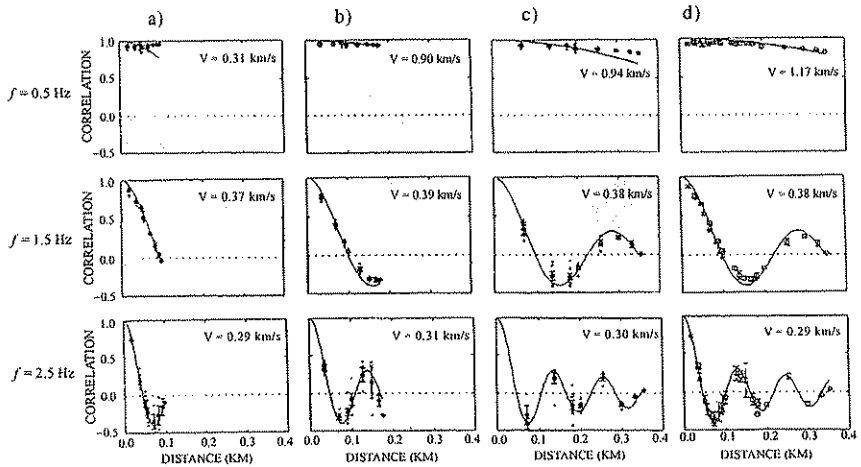

Figure 5.12. An example of fitting the Bessel function of the first kind of zero order to the spatial autocorrelation coefficient $\rho(r)$. (a) Small array, (b) medium array, (c) large array, and (d) a combination of the three arrays.

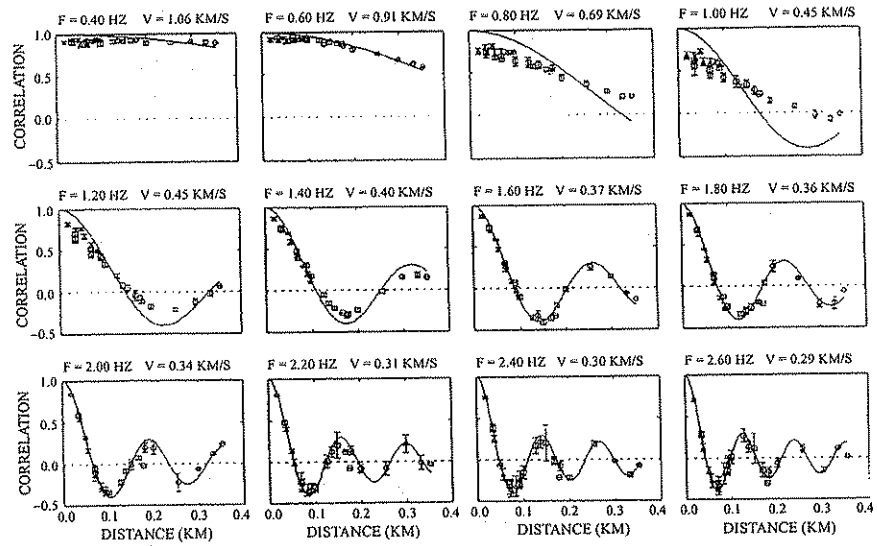

Figure 5.13. An example of combined processing of spatial autocorrelation coefficient from three semicircular arrays of different sizes. Triangles, squares, and circles are the spatial autocorrelation coefficients from the data recorded by the small, medium, and large arrays, respectively. Each graph shows the $r \sim \rho(r)$ curve for $f = 0.4, 0.6, \ldots,$ 2.6 Hz. The solid line is the Bessel function of best fit to $\rho(r)$.

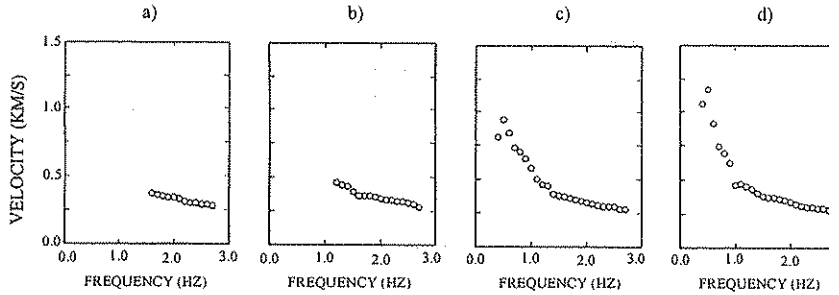

Figure 5.14. Phase velocity estimated by the ESPAC method, obtained by fitti Bessel functions to the $\rho(r)$ values from the data collected by the small array (a medium array (b), large array (c), and combination of the three arrays (d).

In the above example, a Bessel function was fitted to the observed da by the least-squares method, as it is theoretically expected and justified. Bu as seen in the examples, around 1Hz, the correlation coefficient general contains some noise. With the expectation that such cases will occur, futu processing methods will require a quantitative method to assess the appropr ateness of such solutions, and this is an example in which an inappropria value of velocity is obtained at 1Hz, when the spectral power is low.

As seen in the above example, an important characteristic of the ESPA method is that it can easily detect an inappropriate value, which is impossibl in the *f-k* method.

Figure 5.14 shows the estimated phase velocities obtained by fitting Bess functions to the $\rho(r)$ values from the data collected by the arrays of variou sizes.

Figure 5.15 is a comparison of these phase velocities estimated by th ESPAC method (circles) and by the *f-k* method (triangles). In the figur the ESPAC result is an estimate from the combination of the three arrays, whil the results from the *f-k* method for the small and large arrays are shown sepa rately. They are overplotted in the bottom row. From the figure, we can see tha

i) the results are coincident in the frequency range $f \geq 1.2$ Hz;

ii) both methods gave poor results near 1.0 Hz (0.8 Hz $\leq f \leq$ 1.2 Hz perhaps due to the lower power;

iii) in the range $f \leq 0.8$ Hz, the phase velocity from array-S (the size c which is similar to the large semicircular array) via the *f-k* method is

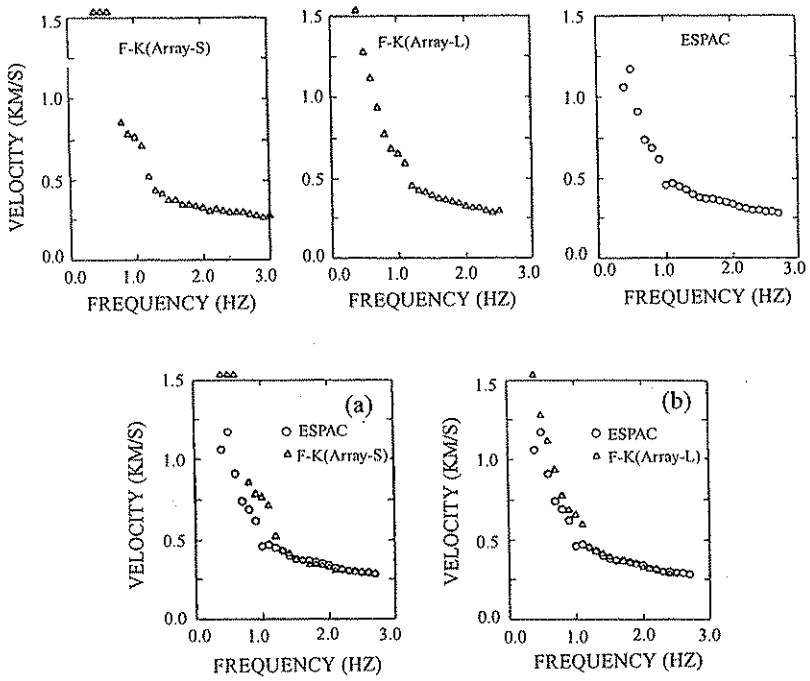

Figure 5.15. Comparison of phase velocities estimated by the ESPAC method and by the f-k method.

larger estimate than the one via the ESPAC method ($c \geq 1.5$ km/s). The reason for this is believed to be that this frequency range is outside the limit for which phase velocity can be estimated; a limit imposed by the size of the array.

By using Array-L (the size of which is about three times as large as the large semicircular array), a result similar to the ESPAC method is obtained. This demonstrates the superiority of the ESPAC method in estimating subsurface structure over the f-k method for arrays of the same size. This is concordant with the numerical simulation by Ling (1994).

In calculating $\rho(r)$ by equation (4.5), it is desirable to have an array with many widely spaced stations. A large number of stations allows a large number of pairs of stations with varying distance r and a wider distribution of azimuth. As a result, the subsurface structure can be estimated more

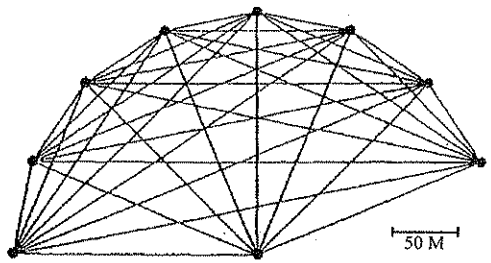

Figure 5.16. All the possible combinations of two stations.

precisely. In this case history, we had enough instruments for nine stations For this array, a diagram of all the possible pairs of stations is shown in Fig· ure 5.16. Table 1 summarizes the number of pairs and the azimuths for eacl possible distance between pairs of stations.

As seen in Table 1, the semicircular array provides a large number of pair: separated by the distance of the radius ($r = 180$ m) and a large number o: pairs of adjacent points ($r = 70$ m); the array's azimuth coverage approache: 180 degrees. Where the distance between stations is larger than the radius o: the array, there are fewer possible combinations and the azimuth coverage i: narrow. As a result, the accuracy of the spatial autocorrelation coefficient may suffer.

Table 5.1. All the possible combinations of two stations, distance betweer the stations, number of combinations and azimuth of the line connecting the stations.

r(m)	N	Angle (degree)							
70	7	−56.25	−33.75	−11.25	11.25	33.75	56.25	78.75	
138	6	−45.00	−22.50	0.00	22.50	45.00	67.50		
180	8	22.50	45.00	67.50	90.00	112.50	135.00	157.50	180.00
200	5	−33.75	−11.25	11.25	33.75	56.25			
255	4	−22.50	0.00	22.50	45.00				
299	3	−11.25	11.25	33.75					
333	2	0.00	22.50						
353	1	11.25							

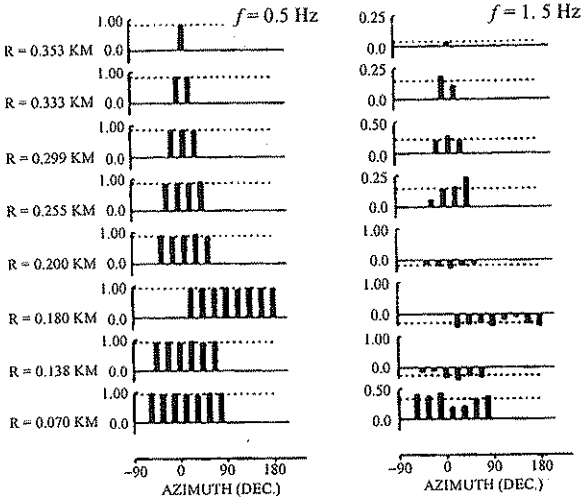

Figure 5.17. Spatial autocorrelation function calculated for all the combinations of stations for 0.5 and 1.5 Hz (sorted by distance).

Figure 5.17 shows the autocorrelation functions at $f = 0.5$ and 1.5 Hz plotted against the distance r of all the combinations of the stations. The dotted lines in the figure indicates the averages. Where an autocorrelation value is absent due to insufficient combinations for a particular r, the dotted line of the average assumes the missing value. This problem of dependency of azimuth coverage on r may be eliminated by using a circular array.

As discussed before, the ESPAC method allows the combination of several data sets obtained at different times. The example here demonstrates that the data sets observed at different times by the three arrays, small, medium and large, could lead to a Bessel function that fits a curve representing the spatial autocorrelation coefficient for the corresponding frequency. This shows that several data sets separated by a considerable time lag could be jointly analyzed by the ESPAC method. This is a merit of the ESPAC method that has not been available in previous methods. With the ESPAC method, even with only a few seismometers available, one can obtain the same result as that found with many seismometers, by repeating observations.

5.2.3.2 Analysis of data from the arbitrary array

The regular semicircular array discussed in the previous section may not be easily arranged at the desired site. In such a case, an arbitrary array may be

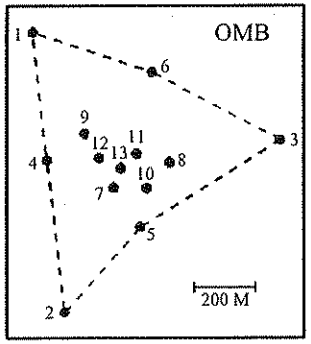

Figure 5.18. Arrangement of the stations of array OMB.

used by virtue of the ESPAC method. A range of distances $[r_0 - \Delta r, r_0 + \Delta r]$ is, in this case, represented by r_0. This section is a case history of thi application.

Figure 5.18 is a diagram of the observation array used in Oma, Aomor Prefecture, at the northern tip of Honshu Island. An analysis of these sam data with the *f-k* method has been shown in Chapter 3. A separate analysi by the ESPAC method is demonstrated here. For arbitrary arrays like this, th conventional SPAC method cannot be applied.

Figure 5.19 shows $r \sim \rho(r)$ curves for $f = 0.4, 0.6, \ldots 2.0$ Hz.

Figure 5.20 is a comparison between the ESPAC method and the *f-* method. It is clear from the figure is that the two results are almost identica for frequencies higher than 1.0 Hz, and the *f-k* method gives considerabl higher velocity at frequencies below 1.0 Hz. It is considered that the ESPAC method gives a velocity closer to the real value. However the *real* velocity i not independently known at this stage.

From the above, the following conclusions for the ESPAC method wer reached:

1. The ESPAC method gives the same result as the *f-k* method in the highe frequency range.
2. The ESPAC method is superior to the *f-k* method in that it
   a) gives a good stable result for the lower frequency ranges,
   b) the computation of the correlation function is simpler, and suitabl for a PC,

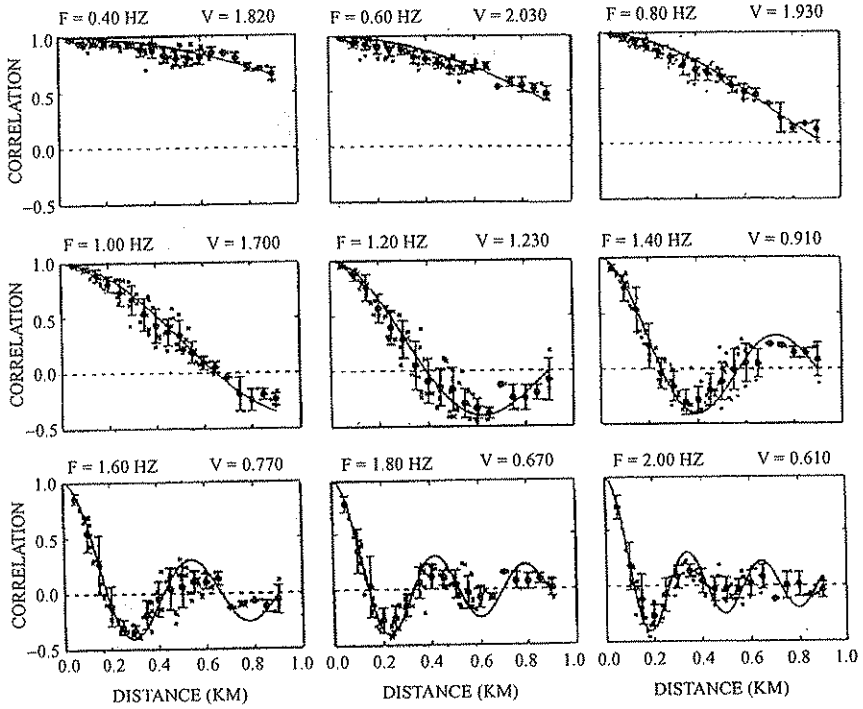

Figure 5.19. An example of fitting the Bessel function of the first kind of zero-order to the spatial autocorrelation coefficient from an arbitrary array. Symbols: the cross is the spatial autocorrelation coefficient calculated for each r_i; the circle is the spatial autocorrelation coefficient calculated and averaged over the distance $[r_0 - \Delta r, r_0 + \Delta r]$, where Δr is 40 m; the solid line is the best-fit Bessel function to $\rho(r)$.

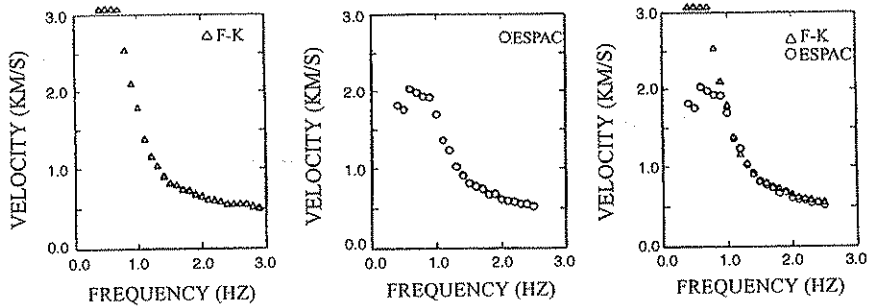

Figure 5.20. Comparison of phase velocities estimated by the ESPAC method and by the *f-k* method (data acquired by the array OMB).

c) a reasonable result can be obtained with fewer stations,

d) several data sets collected at different times can be jointly processe and

e) inappropriate values as calculated by the *f-k* method can be detect by the ESPAC method.

On the other hand, the ESPAC method cannot detect the direction of t source of the wave. Also, if there are surface waves of higher mode mixed with the data, the ESPAC method cannot detect it. In these respects, the *f* method is superior.

5.2.3.3 Analysis of data from the circular array with three-componen seismometers (identification of the Love wave)

In Section 3.5, we discussed how the SPAC method can detect the Love wa from three-component data while the *f-k* method cannot, and the theory ar the method was presented in Section 3.6. This section shows an example its application to long-period microtremor data in order to identify Love wa energy (Matsushima and Okada, 1990b).

The data were collected in a suburb of Hachinohe City, Aomori Prefe ture. Two datasets were collected with arrays of two different radii, 266 and 501 m. Each array comprised four stations of three-component sei mometers; one at the center and three on a circle with a 120-degree inte val. The horizontal-component seismometers are set to record north-sou and east-west components. Each dataset was collected for 46 min at nigh The relative location of the arrays is shown in Figure 5.21. The seismom ters are models PELS74V for the vertical component, and PELS74H for t horizontal component. Both have a natural period of 8 s.

The data were converted to the radial and tangential components, i.e., X_r and X_θ in the left-hand side of equation (3.81), respectively. Applying narro band-pass filters with various central frequencies to these and the vertic component data, the spatial autocorrelation coefficients, ρ_r and ρ_θ of equatio (3.96), were calculated.

Figure 5.22 shows the autocorrelation coefficients of the vertical, radi and tangential components of the data for the array of 868-m diameter (whic is the length of the sides of the triangle of the circle with the diameter

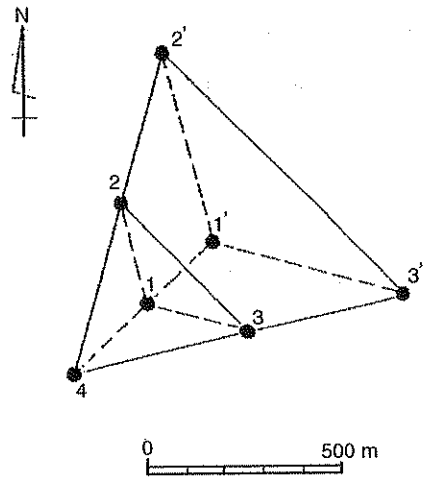

Figure 5.21. Arrangement of three-component seismometers to form two equilateral triangle arrays. The radii of the arrays are 266 m and 501 m.

501 m), plotted against the central frequency of the band-pass filter. The different symbols indicate the different components.

Figure 5.23 is the relationship between the phase velocity of the Rayleigh wave and its period calculated from the vertical component of microtremor records by various array radii using equations (3.78) or (3.80). In this graph the horizontal axis is converted to period from frequency. The symbols in the figure correspond to the radii of the array from which the phase velocities were calculated. The subsurface structure estimated from the relationship between the phase velocity and period is shown in Table 5.2.

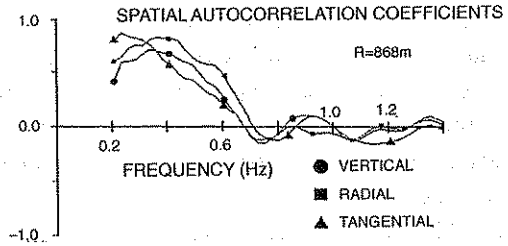

Figure 5.22. Spatial autocorrelation functions for an array with a radius of 868 m.

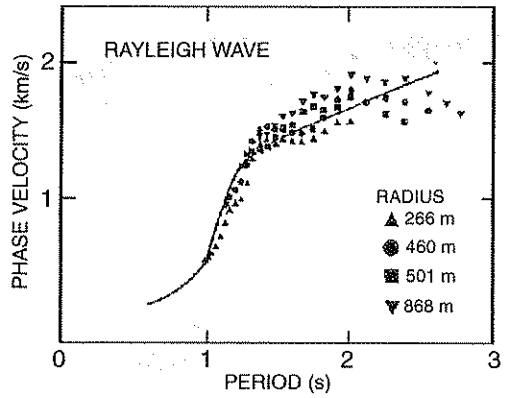

Figure 5.23. Phase velocities of Rayleigh waves obtained from the vertical compone of microtremors. The solid line indicates the theoretical phase velocity curve Rayleigh waves calculated for the structural model in Table 5.2.

The curve in Figure 5.23 is the phase velocity of the fundamental-moc Rayleigh wave theoretically calculated for the subsurface structure model Table 5.2.

Figure 5.24 shows the phase velocity of the Love wave plotted against i period, calculated by equation (3.98) from the spatial autocorrelation functic [equations (3.93), (3.94), and (3.95)], and using the parameter $\lambda(\omega, r)$ derive from equation (3.100).

The curve in Figure 5.24 is the phase velocity of the fundamental-moc Love wave calculated from the S-wave velocity of the subsurface structure

Table 5.2. Model parameters of geological structure at the test site est mated by an inversion technique using phase velocities of Rayleigh wav in microtremors.

Layer	Thickness (m)	S-wave velocity (km/s)	P-wave velocity (km/s)	Densit (g/cm
1	44	0.15	1.58	1.70
2	1256	1.50	3.00	2.22
3	∞	2.40	4.27	2.43

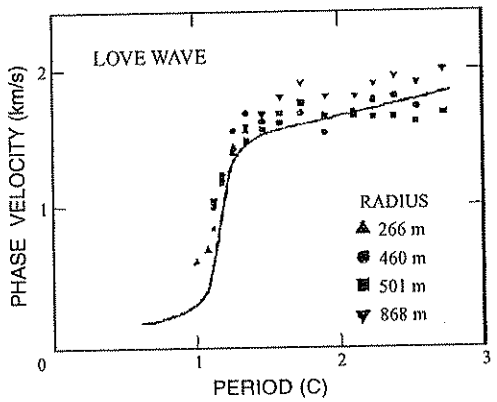

Figure 5.24. Phase velocities of Love waves obtained by the extended SPAC method. The solid line indicates the theoretical phase velocity curve of Love waves calculated for the structural model in Table 5.2.

Table 5.2. This curve generally gives slower velocities than the ones calculated from the observation. However, the general trends of the calculated and observed data are consistent; in particular we see the steep increase in phase velocity through the periods 1 to 1.2 s, and the gradual increase with the periods greater than 1.3 s.

The relationship between period and the power fraction of Love waves $\left\{ = h_0^L(\omega) / H_0(\omega) \text{ [see equations (3.95) to (3.97)]} \right\}$ in microtremors is shown in Figure 5.25. At the period 1 s, the power of the Love wave is about 50%, and the fraction increases at longer periods.

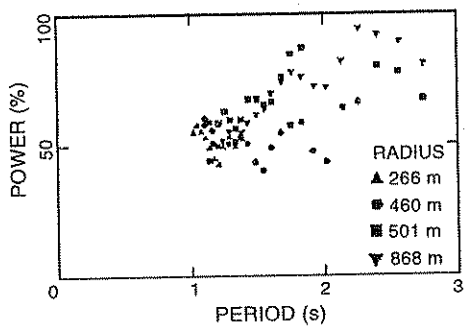

Figure 5.25. Power fractions of Love waves in the horizontal component of microtremors.

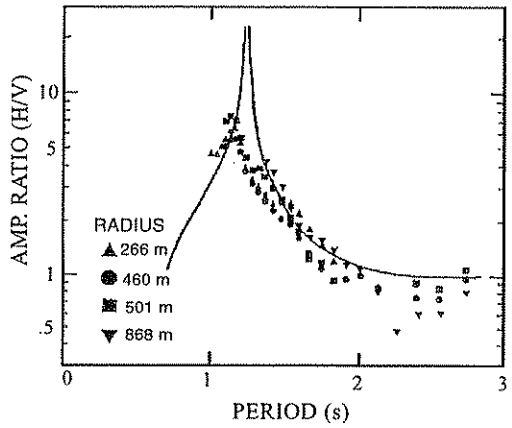

Figure 5.26. Amplitude ratios of vertical and horizontal components of Rayleigh waves. The solid line indicates the theoretical curve calculated for the structural model in Table 5.2.

Figure 5.26 shows the amplitude ratio between vertical and horizontal components (H/V) computed from the ratio of the powers of the vertical component and of the Rayleigh wave contained in the horizontal component. The variation of the amplitude ratio against period generally agrees with the values calculated from the estimated structure (inserted curve), although the peak in the data from observation at 1.1 s slightly offsets from the calculated peak at 1.23 s.

As seen, this comparison between the power ratio or amplitude ratio of the Rayleigh wave can be used to improve or evaluate the estimated subsurface structure model. This demonstrates an advantage of the SPAC method achievable by using three-component data.

Chapter 6

Case histories

Recent studies in Japan contain increasing numbers of cases where one dimensional subsurface S-wave velocity structure is explored using observa tions of microtremors. However, this method is not often used on a stand-alon basis.

With some exceptions, this method has been used for checking the reli ability of results of other methods, by comparing the estimated structures o converting to another measurement. This chapter introduces a few example of such applications.

6.1 Application of the frequency-wavenumber (*f-k*) method

6.1.1 Regional structural survey by long-period microtremors

Figure 6.1 is a map of the central to southern Tokachi Plain, where subsurfac structure was estimated by the microtremor method with 18 locations in th area of a 40-km square. A Bouguer anomaly map referred to for compariso is in Figure 6.2.

At each location, microtremors were recorded with one or two ten-statio arrays. The stations are equipped with a PELS74V vertical-component seis mometer whose natural frequency is 8 s. The recording was by analog method in the early observations, with a digital system being employed in later stud ies. In both cases, the data were recorded independently, i.e., no physical tim

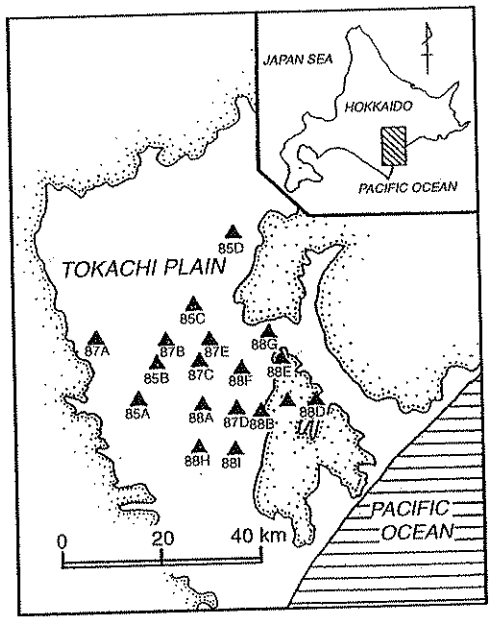

Figure 6.1. Locations of microtremor observations on the Tokachi Plain.

link between stations was used at the time of recording. The duration of each observation was forty-five minutes.

Figure 6.3 is a seven-minute segment of one of the records, and some of the *f-k* spectra estimated from the microtremor data are shown in Figure 6.4. The figure shows the *f-k* spectra for six different periods. The circle in each graph passes through at least one of the maxima of the *f-k* spectra, and its radius indicates the phase velocity posted in the graph.

Figure 6.5 shows the phase velocity of the Rayleigh wave as a function of period at eight of the eighteen locations in the Tokachi Plain. The curves in the graphs indicate the relationship between phase velocity and the period theoretically calculated from the estimated layered-earth structure models.

Figure 6.6 shows examples of the S-wave velocity structures estimated for the same eight stations calculated from the estimated phase velocities of the observed Rayleigh waves. The velocity structure was constrained by an assumption that the maximum number of layers is seven.

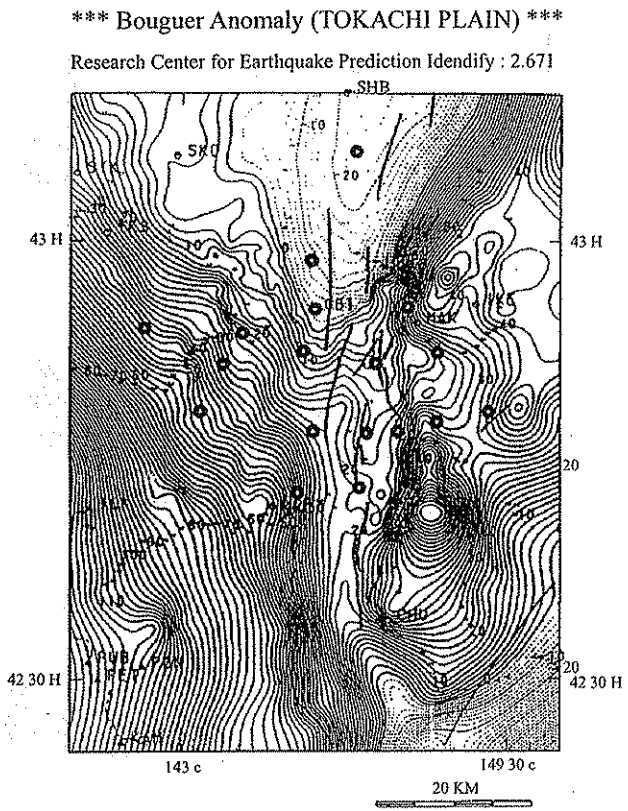

Figure 6.2. Bouguer anomaly map of the Tokachi Plain.

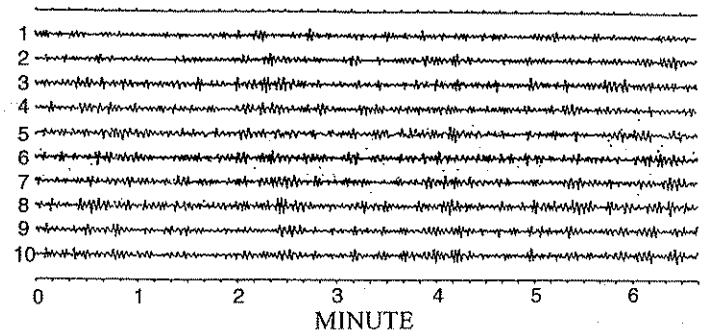

Figure 6.3. A part of the microtremor record obtained with array 88E.

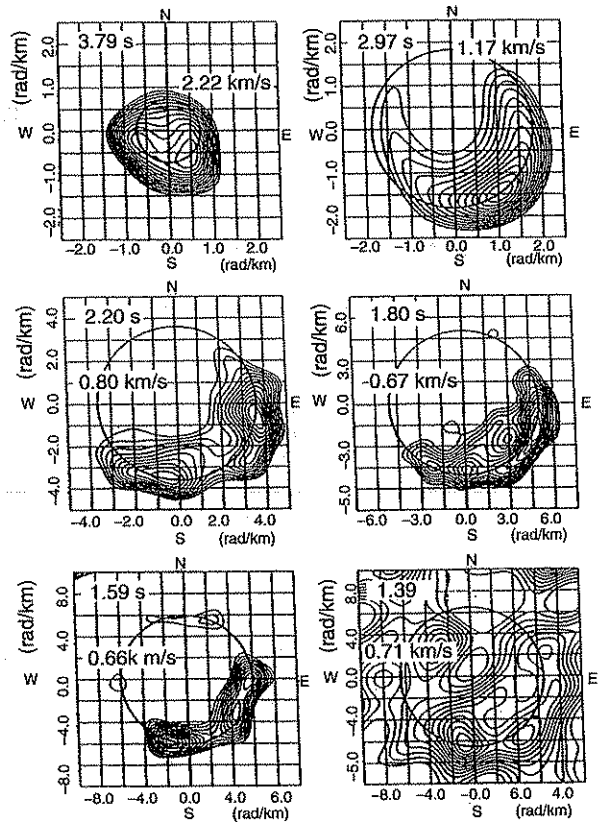

Figure 6.4. An example of the *f-k* spectra computed from the microtremor record obtained with array 88E.

Figure 6.7 shows a cross-section for the estimated S-wave velocity structure along the west-east line C–C′. Figure 6.8 shows a comparison between the section and profiles of the Bouguer anomaly as obtained both from actual observation and from model calculations (assigning assumed densities to each layer). The density of the deepest layer was not directly estimated from the microtremors, but estimated so as to fit the measured values of the Bouguer anomaly. In order to estimate this last layer with confidence from microtremors, phase velocities would need to be estimated out to at least 5 s.

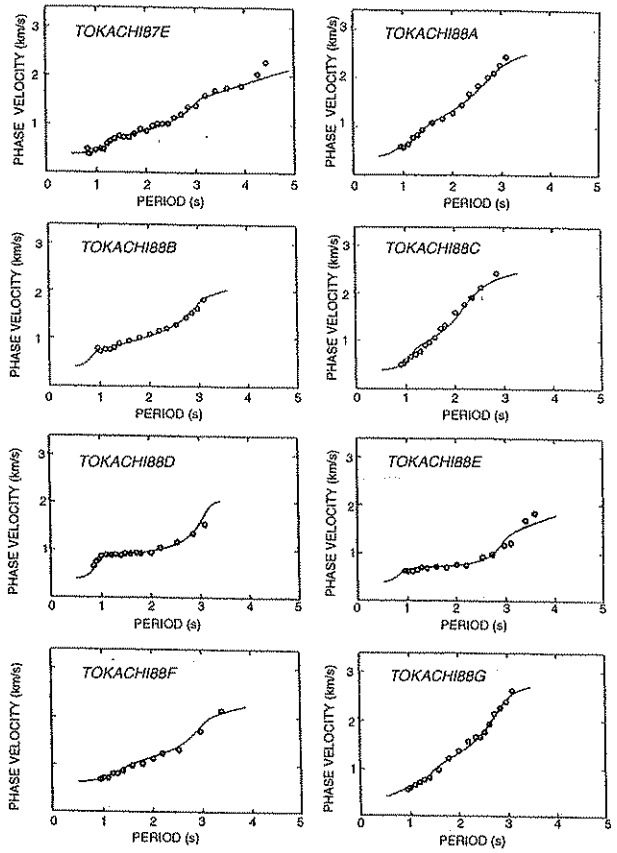

Figure 6.5. Phase velocities obtained at the eight locations in the Tokachi Plain (circles), and those of fundamental mode Rayleigh waves calculated for best-fit models (solid lines).

6.1.2 Comparison of the result with a reflection seismic survey

Two seismic lines were recorded over the sediments from the southern Ishikari Basin to Tomakomai; the 17-km Naganuma line and the 15-km Tomakomai line. They are from a detailed vibrator seismic reflection survey conducted

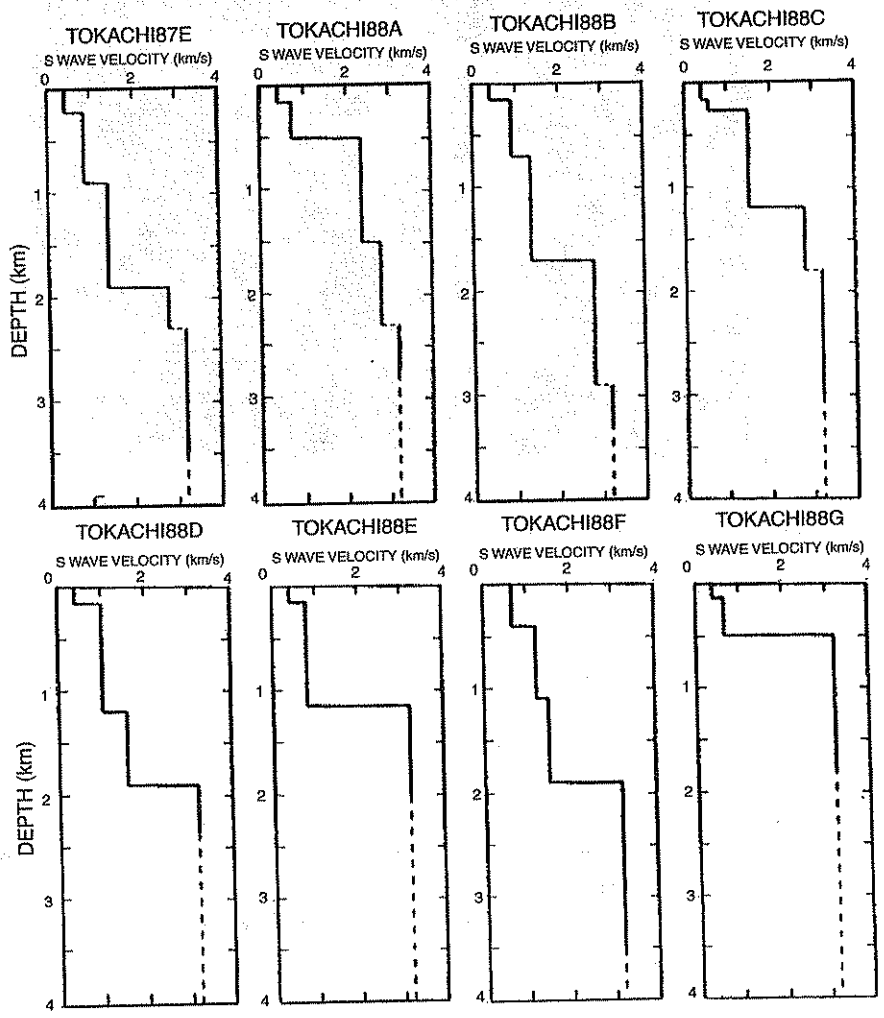

Figure 6.6. S-wave velocity structures at the eight locations in the Tokachi Plain.

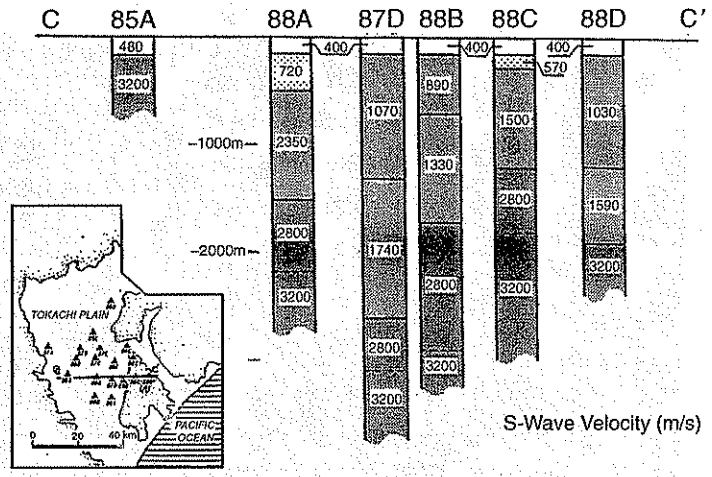

Figure 6.7. S-wave velocity structural cross-section along line C–C′.

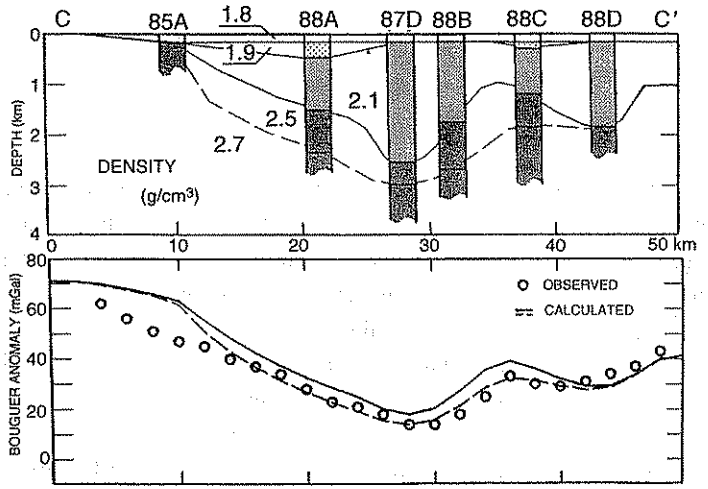

Figure 6.8. Comparison between density model and the calculated and observed Bouguer anomaly along line C–C′.

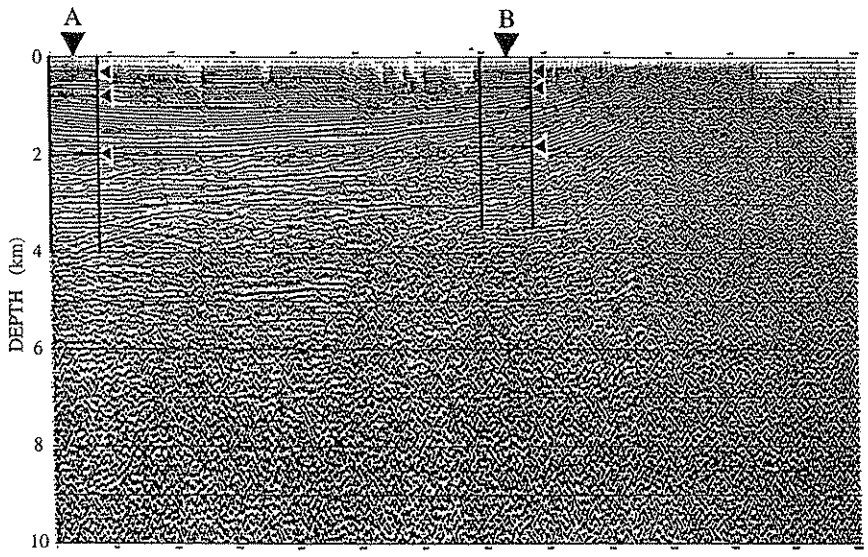

Figure 6.9. Comparison of a depth section of the Naganuma line obtained by a reflection seismic survey, with two S-wave velocity columns derived from microtremor data obtained with arrays A and B (Asano, 1989).

for petroleum exploration (Asano, 1989). Okada et al. (1990) carried out a microtremor survey in this area at eight locations, including two locations on each of these seismic lines. This section shows the results from the microtremor survey.

The scope of the work is to test a possibility in the future of using a microtremor survey method to extend "point" structural data given by well logs, to a line; and "line" structural data from a seismic line, to a plane. Thus, information from a detailed survey could be economically extrapolated by the use of microtremor survey methods.

Figures 6.9 and 6.10 are comparisons of the structures obtained from the microtremor survey method with those from conventional reflection seismic method. (see Asano (1989, 129–146). Most of the boundaries detected by the microtremor method correspond to one of the reflectors. However, not all the reflectors are detected by the microtremor survey method. This is due to the fact that the resolution of depth is strongly dependent on wavelength.

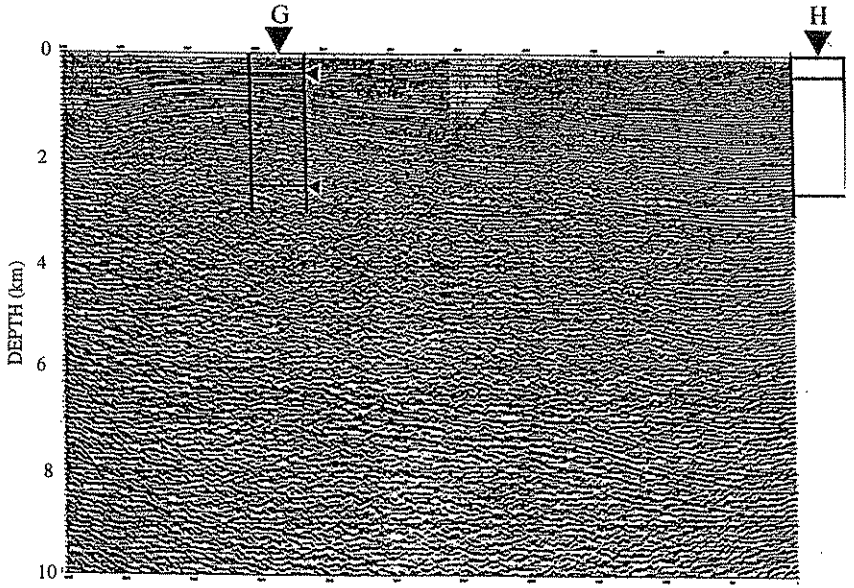

Figure 6.10. Comparison of a depth section of the Tomakomai line obtained by a r
flection seismic survey, with two S-wave velocity columns derived from microtrem
data obtained with arrays G and H (Asano, 1989).

On the other hand, there are occasions where the microtremor metho
clearly "sees" the boundaries defined by the P-wave sonic log, even whe
they are not clear in the reflection seismic section.

Figure 6.11 is a comparison between the P-wave column measured by
by sonic log, and the S-wave column estimated by the microtremor metho
for a location near array G. As is clearly seen, the microtremor survey resu
indicates a boundary at the depth of 2500 m at which the sonic log also show
a clear break. However, the seismic section does not show a strong reflect
at this depth.

It is noted that the microtremor method is not detecting the layer fro
1100 to 1300 m and from 1300 to 2500 m where the velocity gradient
relatively large. In this example, the structure estimated by the microtrem
survey method consists of layers with constant velocities. The question
whether phase velocities from the observations can be explained if some
the constant-velocity layers are replaced by layers with a velocity gradient
still unanswered.

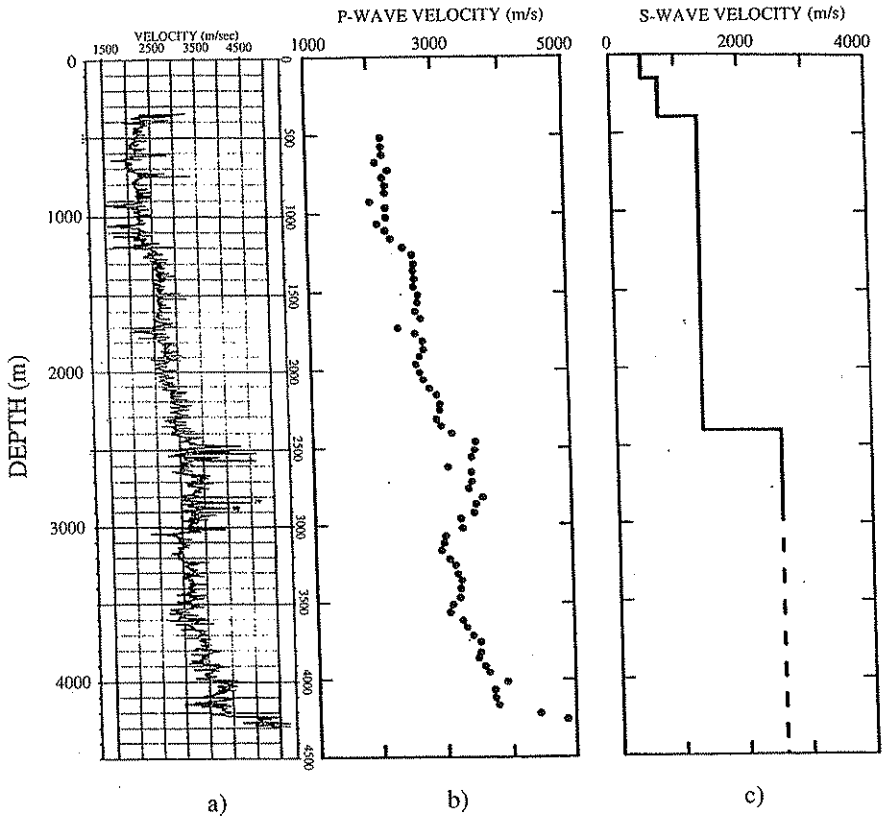

Figure 6.11. (a) P-wave sonic log data near array G; (b) smoothed segment extracted from the sonic log; (c) distribution of S-wave velocity estimated from microtremor observation.

6.2 Application of the spatial autocorrelation method

6.2.1 Evaluating the reliability of the spatial autocorrelation method by comparison with wireline log data

Matsuoka et al. (1996) test the reliability of the SPAC method at several locations where the velocity structure is known from 2 to 3 m to about 3000 m, from well log and refraction surveys.

Figure 6.12 shows good agreement between the phase velocity from tl microtremor method and phase velocity calculated from the known stru ture by logging and refraction surveys at four locations up to 50 m deep. the four locations, four-point circular arrays (equilateral triangle and the ce ter point) with four different radii were used for observation. This experime demonstrates that an array radius of 3 m is sufficient to estimate the structu to a depth of 50 m.

Figure 6.13 is another comparison at a location where the subsurfa structure is precisely known. The microtremors were observed at the Iwatu location using four-point circular arrays with radii of 3, 17, 52, and 1: m. The comparison of the phase velocities shows a very good agre ment.

The velocity structure was estimated for two additional location Kosigaya and Kasukabe in the vicinity of Iwatuki. The two graphs at tl sides of the Iwatuki graph at the bottom of Figure 6.13 present comparison These structure models were estimated using the Iwatutki model as a referen for the initial model of an iteration process.

This example suggests that the SPAC method is able to detect a subsu face boundary using wavelengths up to 10 to 20 times the largest radius of tl arrays. On the other hand, a numerical simulation by Miyakoshi et al. (199(confirmed that the *f-k* method is limited to using wavelengths around two t three times the largest distance between stations, in detecting a subsurfac boundary. These examples have demonstrated that the SPAC method is sup rior to the *f-k* method in estimating subsurface structure from observation microtremors.

6.2.2 Estimating shallow and deep subsurface structures in earthquake damaged areas

On 17 January 1995, the Kobe Earthquake (Hyogoken-nanbu Earthquak caused severe damage to the Kobe area. In order to make a fundament database for the cause and distribution of the damage, the Ministry of Cor struction has been studying the geological structure of the Osaka and Hyog area (Kinki Regional Construction Bureau, Ministry of Construction of Japa 1997). The basement rocks are estimated up to 1000 m deep. Along with othe methods, the microtremor survey method is employed targeting the depth i the order of 1000 m. This section briefly describes some results of this stud (Okada et al., 1997).

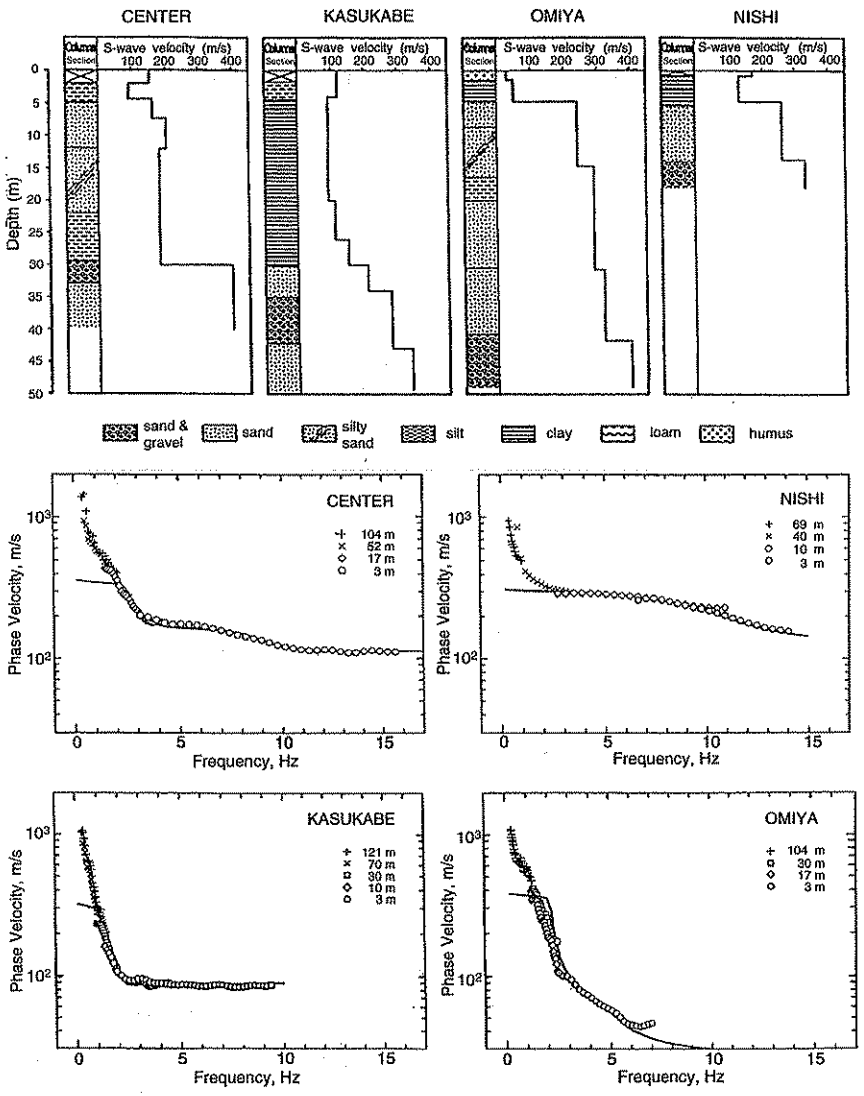

Figure 6.12. (Top) Detailed distribution of S-wave velocity to the depth of 50 meters from well-log and refraction seismic data. (Bottom) Phase velocities of the fundamental-mode Rayleigh wave calculated from microtremor data by the SPAC method, and from theoretical calculation using the velocity distributions shown above (Matsuoka et al., 1996).

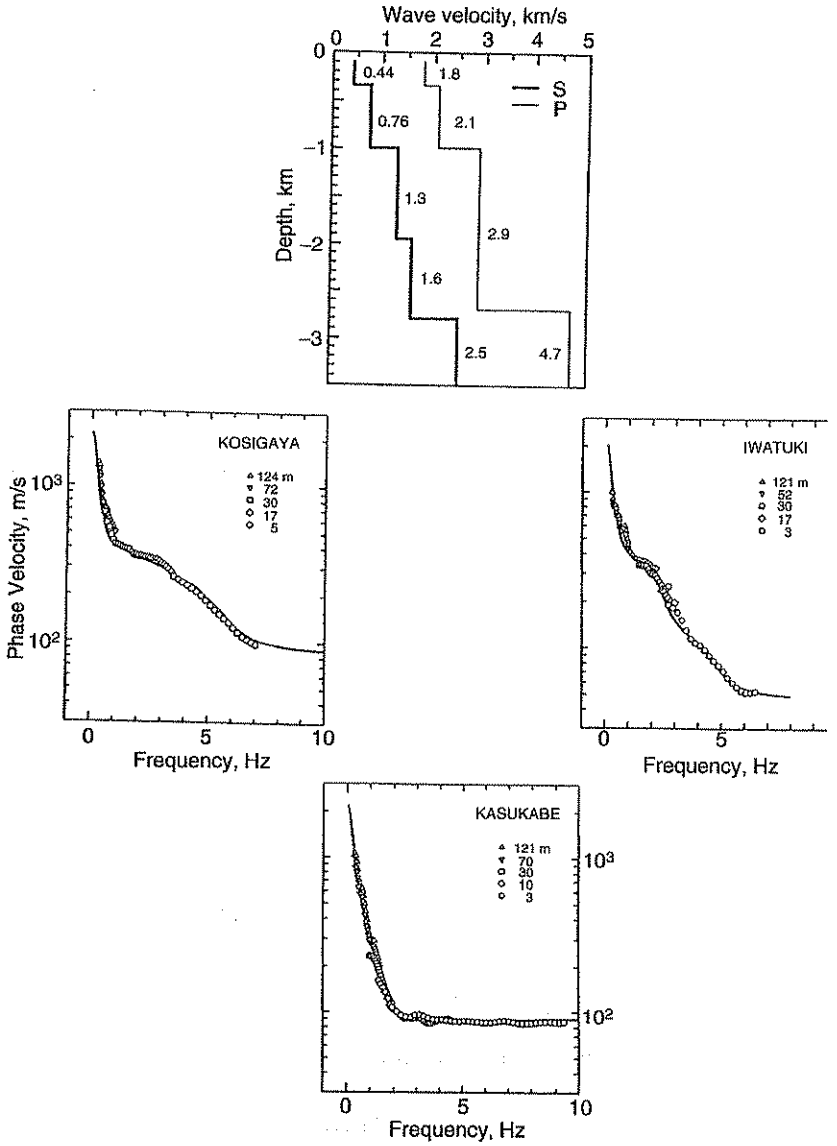

Figure 6.13. (Top) Distribution of S-wave velocity to the depth of 3500 m as es mated from well logs. (Center right) Phase velocities of fundamental-mode Raylei waves, calculated from microtremor data at the same place by the SPAC method a from theoretical calculations using the velocity distribution shown above (Matsuo et al., 1996).

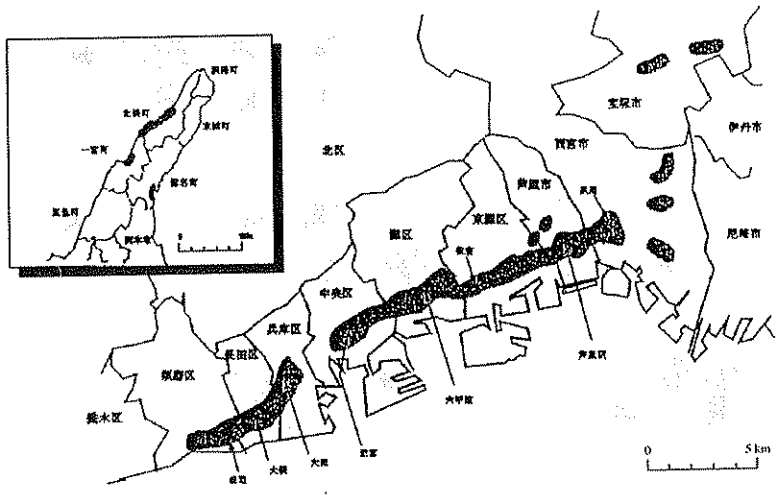

Figure 6.14. Distribution of damage of the 1995 Kobe Earthquake (Osaka Meteorological Bureau, 1995). Dark areas exceeded 7 degrees on the Japanese seismic intensity scale (equivalent to over X on the MMS).

Figure 6.14 is a distribution map of the areas severely damaged by the 1995 Kobe Earthquake, which was the 7th degree on the Japanese seismic intensity scale—the so-called "damage belt." Magnitude of the damage varied widely from place to place. Microtremor surveys were carried out at 45 locations, including the damage belt, in an area measuring 35 km in the east-west direction by 5 km north-south (Figure 6.15).

The area has not been surveyed in detail by conventional seismic methods, and hence the detailed relationship between the distribution of the damage and site effects is largely unknown. The microtremors were analyzed by the SPAC method. The survey was made using eight-station arrays formed by combining two basic four-point arrays of three sizes: large (300–500 m radius), medium (120–200 m) and small (30 m), as reported by Okada et al. (1997).

Incorporating geological information and results of rather scarce "detailed" seismic surveys, the structure of the targeted depth of 10 to 1000+ m was estimated. This depth range corresponds to the depth of granitic basement with an S-wave velocity higher than 2200 m/s. The depth of the basement was estimated to be between 155 m and 1600 m.

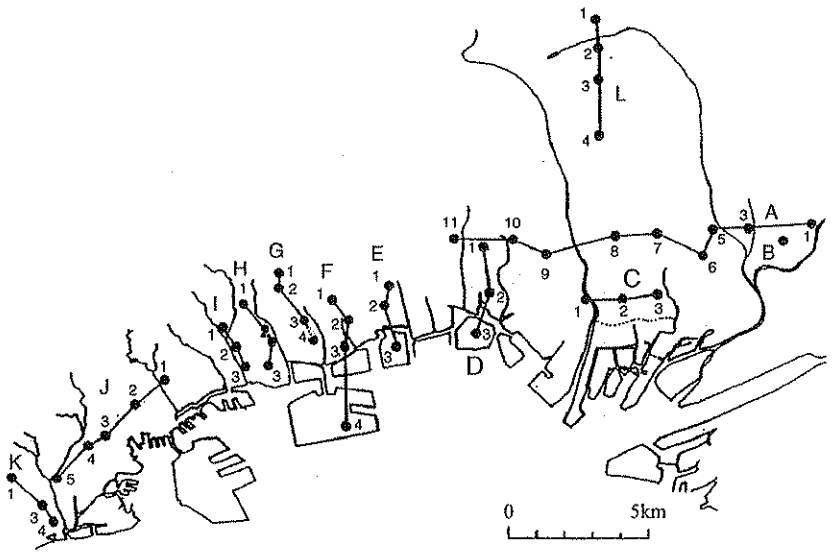

Figure 6.15. Locations of microtremor observations used for analysis of subsurfa structure, in order to investigate factors affecting damage in the 1995 Kobe Earthqual (Okada et al., 1997).

By way of example, the phase velocity profile estimated from microtremo observed at location A8 is illustrated in Figure 6.16. The solid line in the fi ure is the phase velocity of Rayleigh waves, as calculated for the estimat structure.

Cross-section views of the structure along selected lines joining the 45 l cations are shown in Figures 6.17 (east of Ashiya) and 6.18 (west Ashiya).

In each case, the observed phase velocities are assumed to be those fundamental-mode Rayleigh waves, and the data are analyzed for five layer or six layers where an alluvium layer can be distinguished from the diluviu layer. These layers are described in the legend of Figure 6.18. It seem difficult to recognize more layers for the chosen magnitude and length of t observation. The subsurface boundaries were drawn along twelve traverse A, B, . . . , L, as shown in Figure 6.15, where traverse B is of a single point onl In Figures 6.17 and 6.18, these traverses are shown with a letter *T* (for traverse

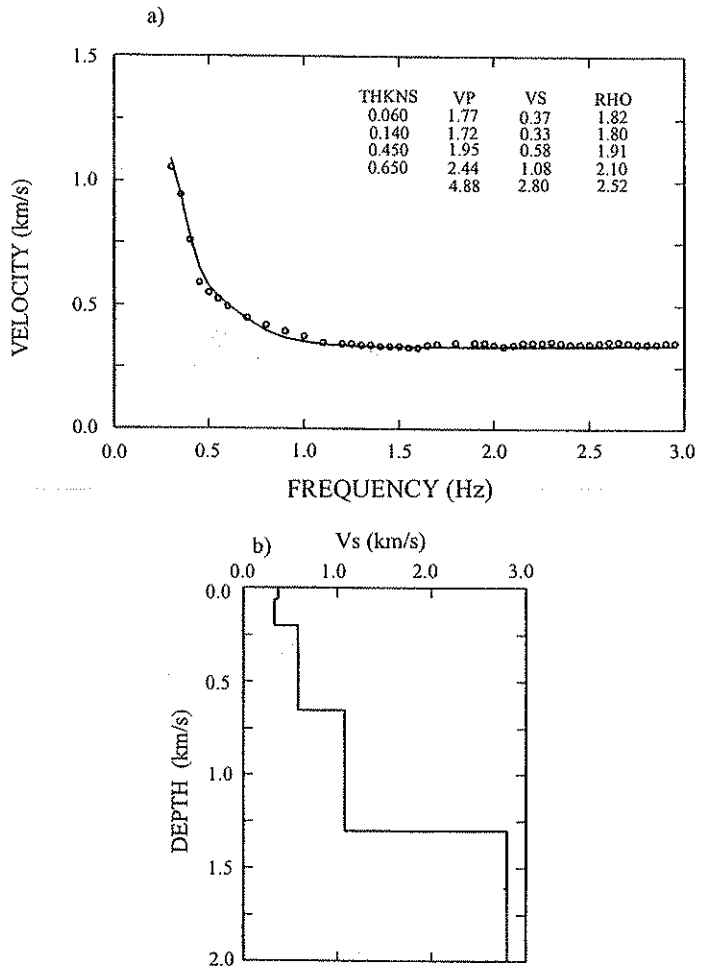

Figure 6.16. (a) Phase velocity calculated for the location A8; (b) estimated S-wave structure.

prefixed to the letters A, B, . . . , L. The layers are interpreted integrating P-wave velocity, S-wave velocity, density, and thickness. The correspondence between S-wave velocity and the estimated geological formation is shown in the legend (Table 6.1). Several layers are left uncolored in the figure; they are the layers where the calculated S-wave velocity does not correspond to any of the "estimated geological formations."

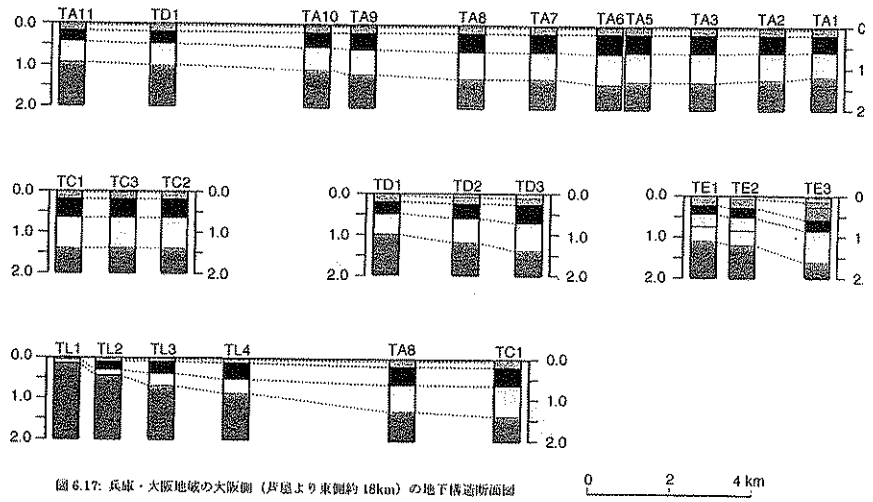

図 6.17: 兵庫・大阪地域の大阪側（芦屋より東側約 18km）の地下構造断面図

Figure 6.17. Subsurface structural cross-section for the Hyogo-Osaka area (east o Ashiya). Labels of the form TA11 refer to Traverse A, Station 11, located as marke on Figure 6.15. See legend in Table 6.1.

While the estimated accuracy of the S-wave velocity is generally abou 10%, accuracy of estimates of the S-wave velocity of the basement is con sidered to be as poor as 20%. As seen in Table 6.1, the estimated range o the basement S-wave velocity (2.20–2.80 km/s) is larger than the range fo other formations. The S-wave velocity of the basement at stations TF1, TF2 TG2, TI2, and TJ1 is even lower, at around 2.0 km/s. Whether these lay ers with low S-wave velocity are really representative of granitic basemen

Table 6.1. Legend for Figures 6.17 and 6.18.

Color	Velocity layer	Estimated formation	S-wave velocity (km/s
blue	I	Alluvial	0.15–0.39
orange	II	Upper Osaka Group	0.33–0.57
black	III	Middle Osaka Group	0.45–0.85
yellow	IV	Lower Osaka Group	0.79–1.28
pink	V	Granitic Basement	2.20–2.80

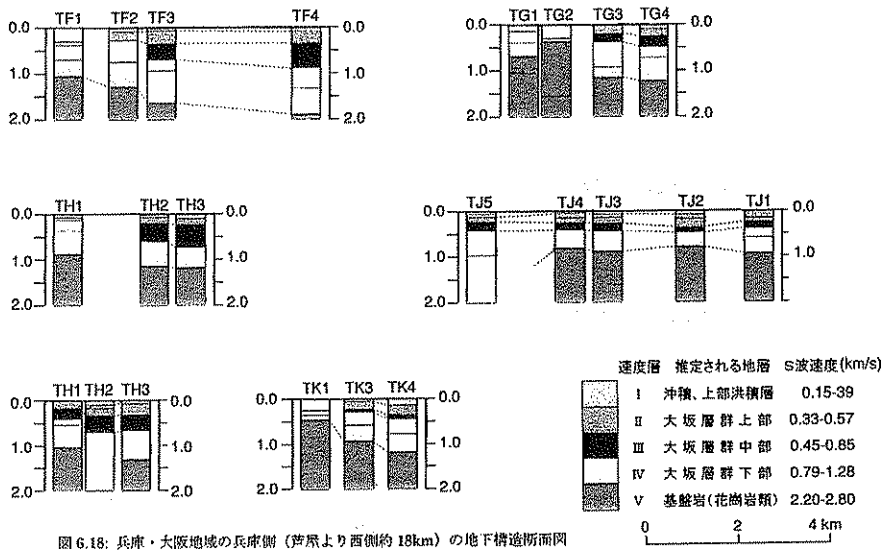

図 6.18: 兵庫・大阪地域の兵庫側（芦屋より西側約 18km）の地下構造断面図

Figure 6.18. Subsurface structural cross-section for the Hyogo-Osaka area (west of Ashiya). See legend in Table 6.1.

cannot be determined by this survey alone. It is noted that the stations with a low-velocity basement are found to be immediately adjacent to faults: TF1 and TF2 on the Ashiya Fault, TG2 on the Gosukebashi Fault, and TI2 and TJ2 on the Suwayame Fault.

To the east of Ashiya, the depth of the basement at TL1, which is located close to the foothills, is estimated to be very shallow at around 0.155 km. The depths of the basement at other locations near the foothills are generally shallow at about 0.45 km, and gradually deepening toward the coast-line, to reach about 1.4 km at locations TD3, and TC1 to TC3. This trend agrees with surface-mapping of the geology. A fault is indicated near TL1, near the Fukuchiyama Line of the Japan Railway in Takarazuka. This coincides with the known structural lineament known as the Arima-Takatsuki Line.

To the west of Ashiya, as in the east, the depth of the basement is small near the foothills, at 0.35 km (station TG2), and gradually increases towards the coast to reach about 1.6 km near location TF3. These agree with the structure expected from surface mapping. The basement is clearly deeper than 1.6 km at TJ5.

Kuroki and Wakizaka (1997) calculated the seismic response taking thi structure into consideration, and suggested a possibility that the origin of th "damage belt" is affected by structure to the full depth of the basement, a well as by the condition of the shallow part of the ground.

The observations of microtremors used in the above example were mad during day-time in the urban area, where there is severe cultural noise an consequently conventional exploration techniques are difficult to apply. Thi is an important result that shows the strength of the microtremor survey metho in estimating subsurface structure in urban areas.

In recent times, application of the SPAC method has been gaining i popularity in Japan. In China, strong interest has been shown in the SPA method since 1984 when our research started. Progress in our research ha been adopted through research information exchange, and applied succes fully in preliminary exploration for geothermal groundwater (Ran and Wan 1994). There are several recent demonstrations of the practical superiorit of the SPAC method over conventional *f-k* methods (e.g., Miyakoshi et al 1996). These case histories and results are not included in this volume.

Chapter 7

Closing remarks

As discussed previously, there are numerous methods utilizing "natural fields among geophysical survey tools. These include gravity, electric, magnetic and electromagnetic methods. These methods measure local disturbances of the natural fields, and identify the causes of these anomalies. Many of these techniques evolved from scientific research of the Earth, and developed mainly in the western world.

Microtremors, the subject of this textbook, can be counted in broad terms as a natural-field technique. Local anomalies in microtremor activity have long been known since early studies, and research efforts to identify the causes were heightened in the West. This research is not an exception; originated from the scientific interest in understanding the Earth through the study of microtremors. But this technique, unlike other geophysical methods was not developed systematically in an organized fashion. The reason is the overwhelming development and rapid evolution of other commercial seismic methods, particularly the reflection seismic method from the 1960s.

A turning point in the research into microtremors was the International Geophysical Year (IGY, 1957–1958), which served as an organized international collaboration of geoscientists. Many researchers in the West and abroad had a great interest in microtremors, which had always been recorded by the seismometers. The main focus of studies at that time was components with periods greater than 1 s, the so-called "long-period microtremors." Before the IGY, individual researchers achieved a good understanding of the source temporal variations, and the relationship with the under-ground structure for long-period microtremors; studies involved searching for a local anomaly and identifying the position of the source. The IGY designated research o

long-period microtremors as one of the projects for international collaboration. Unfortunately, momentum of these studies diminished after the conclusion of the IGY. However, among the branches of microtremor research, study of the technique for the purpose of estimating geological structure *did* survive. From the 1960s until the present, further research impetus has derived from the concurrent development of stimulating theories and of data acquisition and interpretation techniques.

On the other hand, in Japan after the IGY, Kiyoshi Kanai and his group researched microtremors with periods shorter than 1 second (Kanai, 1983). From a series of studies, it was evident that the dominant period of microtremors is related to subsurface geological structure. The results formed the basis of the development of applications of this technology to the field of earthquake engineering. Unfortunately, the technology did not have the technical merit to meet the expectations imposed by that field.

Since 1968, the year of the major Tokachi-Oki earthquake, the demand for quantitative information of geological structure, or basement structure in earthquake engineering terms, down to 1000 m, has rapidly intensified. A consequence has been the desire for development and refinement of techniques to explore deep structure. A concurrent difficulty has been that the information on structure is required for highly developed urban areas or their peripherals, where advanced seismic reflection methods are difficult to apply, both technically and economically. The microtremor survey method, has been devised to address this demand, while minimizing these difficulties.

The principles, theoretical background, and interpretation techniques of the microtremor survey method are not based on an extension of the succession of tremor research dating back to the pre-IGY period. Rather, the theoretical background is based on the theory of a stochastic process which was developed after the 1960s. The data acquisition instruments have been developed specifically for the application to microtremors, taking their unique properties and attributes into account. The interpretation method assumes access to high-speed, high-capacity computers which enable complex and complicated calculations to be performed on a large amount of data. Therefore this textbook omits discussion of studies of the "traditional long-period microtremor surveys," which is based on the tremor research and owes their theoretical derivation to the extension of pre-IGY studies, even though such studies incorporate the use of modern data acquisition and interpretation techniques. This omission is because the technical details of such studies make little contribution to surveys of geological structure.

The technique of the microtremor survey method was developed in re
sponse to the demand generated within the field of earthquake engineering
It has a very short history of development, with little opportunity thus fa
to confirm the viability of its direct application to oil and gas prospecting
However, the method's potential for such an application is irrefutable.

This textbook owes much to the researchers in The Faculty of Science o
Hokkaido University, which has been the center of the development of thi
survey technique for the last ten years. As seen in this textbook, there are a
yet few case histories of applications of the microtremor method. We nov
need to extend the application of the method and the number of case histories
towards commercial viability.

References

*Note: Some Japanese publications do not have titles in English. The English titles are given by the translator at his discretion, and such titles are indicated by an * after the author and the publication year. Most of the publications in Japanese journals contain abstracts in English.*

Aki, K., 1957, Space and time spectra of stationary stochastic waves, with special reference to microtremors: Bull., Earthq. Res. Inst., **35**, 415–456.

Aki, K., 1965, A note on the use of microseisms in determining the shallow structures of the Earth's crust: Geophysics, **30**, 665–666.

Aki, K., and Richards, P. G., 1980, Quantitative seismology—Theory and methods: W. H. Freeman & Co.

Asano, S. (Editor), 1989*, Research into the determination of deep underground structures for the better prediction of earthquake ground motion: A special report of the Study on Natural Disaster Science with Grant-in-Aid for Scientific Research by the Ministry of Education, No.A-63-3, (in Japanese).

Asten, M. W., and Henstridge, J. D., 1984, Array estimators and the use of microseisms for reconnaissance of sedimentary basins: Geophysics, **49**, 1828–1837.

Bendat, J. S., and Piersol, A. G., 1986, Random data, analysis and measurement procedures, 2nd Ed.: John Wiley & Sons, Inc.

Bradner, H., and Dodds, J. G., 1964, Comparative seismic noise on the ocean bottom and on land: J. Geophys. Res., **69**, 4339–4348.

Blackman, R. B., and Tukey, J. W., 1958, The measurement of power spectra: Dover Publ., Inc.

Capon, J., 1969, High-resolution frequency-wavenumber spectrum analysis: Proc. IEEE, **57**, 1408–1418.

——— 1973, Signal processing and frequency-wavenumber spectrum analysis for a large aperture seismic array: Methods in computational physics, **13**, Academic Press Inc.

Capon, J., Greenfield, R. J., and Kolker, R. J., 1967, Multidimensional maximum-likelihood processing of a larger aperture seismic array: Proc. IEEE, **55**, 192–211.

Dobrin, M. B., and Savit, C. H., 1988, Introduction to geophysical prospecting, 4th Edition: McGraw-Hill Book Co.

Ferrazzini, V., Aki, K., and Chouet, B., 1991, Characteristics of seismic waves composing Hawaiian volcanic tremor and gas-piston events observed by a near-source array: J. Geophys. Res., **96**, 6199–6209.

Gutenberg, B., 1958, Microseisms: Advances Geophys., **5**, 53–92.

Haubrich, R. A., 1967, Microseisms: International Dictionary of Geophysics, **2**, Pergamon Press Inc.

Henstridge, J. D., 1979, A signal processing method for circular arrays: Geophysics, **44**, 179–184.

Hidaka, E., 1985, Phase velocity of Rayleigh waves and S-wave velocity distribution estimated from long-period microtremors: M.Sc. thesis, Hokkaido University (in Japanese).

Horike, M., 1985, Inversion of phase velocity of long-period microtremors to the S-wave velocity structure down to the basement in urbanized areas: J. Phys. Earth, **33**, 59–96.

Hough, S. E., et al., 1992, Ambient noise and weak-motion excitation of sediment responses: Results from the Tiber Valley, Italy: Bull. Seis. Soc. Am., **82**, 1186–1205.

Ikegami, R., 1964, On the microseisms observed at Koganei, Tokyo (I): Zisin Ser.II, **17**, 68–88 (in Japanese).

Kanai, K., 1983, Engineering Seismology: University of Tokyo Press (I Japanese)

Kinki Regional Construction Bureau, Ministry of Construction of Japa 1997: A brief report on the investigation of the characteristics of gec logical structure in the Osaka and Hyogo areas: Kinki Technical Offic (in Japanese).

Kudo, K., et al., 1976, Observation of 1- to 5-sec microtremors and thei application to earthquake engineering, Part IV, Elucidation of propagativ characteristics by use of a temporary array net: Zisin, Ser.II, **29**, 323–33 (in Japanese).

Kulhanek, O., 1990, Anatomy of seismograms: Developments in solid Eart geophysics, **18**, Elsevier.

Kuroki, T., and Wakizaka, Y., 1997, Geomorphological and geological fac tors at damaged area caused by the 1995 Hyougoken-Nanbu earthquake Civil Engineering J., **39**, 20–25, Public Works Research Inst., Ministry o Construction (in Japanese).

Lacoss, R. T., Kelly, E. J., and Toksöz, M. N., 1969, Estimation of seismi noise structure using arrays: Geophysics, **34**, 21–38.

Liaw, A. L., and McEvilly, T. V., 1979, Microseisms in geotherma exploration—Studies in Grass Valley, Nevada: Geophysics, **44**, 1097-1115.

Ling, S., 1994*, Research on the estimation of phase velocities of surfac waves in microtremors: Ph.D. thesis, Hokkaido University (in Japanese).

Ling, S., and Okada, H., 1993, An extended use of the spatial autocorrela tion method for the estimation of geological structure using microtremors Proc., 89th Conf. SEGJ. 44–48 (in Japanese).

Malagnini, L., Rovelli, A., Hough, S. E., and Seeber, L., 1993, Site amplifica tion estimates in the Garigliano Valley, central Italy, based on dense arra measurements of ambient noise: Bull., Seis. Soc. Am., **83**, 1744–1755.

Marquardt, C. W., 1963, An algorithm for least square estimation of nonlinea parameters: J. Soc. Indust. Appl. Math., **11**, 431–441.

Matumoto, H., and Takahashi, M., 1977, Development of the portable easy-operation long-period seismometer, Part 2, Peripheral device: Bull. Earthq. Res. Inst., **52**, 11–27.

Matsuoka, T., Umezawa, N., and Makishima, H., 1996, Experimental studies on the applicability of the spatial autocorrelation method for estimation of geological structures using microtremors: Butsuri-Tansa (Geophys. Explor.), **49**, 26–41 (in Japanese).

Matsushima, T., and Ohshima, H., 1989, Estimation of underground structures using long-period microtremors—Kuromatsunai Depression, Hokkaido: Butsuri-Tansa (Geophys. Explor.), **42**, 97–105 (in Japanese).

Matsushima, T., and Okada, H., 1989, A few remarks on the scheme of observation and analysis in estimating deep geological structures by using long-period microtremors: Geophys. Bull., Hokkaido University, **52**, 1–10 (in Japanese).

——— 1990a, Determination of deep geological structures under urban areas: Butsuri-Tansa (Geophys. Explor.), **43**, 21–33.

——— 1990b, An exploration method using microtremors (2)—An experiment to identify Love waves in long-period microtremors: Proc. 82nd SEGJ Conf., 5–8 (in Japanese).

Miyakoshi, K., Okada, H., and Ling, S., 1996, A range of wavelength possible to estimate phase velocities of surface waves in microtremors: Proc. 94th SEGJ Conf., 178–182 (in Japanese).

Nogoshi, M., and Igarashi, T., 1970, On the amplitude characteristics of microtremors (Part 1): Zisin (J. Seismol. Soc. Japan), Ser. 2, **23**, 281–303 (in Japanese).

Ohsaki, Y., 1976*, Introduction to spectral analysis of earthquake ground motions: Kajima Publishing Co. Ltd. (in Japanese).

Okada, H., et al., 1995, Comparison of the frequency-wavenumber spectrum method and the spatial autocorrelation method for estimation of geological structure using microtremors: Proc. 93rd SEGJ Conf., 105–109 (in Japanese).

Okada, H., Ishikawa, K., Sasabe, K., and Ling, S., 1997, Estimation of underground structures in the Osaka-Kobe area by array-network observation of microtremors: Proc. 96th SEGJ Conf., 435–439 (in Japanese).

Okada, H., and Matsushima, T., 1989, An exploration method using microtremors (1),—A theory to identify Love waves in microtremors. Proc. 81st SEGJ Conf., 15–18 (in Japanese).

Okada, H., Matsushima, T., Moriya, T., and Sasatani, T., 1990, An exploration technique using long-period microtremors for determination of deep geological structures under urbanized areas: Butsuri-Tansa (Geophys. Explor.), **43**, 402–417 (in Japanese).

Okada, H., and Sakajiri, N., 1983, Estimates of an S-wave velocity distribution using long-period microtremors: Geophys. Bull., Hokkaido University, **42**, 119–143 (in Japanese).

Osaka District Meteorological Observatory, JMA, 1995, The 1995 Hyogoken Nanbu earthquake and its aftershocks: Report of the Coordinating Committee for Earthquake Prediction, Ed. by Geographical Surv. Inst **54**, 584–692 (in Japanese).

Peterson, J., 1993, Observation and modeling of background seismic noise U.S. Geol. Surv. Open-File rept., Albuquerque, 93–322.

Priestley, M. B., 1981, Spectral analysis and time series, vol. 1: Academi Press Inc.

Project Team for the Development of Small-Size Long-Period Seismometers 1974, Development of the portable easy-operation long-period seismometer: Spec. Bull. Earthq. Res. Inst., **13**, 17–22 (in Japanese).

Ran, W., and Wang, Z., 1994, The long-wave microtremor method and its advances: Geophys. and Geochem. Expl., **18**, 28–34 (in Chinese).

Sakaji, K., 1998, Temporal variation of the power spectra of microtremor observed at soil and rock sites: Graduation thesis, Hokkaido University (in Japanese).

Santo, T. A., 1960, Where do swells turn into microseisms? Zisin, Ser.II, **13**, 150–162 (in Japanese).

———1963, Where do swells turn into microseisms? Microseisms of Scandinavia: Zisin, Ser.II, **16**, 165–180 (in Japanese).

Schwab, F. A., and Knopoff, L., 1972, Fast surface wave and free mode computations: Methods in Computational Physics, **11**, Academic Press Inc.

Society of Exploration Geophysicists of Japan, 1989: Illustration of Geophysical Exploration: Soc. Expl. Geophys. of Japan (in Japanese).

Sunahara, Y., 1981, Stochastic system theory, vol. 1: Asakura Press (in Japanese).

Tokimatsu, K., Shinzawa, K., and Kuwayama S., 1992, Use of short-period microtremors for V_s profiling: J. Geotech. Engrg., **118**, 1544–1558.

Toksöz, M. N., 1964, Microseisms and an attempted application to exploration: Geophysics, **29**, 154–177.

Toksöz, M. N., and Lacoss, R. T., 1968, Microseisms—Mode structure and sources: Science, **159**, 872–873.

Yaglom, A. M., 1962, An introduction to the theory of stationary random functions (translated and edited by R. A. Silverman): Dover Publications Inc.

Yamamoto, H., 2000, An experiment for estimating phase velocities of Love waves from three-component microtremor array observations: Butsuri-Tansa (Geophys. Explor.), **53**, 153–166 (in Japanese with English abstract).

References for general reading

Akaike, H., and Nakagawa, T., 1972, Statistical analysis and control of dynamic systems (in Japanese): Science Press, Tokyo

Aki, K. and Richards, P. G., 1980, Quantitative seismology, Theory and methods, Vol. II: W. H. Freeman and Company, 559–932.

Haubrich, R. A., and McCamy, K., 1969, Microseisms: Coastal and pelagic sources: Rev. Geophysics, **7**, 539–571.

Kanai, K., 1969, Engineering seismology: Kyoritsu Publ. Co., Ltd. (in Japanese).

———1983, Engineering Seismology: University of Tokyo Press (in Japanese).

Index